Long Waves And Sea Level Variations

Final Project Assignment

COLLOUARD Nolwenn

Ensi 11 - Hyo

Ifremer Tutors : Franck Dumas, Fabrice Ardhuin
ENSTA-BRETAGNE Reporter : Nathalie Debese

August 2011

Abstract

Infragravity waves, called “long waves”, which period is between one and ten minutes, are an important part in coastal hydrodynamics. However they are often neglected in models and studies but their effects can be deciding for sedimentary transportation on the coast and marine submsersions. Their amplitude can be one meter. But their generation and liberation is still not well understood.

In coastal areas, the long waves can be amplified in harbors such as in Port-Tudy where the seiches are due to infragravity waves. They create strong currents which can cause damages and can stop port activities.

This study is part of the final project for the studies at ENSTA-BRETAGNE and for the master in Marine Geophysics at IUEM. The subject is the long waves and sea level variations. The aim is to quantify the long waves amplitude using a spectral analysis of existing data (tide gauge data and pressure data) and to model their propagation and generation.

The study was realized with data from Ifremer[1], the SHOM[2] and MEDDTL/DDTM17/SPC-Littoral Atlantique.

[1]Institut Français pour le Recherche et l’Exploitation de la MER
[2]Service Hydrographique et Océanographique de la Marine

Acknowledgements

I could not begin my report without having few words for the people who guided and helped me during this project.

First I would like to thank my tutors Franck Dumas and Fabrice Ardhuin for their trust all along the project, for having answered my questions and guided me during this intership. Without them this project could not have been possible.

Then I would like to thank Ronan Creach from the SHOM who showed interest in my project and gave me information and tide gauge data. These data were especially important for Royan harbor and without it I could not have obtained interesting results.

Finally I would like to thank all people who have read my report and especially Julien Lengrand-Lambert and Mathias Obreski for their constructive rereadings.

Thank to all people who contributed to make my internship pleasant at Ifremer.

Contents

Introduction

The infragravity waves, called “long waves”, which period is between one and ten minutes, are an important part of the coastal hydrodynamics. They are often neglected in models but their effects can be deciding in sedimentary transportation and marine submersions. They can be amplified in small harbors due to the natural resonances at these periods. For example in Port-Tudy, they cause seiches and creates strong currents which can stop port activity for some time. Therefore it is necessary to characterize their dynamics and to establish their statistics from the open ocean to the coastal zone. However their generation is still not well understood.

The aim is to quantify the long waves amplitude by spectral analysis of existing data (tide gauge and pressure measurements at the seabed) and data from models. Then the aim is to outline a numerical modeling of changes in sea level associated with the waves via a twodimensional numerical model forced by a wave field.

This report presents my work at Ifremer for a time period of five months and is divided into different parts. First I will present the internship and its context. Then the long waves will be presented, their generation and calculations. Second, I used a model realized by L.Leballeur in 2008 to model the infragravity waves propagation and generation. Finally I will present the seiche detection in Groix and Royan harbors. All results and details are explained in details in the appendices.

1

General Presentation

In this chapter, I am going to present the Ifremer and the context of the internship, and then the objectives and tasks to accomplish.

1.1 Presentation Of Ifremer.

Ifremer (Institut Français de Recherche pour l'Exploitation de la MER) is a public organization which is industrial and commercial (EPIC). It is placed under the supervision authority of the French departments "Enseignement Supérieur et de la recherche", "Développement durable et de la mer", "Alimentation" and "Agriculture et Pêche". The institute works not only with the French scientific community but also with many partners in other countries. It acts through many tasks related to ocean resources, their sustainable use, their monitoring...and the missions are :

- To know, evaluate and highlight the resources of the oceans and enable their durable exploitation.
- To improve the methods of supervision, evolution prediction, protection of marine and coastal areas.
- To promote the economic development of the marine world.

There are about 1400 workers at Ifremer, and five different centers located on the French coast and overseas. The institute owns a set of fish farming and experimentation and also seven ships. The following figure 1.1 shows the organization chart:

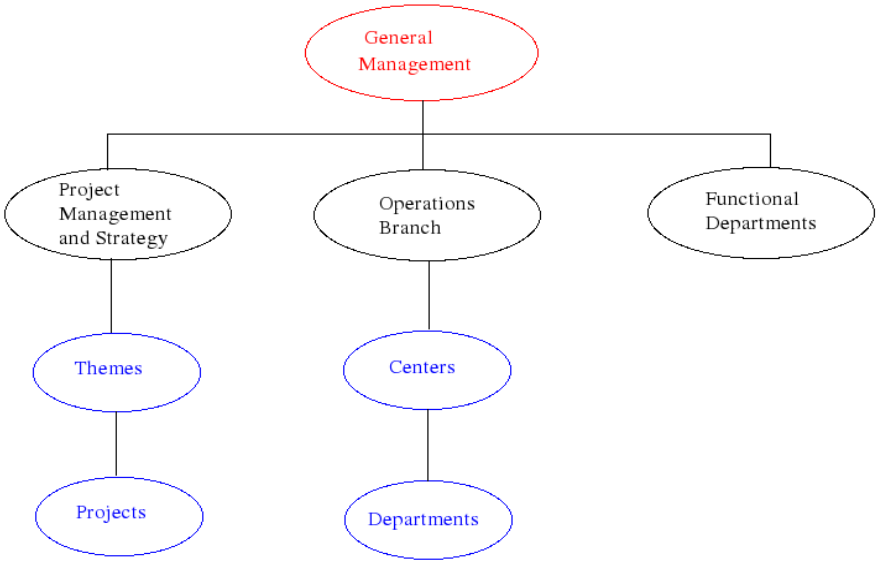

Figure 1.1: *Organization chart of Ifremer.*

The project management and strategy coordinates the science and technologies activities. The centers, departments and laboratories are attached to the operations branch.

During my internship I worked in the Department "Dynamique de l'Environnement Côtier" (Dyneco) mostly located in Brest, and more precisely in the laboratory of "Physique Hydrodynamique Sédimentologie" (Physed). This laboratory conducts research, expertise and collection procedures to evaluate and predict the environmental conditions of the coastal zone. It also develops numerical models for the implementation of systems dedicated to information and decision support for the needs of operational oceanography and sediment hydrodynamics. The department Dyneco carries on projects that focus on :

- Coastal hydrodynamic circulation.
- Sediment movements.
- Ecosystems.
- And generally the evolution of the coastal environment quality.

1.2 Context Of The Internship.

The environmental sciences are growing steadily since mankind has realized the importance of preserving its living environment and learning how to manage it better. The coastal

oceanography is part of the applied sciences that aim at describing the coastal environment, which is an important resource for humans. But these coastal areas are fragile and human infrastructures must be studied first, then controled as the ocean response can be very unpredictable and harmful. Therefore a better understanding of dynamic phenomena is needed to cope with its risks, especially in coastal areas.

In coastal areas, long waves, which period is between one and ten minutes, are present and are an important part of the coastal hydrodynamics. They are often neglected in models but their effects can be deciding in sedimentary transportation and marine submersions. For example, the measurement projects of the sea level by satellites to achieve a higher spatial resolution, such as the SWOT[1] project, require a precise knowledge of these waves. They are one of the main terms of the error budget for the measurement of the dynamic ocean height at high resolution. It is therefore necessary to characterize their dynamics and to establish their statistics from the open ocean to the coastal zone.

Moreover, the long waves can be amplified in small harbors. For example in Port-Tudy, they cause seiches and creates strong currents which can stop port activity for some time.

1.3 Objectives And Conduct Of The Study.

The study of these long waves covers the seiche study in Port-Tudy and Royan harbors. The aim is to quantify the long waves amplitude by spectral analysis of existing data (tide gauge and pressure measurements at the seabed) and data from models. Then the aim is to outline a numerical modeling of changes in sea level associated with the waves via a two-dimensional numerical model forced by a wave field.

Initially, a bibliography study was necessary to understand the subject and be aware of the work already done, and to know how to calculate the infragravity wave spectrum. Then the work was divided into three different parts : hydrodynamic modeling with the code from L.Leballeur ([Leb08]), long waves theoritical calculations and seiche study in Royan and Port-Tudy.

The modeling part consists of adapting the code of L.Leballeur ([Leb08]) to force it with infragravity waves. These waves are calculated theorically from a wave field.

Using data from tide gauges at Port-Tudy and Royan, a spectral analysis on an hour of data recording was performed. In Groix, I also used data from pressure sensors which were placed on the seabed around the island. With this study, the infragravity waves were detected. The aim was also to detect a seiche and to study the conditions outside and inside the harbor to see the relation between seiches and long waves.

The different tasks are summed up here, in relation with the internship objectives:

[1]Surface Water Ocean Topography, http://ctoh.legos.obs-mip.fr/altimetry/future-missions/swot

- Documentation : Bibliography, comprehension of the code from L.Leballeur.
- Theoritical calculation of the infragravity waves generation.
- Hydrodynamic modeling : L.Leballeur code ([Leb08]).
- Groix study : tide gauge and pressure sensors data analysis, analysis of WAVEWATCH III model results.
- Seiche in Royan : tide gauge data analysis, analysis of WAVEWATCH III model results, analysis of observed spectrum by a buoy.
- Report redaction.

I first made a bibliographic work then I adapted the code from L.Leballeur ([Leb08]). At the same time, I obtained data from the tide gauge in Groix so I started the data processing and analysis. Then I realized the theoritical calculation of the infragravity waves generation. Finally, I had data from the tide gauge in Royan and the data from the pressure sensors which were placed on the seabed around Groix.

2

The Long Waves

2.1 Definition.

Everyone has already seen waves, whether at a beach, in a puddle, a lake...Waves are a very complex natural phenomenon. From a standpoint of physics, they correspond to surface gravity waves which are sometimes progessive and standing. These waves propagate causing almost no material transport (Stokes drift). These oscillations of the air-water surface are maintained by an exchange between kinetic and potential energy until these energies are dissipated. They can have different periods depending on their mode of generation and the forces that generate them. The energy thus varies depending on the wavelength as *Oltman-Shay and Hathaway* have explained [OH89]. The following figure 2.1 shows the approximate distribution of ocean surface wave energy:

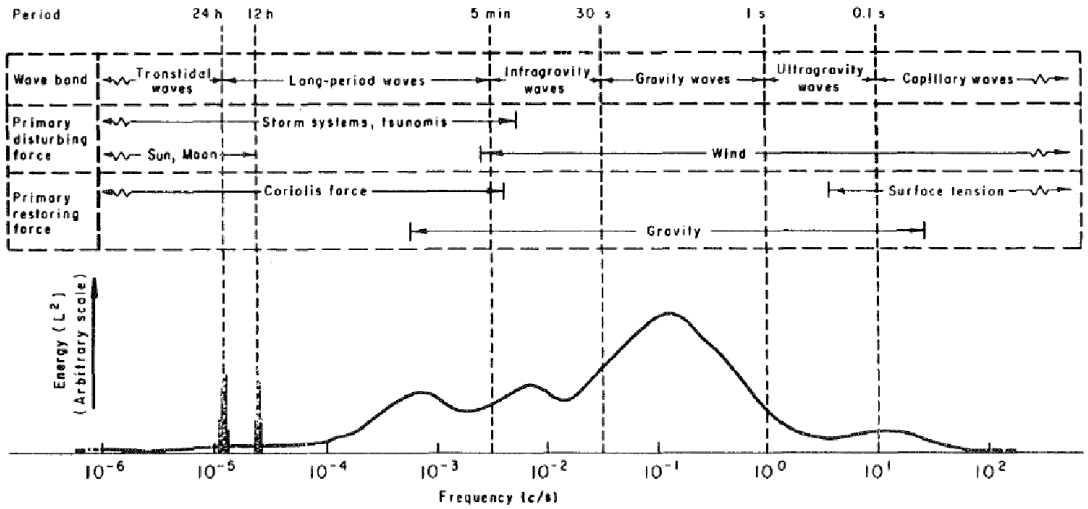

Figure 2.1: *Approximate distribution of ocean surface wave energy illustrating the classification of surface waves.*

Infragravity waves are long waves with low frequencies. The energy in the infragravity band is usually negligible compared to that contained in the incident waves (<1 %). That is why they are generally neglected and filtered. This trend can be reversed when they reach the surf zone in the coast. In these areas, they can cause damages and can be deciding for sedimentary transportation and marine submsersions.

However, they act on the wave field and modify it. It is thus possible to assimilate infragravity waves to the modulating signal, which change the wave field as shown in the following figure 2.2:

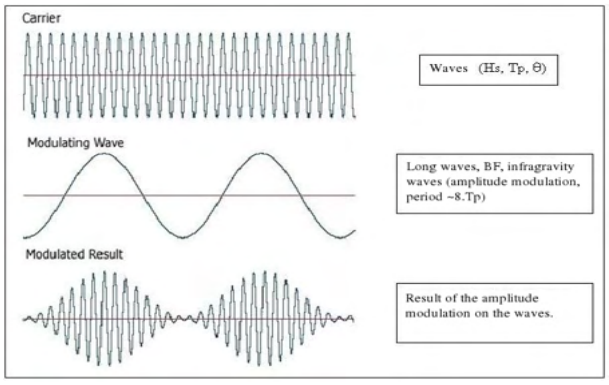

Figure 2.2: *Wave modulation by a long wave, low frequency.*

The resulting signal corresponds to the mixture of the two previous signals and is recorded by the sensors. The infragravity waves and their generation are not well understood.

2.2 Generation Of The Infragravity Waves.

Several hypotheses were put forward to explain the long wave generation.

Initially, although the infragravity waves are generated because of pressure variations and meteorological conditions ([OGS93]) for the long periods, another possible mechanism is that they are liberated during the breaking processes close to the coast ([LS64]) for shorter periods.

Then *Oltman-Shay* showed that the infragravity energy is associated with the incident wind waves ([OH89]). He saw a significant correlation between the fluctuation of wind wave heights (groupiness) and the infragravity motions.

A possible mechanism has been proposed by *Gallagher* ([Gal71]) who showed theorically that certain directional distributions of the incident wave field can resonantly excite edge waves. Edge waves are in that case the waves which are trapped in shallow water by reflection and refraction.

Finally non linear interactions between first-order free waves (sea and swell) of nearly equal frequency is one last possible mechanism of generating infragravity waves bound to groups of higher-frequency waves. Phase coupling between infragravity waves at sea and swell has been observed between eight and eighteen meter depth ([OGS92] and [Her94]).

If one focus on the previous possible mechanism, infragravity waves are forced with wave groups with a high amplification near the coast, propagate at their speed and are 180°out of phase with the shortwave envelope. The probablilities to obtain infragravity waves is high if the wave frequencies are relatively close to each other. The swell contains then the best waves for the formation of the infragravity waves.

Here is an example of infragravity wave generation with two waves that have close frequencies. If one has two monochromatic waves, with frequencies f_1 and f_2, the resulting signal has a frequency of $f_1 + f_2$ and $f_1 - f_2$. However due to the non linearity of the interaction, an infragarvity wave is created and propagates in the same direction as the swell with the group speed. Here is an example of the resulting signal when two signals interact (fig. 2.3 and fig. 2.4):

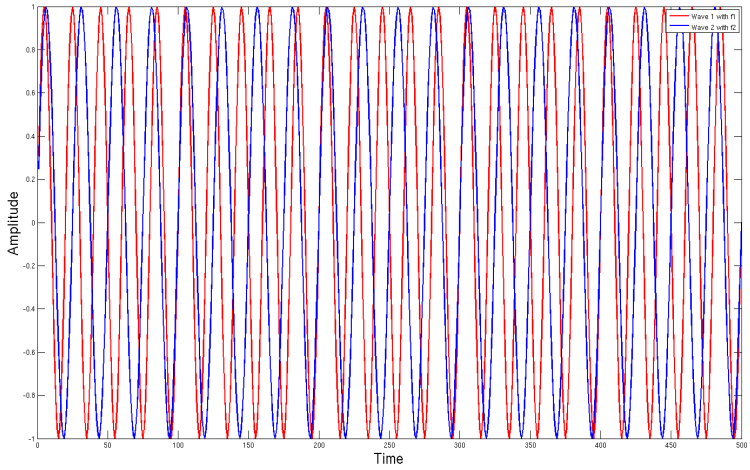

Figure 2.3: *Propagation of two different waves (in red and in blue) with close frequencies.*

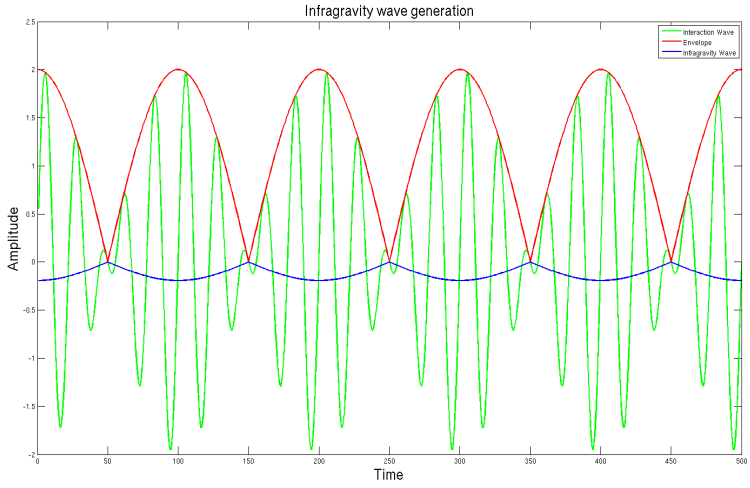

Figure 2.4: *Infragravity wave generated with wave interactions. The envelope is in red, the green signal is the resulting signal of the interaction between the two waves and the blue signal represents the infragravity wave.*

The difference between the two wave frequencies is 0.01 Hz as shown on the figure 2.3. The green wave on the previous figure 2.4 is modulated by the low frequency wave. As the infragravity wave propagates with the wave group, the infragravity spectrum is the same as the envelope spectrum.

When the waves break at the coast, infragravity waves are liberated in free waves. They lose very little energy and therefore can propagate on long distances. The other waves lose

very quickly their energy. Then the infragravity waves propagate onshore in the same direction as the swell ([OGS92]).

2.3 Calculations Of The Infragravity Waves Characteristics.

In this section, one will consider that the infragravity waves are generated by wave interactions. However, only the difference interaction $(f_1 - f_2)$ is taken into account to be sure to get infragravity waves.

The long waves characteristics are calculated when the infragravity band frequency is not recorded by the buoy and is not predicted by the model. This was the case in this study. To characterize them, one needs to know their spectrum and their significative height. Several theoretical methods exist to calculate the infragravity waves. These methods depends on if the wave spectrum is known or if it is the surface elevation.

First if the wave spectrum is known without the long waves frequencies, the infragravity spectrum can be calculated and the long waves caracteristics can be calculated too.

Then if the surface elevation is known, two different methods are possible. The surface elevation for the infragravity waves can be calculated with the Hilbert transform or directly with the coupling coefficient. This coefficient will be explained later. However the calculation with the coefficient is not required for the project so I will give the formula but I did not use it.

2.3.1 Using The Spectrum.

Here one considers that the wave spectrum is known but not the infragravity spectrum. Therefore one needs to calculate it.

A perturbation expansion in weak nonlinearity shows that the interaction between two surface gravity waves with slightly different frequencies f and $f+\Delta f$ excites a forced secondary wave with the difference frequency Δf.

The spectral density of the surface elevation variance for the forced waves is then ([ADP10], [Her94]) (eq. 2.1):

$$E_{forced}(f) = 2 \int\int\int C^2(f + \Delta f, -f, \Delta\theta + \pi) E(f + \Delta f, \theta_1) E(f, \theta_2) df d\theta_1 d\theta_2 \tag{2.1}$$

$E(f, \theta)$ is the spectral density of the wave energy. C is the coupling coefficient for the surface elevation. However this formula is valid for flat bottom and homogeneous spatial conditions. The expression of this coefficient is given by *Okihiro et al.* ([OGS92]):

$$C = -\frac{g k_n k_{n+j} cos(\Delta\theta)}{2\omega_n \omega_{n+j}} - \frac{\omega_n \omega_{n+j}}{2g} + \frac{\omega_n^2 + \omega_{n+j}^2}{2g}$$

$$-\frac{g\omega_j}{(g\Delta k tanh(\Delta kh)-\omega_j^2)\omega_n\omega_{n+j}}\left(\omega_j\left(\left(\frac{\omega_n\omega_{n+j}}{g}\right)^2+k_n+k_{n+j}cos(\Delta\theta)\right)-\frac{1}{2}\left(\frac{\omega_n k_{n+j}^2}{cosh^2(k_{n+j}h)}-\frac{\omega_{n+j}k_n^2}{cosh^2(k_nh)}\right)\right)$$

Then as the long wave spectrum is known, the significative height of the infragravity waves is calculated with the following formula 2.2:

$$H_{IG}=\int E_{2d}(f)df \tag{2.2}$$

The angular spectral density is integrated on the infragravity band frequency.

To calculate the significative infragravity wave height using this method, I adapted the Matlab program of F.Ardhuin which calculates the second order spectrum with an observed spectrum. I used this program to know the second-order spectrum using data from models and from a buoy.

2.3.2 Using The Surface Elevation.

Here one considers that the full wave spectrum is not known, but only the surface elevation. In few articles, *Okihiro, Forristall, Reniers* ([OGS92],[For00], [RVBT02]) give methods to calculate the second order wave spectrum. With the surface elevation, the long waves can be known with the Hilbert transform or with the coupling coefficient given previously. I will present the methods.

At the lowest order, the sea surface elevation is assumed to be a linear sum of free waves (sea and swell) :

$$\eta=\sum_{n=1}^{N}a_n cos(\mathbf{k}_n x-\sigma_n t+\phi_n) \tag{2.3}$$

t is the time, x is the position vector in plane. σ_n, ϕ_n and k_n are respectively the frequency in radian, the phase and the vector wave number of Fourier wave component n. a_n is its amplitude.

Using the Hilbert transform, the surface elevation envelope can be calculated. The exact definition of the Hilbert transform is the following formula 2.4:

$$Hs=(h*\eta)(t)=vp\left\{\int_{-\infty}^{\infty}\eta(\tau)h(t-\tau)d\tau\right\} \tag{2.4}$$

Where $h(t)=\frac{1}{\pi t}$ and η is the signal. vp is the abrevation for Cauchy eigen value. And vp is equal to the following expression 2.5:

$$vp\left\{\int_{-\infty}^{\infty}\eta(\tau)h(t-\tau)d\tau\right\}=\lim_{\epsilon\to 0}\left\{\int_{-\infty}^{\tau-\epsilon}\eta(\tau)h(t-\tau)d\tau+\int_{\tau+\epsilon}^{+\infty}\eta(\tau)h(t-\tau)\right\} \quad (2.5)$$

The Hilbert transform is direclty calculated by Matlab. The following figure shows the result (fig. 2.5):

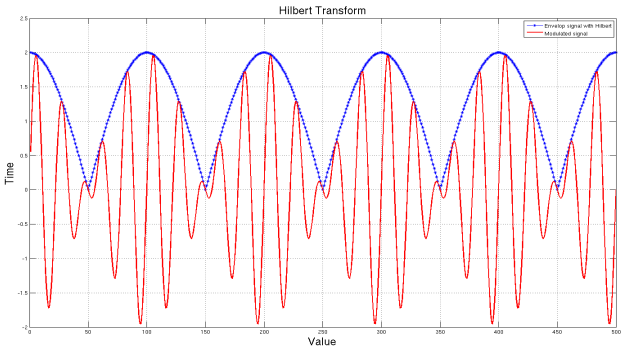

Figure 2.5: *Hilbert transform (in blue) of a signal in red.*

The red signal represents the wave and the blue one is calculated with the Hilbert transform. It corresponds to the envelope signal which is the infragravity wave.

Using the coupling coefficient, *Okihiro and al* gives the second-order (bound wave) sea surface elevation with only the different frequencies retained with the following formula 2.6:

$$\eta_{forced}(\omega_j)=\sum_{n=n_{lo}}^{n_{hi}-j}\sum_{q=1}^{n_\theta}\sum_{r=1}^{n_\theta}C_e A_{n,q}A_{n+j,r}cos(\Delta kxcos\theta_b+\Delta kysin\theta_b-\omega_j t+\Delta\Phi)\delta\omega\delta\theta \quad (2.6)$$

$n_{lo}\delta\omega$ and $n_{hi}\delta\omega$ are the lowest and highest free wave frequencies. $\nu_\theta=\frac{360}{\delta\theta}$ is the number of directional bands at each frequency. The bound wave frequency is $\omega_j=\omega_{n+j}-\omega_n$. h is the depth, A and Φ are the first-order free wave amplitude density and phase.

Then as the surface elevation of the infragravity waves is known, the spectrum can be calculated using a frequency analysis. The caracteristics can be then calculated using the spectrum such as their significative height, frequency. These caracteristics will serve to force the model of L.Leballeur ([Leb08]) (see chapter 3).

2.4 Comparison Of The Methods.

With a more complicated and realistic surface elevation that the signal in the figure 2.5, the Hilbert transform is still satisfying (fig. 2.6). This surface was created with a sum of forty cosinus with a random phase.

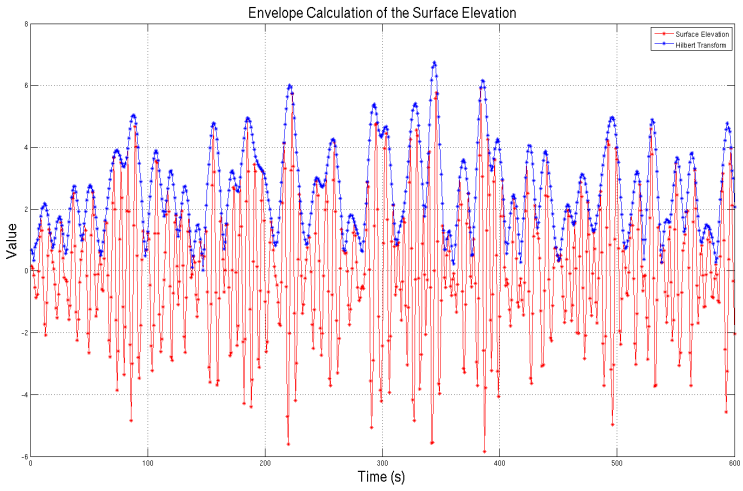

Figure 2.6: *Hilbert transform of a surface elevation. The initial surface elevation is represented in red and the envelope is in blue.*

Then the frequency analysis of the raw signal shows that the spectrum energy is concentrated between 0.1 and 0.2 Hz (fig. 2.7):

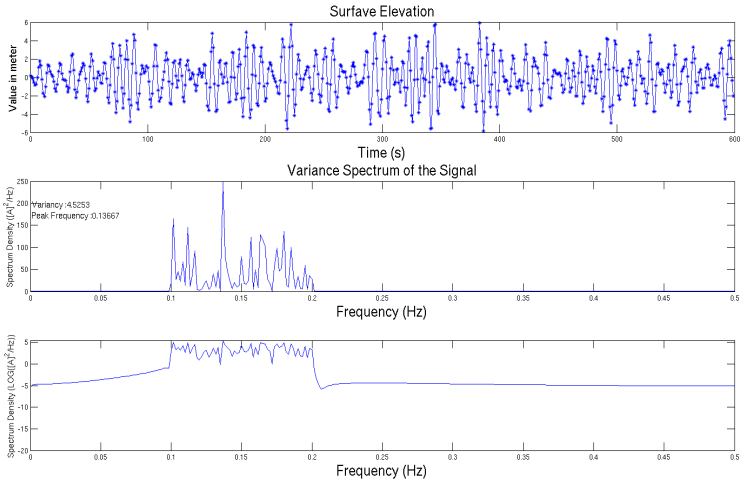

Figure 2.7: *Frequency analysis of a surface elevation.*

Using the Hilbert transform of the same surface elevation, the resulting spectrum frequencies are less than 0.1 Hz (fig. 2.8):

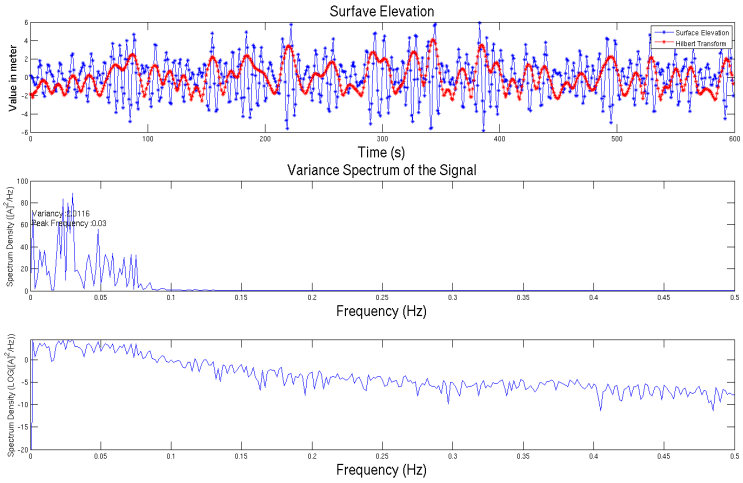

Figure 2.8: *Frequency analysis of the Hilbert transform of a surface elevation (Hilbert transform of the signal in red).*

The infragravity wave frequencies are present. Then when the spectrum of the raw surface elevation is used to calculate the second-order spectrum with the coupling coefficient, the result is the following (fig. 2.9):

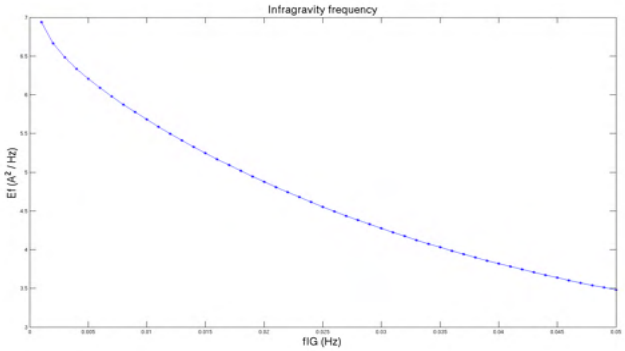

Figure 2.9: *Second-order spectrum calculated with the first order spectrum.*

Using the figures 2.8 and 2.9, the energy is contained in the infragravity frequencies.

2.5 Relation Between Infragravity Waves And 'Seiches' ?

In this project, the main aim is to see the relation between seiches and long waves. First here is a definition of seiche:

What people call “seiches” in french are actually the water level oscillations in basins ,lakes or harbors. These oscillations have a period between one and ten minutes, which depends on the basin form. The seiches can last between few hours and few days after the first impulsion. The waves are standing and they can be considered as the sum of two progessive waves which propagate in two different directions.

Okihiro and al ([OGS93]) have showed that seiches are due to the harbor geometry and are caused by the amplification of waves at the “natural frequencies”. In response to forcing that is broad banded frequency, oscillations within the harbor at these natural frequencies increase significantly in magnitude before the energy input from the exciting source is balanced by losses such as those due to friction, flow separation, boundary absorption, and radiation from the harbor entrance.

To sum up, long waves create seiches in harbors because they coincide with the resonance frequency of the basin. The long wave enters the semi-enclosed space and is trapped. There may then form a standing wave formed by the superposition of the incident wave and the wave reflected from the wall. It can be a problem in harbors for marine activities. For example in the harbor of Groix, because of a seiche, the harbor can be empty and full within few minutes which can create strong currents in the harbor.

However the seiches are often unnoticed due to their low amplitude. The large harbors have generally resonance frequency close to few minutes and the forcing is due to pressure variations of the atmosphere. For smaller harbors, the resonance frequency is less than ten minutes, in a frequency band where wave groups generate an important infragravity signal. The seiche height can sometimes reaches twenty to thirty times the long waves amplitude at the harbor entrance ([OGS93]).

Devaux ([ADP10]) has established a predictive linear relation between the significative height of the seiches and infragravity wave : $Hseiche = 6H_{IG}$. This relation has been established by an empirical method and with tide data from Brest, Port-Tudy and Cherbourg harbors. So as the significative height of the long waves can be predictible, the seiche height can be estimated.

But today, although the seiche height can be predicted, the phenomena is unpredictible.

3

Infragravity Waves Modeling

3.1 Model Used.

To propagate the infragravity waves, I used the code from L.Leballeur ([Leb08]) realized during his last internship at ENSIETA in 2008. This code is a 1D cross-shore model which is composed of three elements:

- A dynamic model of coastal circulation.
- A wave propagation model.
- A coupling of the two previous models.

I first understood the code and checked it worked. Then I adapted it with the desired parameters. I had problems with the dynamic model of coastal circulation which I achieved to solve. Therefore in this chapter, I will present the model and the tests I have done.

Concerning the wave propagation and coupling models, I am going to present them and to give results but the model details are explained in appendices C and D.

In this chpater, the coastal circulation with a forcing by infragravity waves in a flat ground channel will be presented. Then some parameters are going to be tested to see their influence. But at this step, the model did not give the wanted results so I modified it. The modifications were done so that the schema become totally linear.

3.2 Hydrographic Model Of The Mean Circulation.

3.2.1 Model Equations.

The model used is a hydrodynamic model of circulation with the continuity and simplified momentum equations. The system is then the following 3.1:

$$\frac{\partial u}{\partial t} + g\frac{\partial \bar{\eta}}{\partial x} = 0 \tag{3.1a}$$

$$\frac{\partial \bar{\eta}}{\partial t} + \frac{\partial}{\partial x}((h+\bar{\eta})u) = 0 \tag{3.1b}$$

Then the equations 3.1 are discretized on a staggered grid as shown on the following figure 3.1:

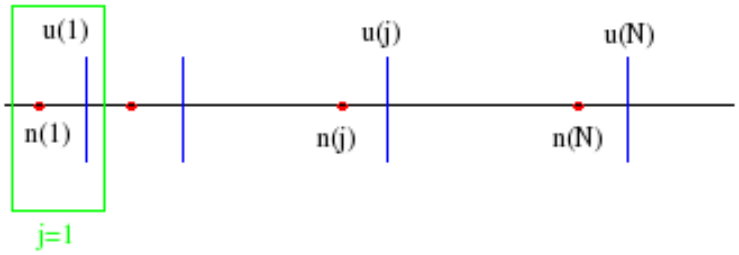

Figure 3.1: *Discretization grid used in the model. j is a grid computing.*

A grid computing is composed of η and u. The variables are not defined in each point of the grid but one point on two alternate. So the continuity equation is applied on η and the momentum equation is applied on u. The discrete variables for the surface elevation η_j are calculated in the center of the intervals whereas the speed u_j and the bathymetry h_j are calculated at the edges. Then the first indice corresponds to the offshore and the indice N correspond to the coast.

Then the schema used is a trapezoidal schema with which you can give a weight to the explicit ($1-\theta_1$ and $1-\theta_2$) and implicit (θ_1 and θ_2) parts of the equation. This schema is neutral and inconditionnally stable. The following equations 3.2 represent the discretization:

$$\eta_j^{n+1} + \theta_1\frac{\Delta t}{\Delta x}\left((hu)_{j+1/2}^{n+1} - (hu)_{j-1/2}^{n+1}\right) = \eta_j^n - (1-\theta_1)\frac{\Delta t}{\Delta x}\left((hu)_{j+1/2}^{n} - (hu)_{j-1/2}^{n}\right) \tag{3.2a}$$

$$u_{j+1/2}^{n+1} + g\theta_2\frac{\Delta t}{\Delta x}\left(\eta_{j+1}^{n+1} - \eta_j^{n+1}\right) = u_{j+1/2}^{n} - g(1-\theta_2)\frac{\Delta t}{\Delta x}\left(\eta_{j+1}^{n} - \eta_j^{n}\right) \tag{3.2b}$$

3.2.2 System To Resolve

With this trapezoidal scheme, the system resolution is done with a tridiagonal linear system. Indeed the equations are coupled which means that u_j^{n+1} is expressed with η_j^{n+1} and η_j^{n+1}. It is the same thing with η_j^{n+1} which is expressed with u_{j+1}^{n+1} and u_j^{n+1}. The second

member is then totally known because all variables at the moment n are known. The unknown vector is the following vector 3.3:

$$X = (u_1^{n+1}, \eta_2^{n+1}, u_2^{n+1}, ..., \eta_j^{n+1}, u_j^{n+1}, ..., \eta_{N-1}^{n+1}, u_{N-1}^{n+1}) \tag{3.3}$$

The term in η_1^{n+1} is not calculated in X because it corresponds to the offshore boundary condition and so is forced. Then with the last line of the matrix, I forced $u_{N-1} = 0$ which means that the boundary condition simulates a wall.

The system has the following form 3.4:

$$\begin{pmatrix} a^{\text{cty}} & b^{\text{cty}} & c^{\text{cty}} & 0 & 0 \\ 0 & a^{\text{qdm}} & b^{\text{qdm}} & c^{\text{qdm}} & 0 \\ \vdots & \ddots & \ddots & \ddots & \ddots \\ 0 & 0 & 0 & \ddots & \ddots \end{pmatrix} \begin{pmatrix} \eta_1 \\ u_1 \\ \eta_2 \\ u_2 \\ \vdots \\ \eta_{N-1} \\ u_{N-1} \end{pmatrix} = \begin{pmatrix} y_1^{\text{cty}} \\ y_1^{\text{qdm}} \\ y_2^{\text{cty}} \\ y_2^{\text{qdm}} \\ \vdots \\ y_{N-1}^{\text{cty}} \\ y_{N-1}^{\text{qdm}} \end{pmatrix} \tag{3.4}$$

The coefficients for the continuity equation are:

$$\begin{cases} a_2(j-1) &= -g\frac{\Delta t}{\Delta x}(h_{j-1} + \frac{\eta_j^n - \eta_{j-1}^n}{2}) \\ b_2(j-1) &= 1 \\ c_2(j-1) &= \frac{\Delta t}{\Delta x}(h_j + \frac{\eta_{j+1}^n - \eta_j^n}{2}) \end{cases} \tag{3.5}$$

The coefficients for the mouvment equation are:

$$\begin{cases} a_2(j-1)+1 &= -g\frac{\Delta t}{\Delta x} \\ b_2(j-1)+1 &= 1 \\ c_2(j-1)+1 &= g\frac{\Delta t}{\Delta x} \end{cases} \tag{3.6}$$

The second member of the system has the following form:

$$\begin{aligned} y_2(j-1) &= \eta_j^n - (1-\theta_1)(c_2(j-1)u_j^n + a_2(j-1)u_{j-1}^n) \\ y_2(j-1)+1 &= u_j^n - (1-\theta_2)(c_2(j-1) + 1\eta_{j+1}^n - c_2(j-1) + 1\eta_j^n \end{aligned} \tag{3.7}$$

Then the system is solved by inverting the matrix 3.4 with the LU method (see appendix A).

3.2.3 Boundary Conditions

The indice $j = 1$ represents the wide sea and the indice N represents the shore. For $j = 1$, which is the wide sea, one only has u in the first computing grid so the boundary condition is needed for η. In this case, η is the forcing wich can be for example the tide. At the end of the grid, in the shore, one ends again with u. Here one considers that the boundary condition is $u_{N-1} = 0$ which means that there is a "wall". Therefore the boudary conditions are used in the momentum equation. Considering the boundary conditions, the coefficients for $j = 1$ and $j = N$ become:

▷ For $j = 1$:

$$\begin{cases} a_2 & = 0 \\ b_2 + 1 & = 1 \\ c_2 & = g\frac{\Delta t}{\Delta x} \end{cases} \tag{3.8}$$

▷ Then for $j = N$ one has:

$$\begin{cases} a_N & = -g\frac{\Delta t}{\Delta x} \\ b_N & = 1 \\ c_N & = 0 \end{cases} \tag{3.9}$$

Now with this model, one forces the system with a tide, an infragravity wave... Moreover some parameters can be added such as the viscosity, friction...

3.2.4 Results With A Tide Forcing

First the forcing used is the tide. The considered channel has a constant bathymetry and a wall is at the end of the channel. The tide period is relatively high therefore the simulation time must be long enough to see free surface oscillations. Here the time simulation is 48 hours. Then the cross-shore distance is 50 km. The results are shown on the following figure 3.2:

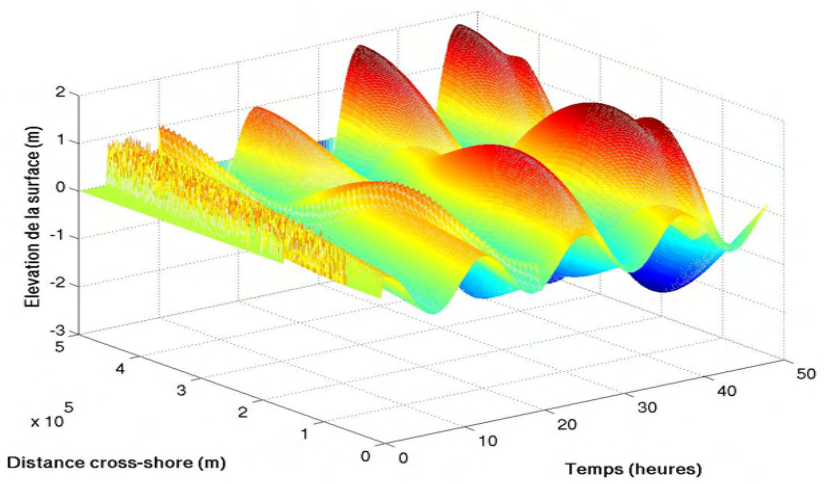

Figure 3.2: *Result of the circulation model after 48 hours. The forcing is a tide forcing. The cross-shore distance is 500 km and the bathymetry is constant. At the coast, a wall keeps all movements.*

The tide is propagating as a sinusoidal wave and reflects at the coast. Therefore the wave will be stationary if the time simulation is increased.

3.2.5 Resuls With Infragravity Waves Forcing

In a second time, the model is forced with an infragravity wave. The cross-shore distance, the simulation time and the bathymetry stay the same. The following figure 3.3 shows the results:

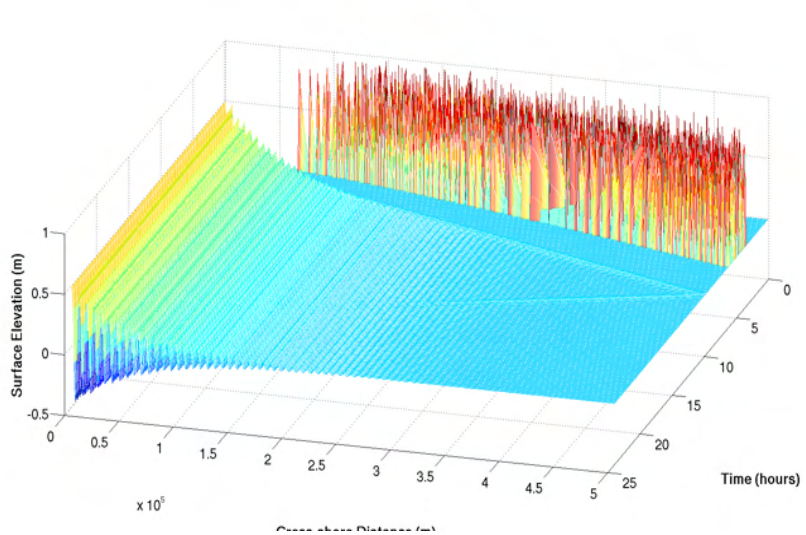

Figure 3.3: *Result of the circulation model with an infragravity wave forcing. The simulation duration is 48 hours, the cross-shore distance is 500 km.*

After 300 km which corresponds to about 120 wavelenghts, the wave is completely attenuated. The noise was a problem in the fortran program and does not have a physical reality. However the infragravity waves have a period of 4 minutes. The speed is $\sqrt{gh}$ with h the depth and $g = 9.81m/s^{-2}$. Here the depth is 20 m so the speed is 14 m/s. To study the propagation, only about 20 wavelengths are sufficient so the cross-shore distance is reduced to 50 km. Then as the period is low, the propagation is studied on one hour. With these parameters the following results are obtained (fig. 3.4):

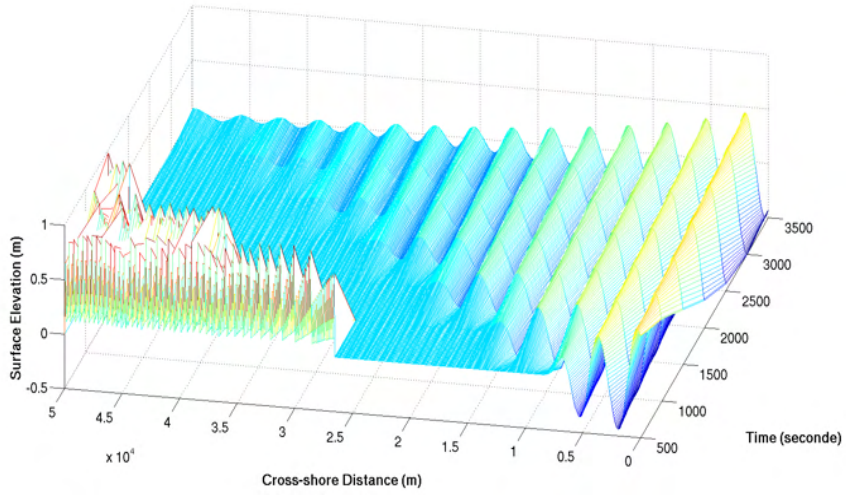

Figure 3.4: *Result of the circulation model with an infragravity wave forcing. The simulation duration is one hour, the cross-shore distance is 50 km.*

No viscuosity or friction were added so the solution is known and is supposed to be a sinusoidal. But here the waves are still completely attenuated which is a problem. This attenuation is due to numerical dissipation of the model. In the following parts, I am going to try to choose the parameters so that the model does not attenue the waves any more.

3.2.6 Influence Of The Parameters.

The parameters which influence the model are :

- dt : time interval.
- $dx = \frac{nbcouche}{width}$: space interval.
- $\theta_{continuity}$ and θ_{qdm}.

The last two figures (fig. 3.3 and fig. 3.4) have $\theta_{continuity} = 1$ and $\theta_{qdm} = 0.5$. In this part, different $\theta_{continuity}$ and θ_{qdm} will be tested.

When $\theta_{continuity}$ and θ_{qdm} are equal to 0.5, the following results are obtained (fig. 3.5). The other parameters are $dx = 50$ and $dt = 5$.

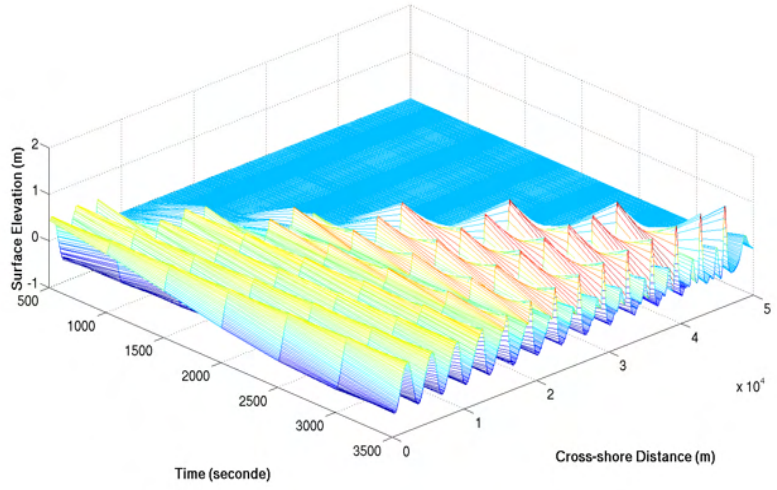

Figure 3.5: *Result of the circulation model with* $\theta_{continuity} = 0.5$ *and* $\theta_{qdm} = 0.5$.

The waves are little amplified and the form changes. $\theta_{continuity}$ and θ_{qdm} have the same effect if there value is interchanged (see appendix B). However the wave is still attenuated. Different values of the parameters were tested (see appendix B). But in all cases, the waves are attenuated. Finally the best values for $\theta_{continuity}$ and θ_{qdm} are 0.5 and 0.54 (fig. 3.6):

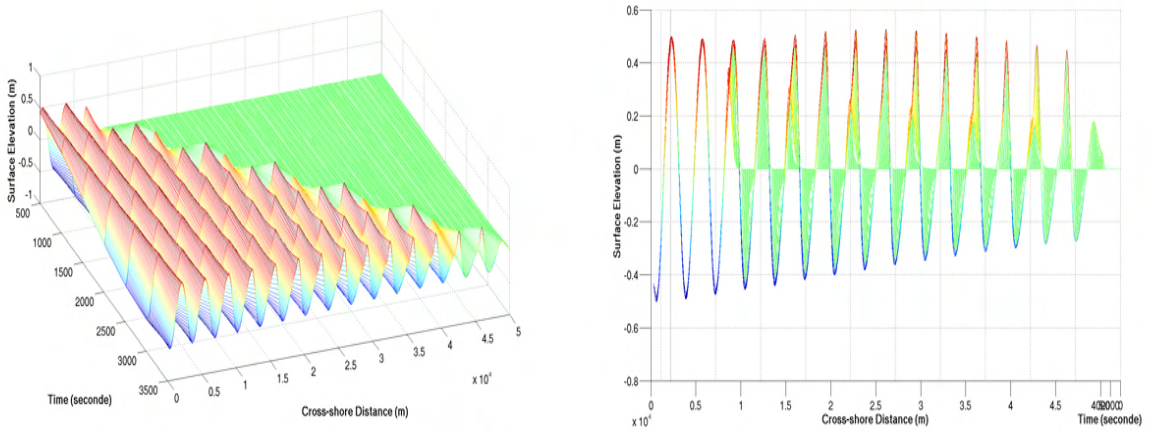

Figure 3.6: *Result of the model with* $\theta_{continuity} = 0.5$ *and* $\theta_{qdm} = 0.56$.

The wave is less attenuated but the surface is oscillating. But the waves do not propagate on a distance long enough.

Therefore in the next paragraph, I have tested the explicit scheme and try to find δt so that the schema is stable in theory.

3.2.7 Explicit Schema.

In this next part, the explicite schema has been tested. To have the explicit scheme, $\theta_{continuity}$ and θ_{qdm} are equal to zero. Then the model needs to be stable. The stability condition is :

$$\sqrt{gh}\frac{dt}{dx} < 1 \tag{3.10}$$

Here the parameters dt and dx are the adjustable parameters so that the stabily condition is respected.

However it gives nothing, with 0, the system exploses, even if in theory the condition is respected. I obtained the same results if we modify dx instead of dt. In some cases, the system does not explose but it implies to have low dt which means that the calculation time can be too high (see appendix B).

3.2.8 Linear System.

In this section, I modified the model to make it completely linear. Indeed a part was non linear. Then one will see whether the waves are still attenuated or not. The initial model was the following 3.11:

$$\frac{\partial u}{\partial t} + g\frac{\partial \bar{\eta}}{\partial x} = 0 \tag{3.11a}$$
$$\frac{\partial \bar{\eta}}{\partial t} + \frac{\partial hu}{\partial x} = 0 \tag{3.11b}$$

h was the total depth which means that $h = depth + \bar{\eta}$. In this case, $depth = constant = H$ and $\bar{\eta} = 0$ so the equations become 3.12:

$$\frac{\partial u}{\partial t} + g\frac{\partial \bar{\eta}}{\partial x} = 0 \tag{3.12a}$$
$$\frac{\partial \bar{\eta}}{\partial t} + H\frac{\partial u}{\partial x} = 0 \tag{3.12b}$$

The previous equations are linear. Then the staggered grid stays the same and also the resolution. The system to solve becomes 3.13:

$$\eta_j^{n+1} + \theta_1 \frac{\Delta t}{\Delta x} H \left(u_{j+1/2}^{n+1} - u_{j-1/2}^{n+1} \right) = \eta_j^n - (1-\theta_1)\frac{\Delta t}{\Delta x} H \left(u_{j+1/2}^n - u_{j-1/2}^n \right) \tag{3.13a}$$
$$u_{j+1/2}^{n+1} + g\theta_2 \frac{\Delta t}{\Delta x} \left(\eta_{j+1}^{n+1} - \eta_j^{n+1} \right) = u_{j+1/2}^n - g(1-\theta_2)\frac{\Delta t}{\Delta x} \left(\eta_{j+1}^n - \eta_j^n \right) \tag{3.13b}$$

With this linearization, I used the same parameters which are:

- $tfin = 3600$ sec (simulation time).
- $dt = 5$ sec (interval time).
- long = 50 km (total cross-shore distance).
- nb couche l = 1000 (number of stitches on the horizontal).
- period = 240 sec (wave period).
- channel with a flat seabed.
- Boundary condition a the end of the channel : a wall.
- $\theta_{qdm} = 0.54$
- $\theta_{continuity} = 0.5$

The schema is unconditionally neutral if $|\lambda|^2 = 1$ which means that the schema is unconditionally stable. λ is the amplification factor. One defines:

$$\begin{cases} u^n_{j+1/2} = \hat{u}^n exp(ikj\Delta x) \\ \eta^n_j = \hat{\eta}^n exp(ikj\Delta x) \end{cases}$$

By replacing the previous forms in the equations one obtains 3.14:

$$\begin{aligned} &\frac{\hat{\eta}^{n+1} - \hat{\eta}^n}{\Delta t} exp(ikj\Delta x) + \frac{\theta_1 H}{\Delta x}\left(\hat{u}^{n+1} exp(ik(j+1/2)\Delta x) - \hat{u}^{n+1} exp(ik(j-1/2)\Delta x)\right) \\ &\qquad + (1-\theta_1)\frac{H}{\Delta x}\left(\hat{u}^n exp(ik(j+1/2)\Delta x) - \hat{u}^n exp(ik(j-1/2)\Delta x)\right) = 0 \\ &\frac{\hat{u}^{n+1} - \hat{u}^n}{\Delta t} exp(ik(j+1/2)\Delta x) + \frac{g\theta_2}{\Delta x}\left(\hat{\eta}^{n+1} exp(ik(j+1)\Delta x) - \hat{\eta}^{n+1} exp(ikj\Delta x)\right) \\ &\qquad + \frac{g(1-\theta_2)}{\Delta x}\left(\hat{\eta}^n exp(ik(j+1)\Delta x) - \hat{\eta}^n exp(ikj\Delta x)\right) = 0 \end{aligned} \quad (3.14)$$

Here $\theta_1 = \theta_{continuity}$ and $\theta_2 = \theta_{qdm}$. The amplification factor λ is equal to :

$$\lambda = \frac{\hat{u}^{n+1}}{\hat{u}^n} = \frac{\hat{\eta}^{n+1}}{\hat{\eta}^n}$$

After simplifications the final equations are the following 3.15:

$$(\lambda - 1)\hat{\eta}^n + \frac{\theta_1 H \Delta t}{\Delta x}\hat{u}^n 2isin(\frac{k\Delta x}{2})(\lambda - 1) + \frac{H\Delta t}{\Delta x}\hat{u}^n 2isin(\frac{k\Delta x}{2}) = 0 \quad (3.15a)$$

$$(\lambda - 1)\hat{u}^n + \frac{g\theta_2 \Delta t}{\Delta x}\hat{\eta}^n 2isin(\frac{k\Delta x}{2})(\lambda - 1) + \frac{g\Delta t}{\Delta x}\hat{\eta}^n 2isin(\frac{k\Delta x}{2}) = 0 \quad (3.15b)$$

Then after having $\hat{\eta}^n$ with the first equation and replacing it into the second equation, it leads to 3.16:

$$(\lambda - 1)^2 + 4\left(\frac{C_g \Delta t}{\Delta x}\right)^2 sin(\frac{k\Delta x}{2})\left(\theta_1\theta_2(\lambda - 1)^2 + (\theta_1 + \theta_2)(\lambda - 1) + 1\right) = 0 \quad (3.16)$$

With $C_g = \sqrt{gH}$ because in this case the water is shallow. Then one defines the factor b as the following :

$$b = \left(\frac{4C_g \Delta t}{\Delta x}\right)^2 sin^2(\frac{k\Delta x}{2})$$

One can notice that $b > 0$. Then b is fixed because the person defines it with the model. The equation to solve is then 3.17:

$$\lambda^2\left(1 + \theta_1\theta_2\frac{b}{4}\right) + \lambda\left(-2 + \frac{b}{4}(\theta_1 + \theta_2 - 2\theta_1\theta_2)\right) + \frac{b}{4}(\theta_1\theta_2 - \theta_1 - \theta_2 + 1) + 1 = 0 \quad (3.17)$$

After simplifications, the final equation to solve is the following 3.18:

$$\lambda^2 - 2\lambda\left(1 - \frac{(\theta_1+\theta_2)/2.b/4}{1+\theta_1\theta_2.b/4}\right) + 1 + \frac{(1-\theta_1-\theta_2)b/4}{1+\theta_1\theta_2.b/4} = 0 \tag{3.18}$$

The equation depends on θ_1 and θ_2. The schema is unconditionally neutral if $|\lambda|^2 = 1$. So one needs to find the solution of the previous equation and to calculate $|\lambda|^2$.

The equation is solved with the method for a second degree polynomial equation. After calculations and simplifications, I obtained$|\lambda|^2$:

$$|\lambda|^2 = 1 + \frac{(1-\theta_1-\theta_2)b/4}{1+\theta_1\theta_2.b/4} \tag{3.19}$$

Therefore : $|\lambda|^2 = 1 <=> \theta_1 + \theta_2 = 1$. This theoretical result is confirmed with the model. However when θ_1 or θ_2 are equal to 0,0.1,1 and 0.9, the model exploses. The following figures 3.7 and 3.8 show some results:

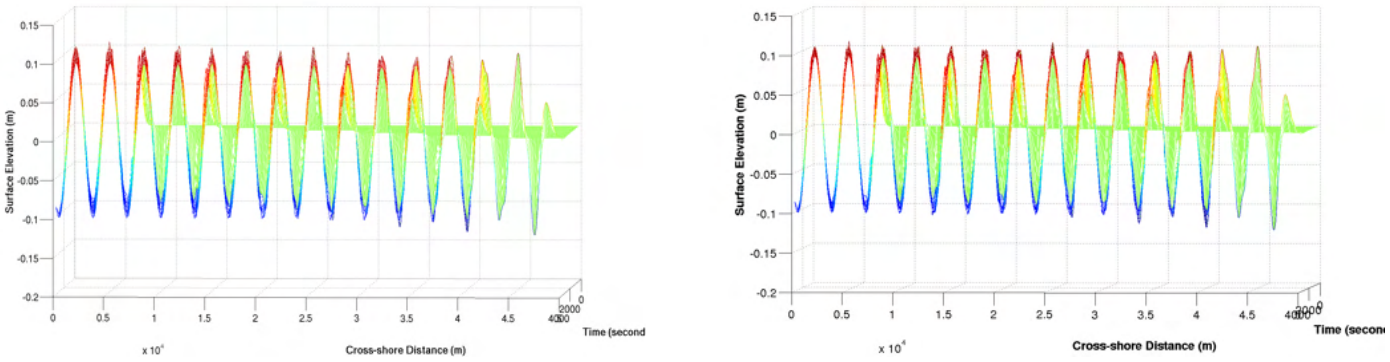

(a) *Surface elevation depending on the cross-shore distance.*θ_1 *and* θ_2 *are equal to 0.5.*

(b) *Surface elevation depending on the cross-shore distance.*$\theta_1 = 0.6$ *and* $\theta_2 = 0.4$.

Figure 3.7: *Results with the linearized circulation model.*

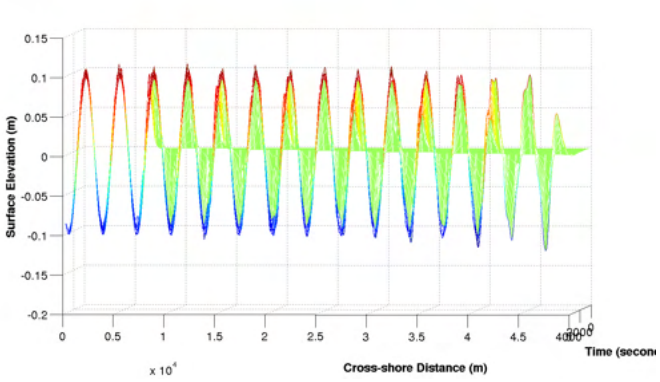

(a) *Surface elevation depending on the cross-shore distance.*$\theta_1 = 0.7$ *and* $\theta_2 = 0.3$.

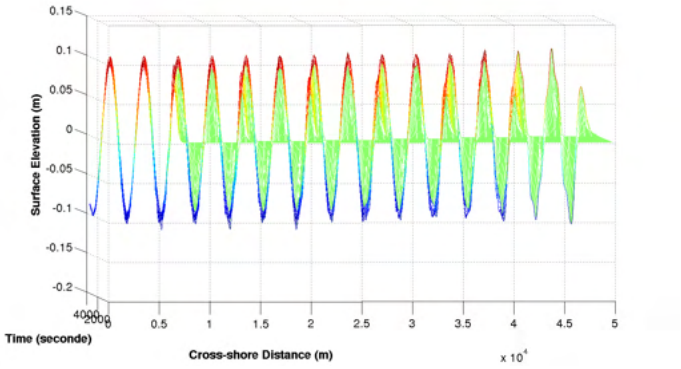

(b) *Surface elevation depending on the cross-shore distance.*$\theta_1 = 0.8$ *and* $\theta_2 = 0.2$.

Figure 3.8: *Results with the linearized circulation model.*

Now with these parameters, the model does not attenuate the waves at all, which is what one expected.

3.3 Wave Propagation Model.

The wave propagation model is based on a energy model which calculates the wave height. The model takes into account the dissipation and the breaking. The equation details are presented in the appendix C. The resolution is made with a Runge-Kutta method (see appendix A).

To test the model, I simulated a flat channel and I forced it with the first significative height H_s offshore. The model evaluates the other heights in each point of the grid: the waves are propagating.

The significant wave height does not change which was expected because here the bathymetry is constant and H_s is modified with the depth.

3.4 Coupling Model.

The model couples the circulation and propagation models. The Phillips formulation is used to solve the total transportation. The movement equation is solved with a non-conservative form. Then the equation is simplified to have only the term in the cross-shore

direction. The equations used are the following 3.20:

$$\frac{\partial U}{\partial t} + U\frac{\partial U}{\partial x} + g\frac{\partial \bar{\eta}}{\partial x} = \frac{-1}{\rho(h+\bar{\eta})}\frac{\partial S_{xx}}{\partial x} - \tau_{bottom} \tag{3.20a}$$

$$\frac{\partial \bar{\eta}}{\partial t} + \frac{\partial}{\partial x}((h+\bar{\eta})u) = 0 \tag{3.20b}$$

The principle is the following :

1. With the wave heights, periods and directions, the wave propagation model calculates the wave number, the energy and wave parameters in each point of the grid. Then the radiation stresses S_{xx_j} can be deduced which are the forcing for the circulation model.
2. The radiation stresses S_{xx_j} and the bottom stresses τ_{bottom} previously calculated can force the wave circulation model. As data output, the free surface elevation is given in each point of the grid.

More details (explainations of S_{xx} and τ_{bottom}) are presented in appendix D.

I only tested the model with a flat channel and with a constant forced S_{xx}. The circulation model was not linear. The next step would be to use the linearized circulation model, to introduce a forcing with infragravity waves calculated theoritecally from a wave field and to parametrize the bottom friction.

3.5 The Next Step.

The next step, after having used the coupling model with long waves, would be to try to model the waves breaking. Thus the seabed will have a hump. During the breaking, infragravity waves would be liberated and propagate freely.

4

Study Case In Groix

In Port-Tudy the seiche has a peak at the frequency 0.0038 Hz (4.4 minutes period), which covers a frequency band of 0.0001 Hz ([Dev09]). In the harbor, the highest seiches happen generally when the wind is South-West, between 210° and 250° ([Fle04]). The seiche can last half a day to two days after the first impulsion and creates strong currents. For example a one meter amplitude seiche causes a current of eight knots in the harbor ([Fle04]). Generally three or four seiches happen in a year. Their amplitude is about seventy centimeters. They usually happen during neap tide and in high or low tide. Here the aim is to see whether a seiche happened or not and in what conditions (swell, wind...).

Concerning the Groix harbor, pressure sensors were placed on the seabed around the island. An atmospheric pressure sensor was placed in the harbor. Moreover, before February 2011, the tide gauge was not numerical. So I obtained the data for the considered period, which almost corresponds to the immersion period of the pressure sensors. However for this period, I did not know whether a seiche happened or not. So the best method was to analyse first the observed tide to try to detect a seiche.

The data from the tide gauge are from the SHOM[1]. The captor is situated in the harbor and the measurements are done with a radar rangefinder (see fig.4.3 and fig. 4.4). The tide is measured every minute between March 23 and April 5 2011. After April 5, the data were recorded every fifteen seconds. Therefore the analysis was cut into two parts. Between March 23 and April 5, I used the files with the data recorded each minute. Then I used the files with the data recorded every fifteen seconds.

Because of a problem with the data transmission, I did not obtain tide data after May 12 2011.

[1]Service Hydrographique et Océanographique de la Marine.

4.1 Harbor Configuration.

The harbor is situated on the North coast of the island, so is relatively well protected from swell and wind. Indeed in this region, most of the time the wind does not come from the north. The following photos (fig. 4.1 and fig. 4.2) show satellite views of the harbor and its orientation :

Figure 4.1: *Harbor location in the South of Lorient (on the top photo) and its orientation (on the down photo).*

Figure 4.2: *Port-Tudy in Groix.*

The west dyke protects the harbor from the west swell, and the continental coast protects

the harbor if the swell comes from the east and north. However, the wind does not often comes from the north. The wind and swell are most of the time in the directions south east-south and west-south. But the swell is diffracted and turns around the island to go into the harbor. Then the swell is attenuated but not the long waves. So in the harbor, in theory the long waves are present and must be seen by the tide gauge in addition to the tide. Indeed the well stilling used by the SHOM filters the swell.

The tide gauge location is indicated with a red cross in the figure 4.2. At this place, the tide gauge does not record the swell. The following figures 4.3 and 4.4 show the tide gauge location in the harbor and its installation.

Figure 4.3: *Tide gauge installation in Groix harbor. Tide gauge hut (on the left photo) and well stilling (on the right photo).*

Figure 4.4: *Radar rangefinder in Groix (on the bottom left corner of the photo).*

4.2 Seiche Detection.

In this case, the interesting period corresponds to the time recording period of the pressure sensors. Indeed if a seiche happens during that period, one will be able to study the waves outside the harbor.

As I previously wrote, first I had tide data where the measurements were preformed every minute between March 23 and May 12 2011. Then I obtained tide data which were recorded every fifteen seconds between April 5 and May 12 2011. Therefore I used the data recorded every minute between March 23 and April 5 2011 and then I used the data recorded every fifteen seconds.

The method that I used to detect a seiche is described in appendix E.

4.2.1 Seiche Detection Using Data Recorded Every Minute.

The following figure 4.5 shows the observed tide between March 23 and April 5 2011 in the harbor :

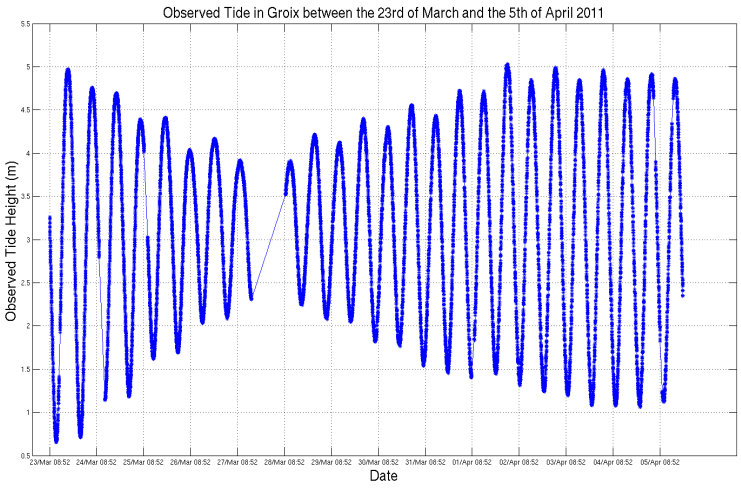

Figure 4.5: *Observed tide in Groix between March 23 and April 5 2011. The data were recorded every minute.*

The file was cut between March 27 and March 28 2011 because of a too long time interval. The following figure 4.6 shows an example of the observed tide in comparison with the predicted tide. The other figures are presented in appendix F.

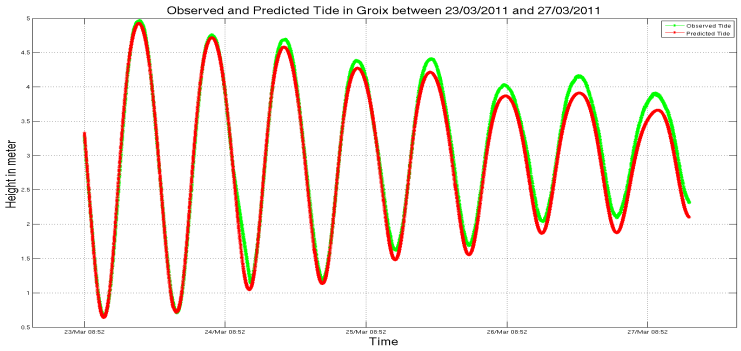

Figure 4.6: *Observed (in green) and predicted (in red) tides in Groix between March 23 and March 27 2011.*

The difference between the observed and predicted tides is less than twenty centimeters. So no seiche happened. The following figure 4.7 shows an example of this difference :

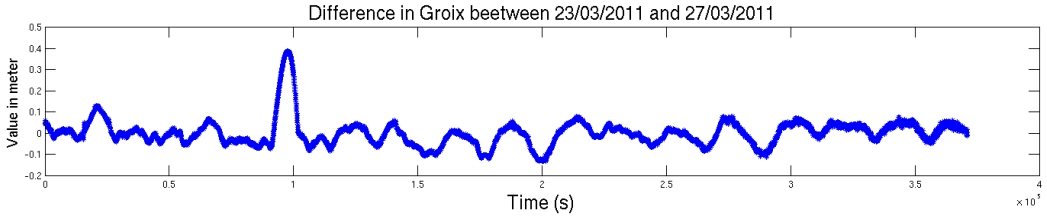

Figure 4.7: *Difference between observed and predicted tides in Groix between March 23 and March 27 2011.*

On the previous figure, the peak amplitude is due to the interpolation of the observed tide. At the end, one can not be sure that a seiche happened during that period.

4.2.2 Seiche Detection Using Data Recorded Every Fifteen Seconds.

I used the same method as previously (see appendix E). Between April 5 and May 12 2011, I detected no significant seiche at all. The files have to be cut because of too long time intervals. The following figure 4.8 shows an example of the the difference between the observed and predicted tides between April 5 and April 20 2011. The oscillations that one can sometimes observe are not high enough and last not long enough to be sure that is a seiche.

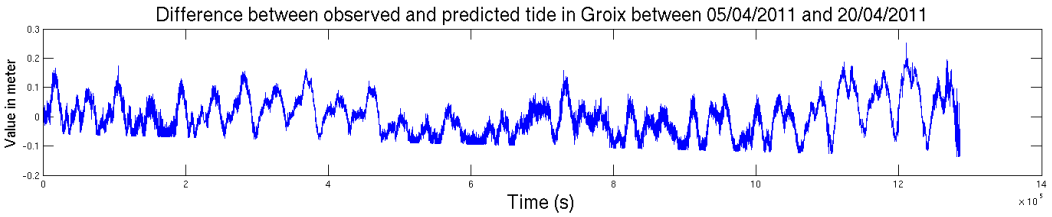

Figure 4.8: *Difference between observed and predicted tides in Groix between April 5 and April 20 2011. The data were recorded fifteen seconds.*

But the infragravity waves inside and outside the harbor can be still studied to be compared. Indeed they were recorded by the tide gauge.

4.3 Frequency Analysis Using One Hour Of Data.

In this part, the observed tide inside the harbor will be studied to detect the infragravity frequencies and to see their time evolution. A frequency analysis is realized using one hour of data to reduce the tide. Here are an example of the results of the frequency analysis (fig. 4.9):

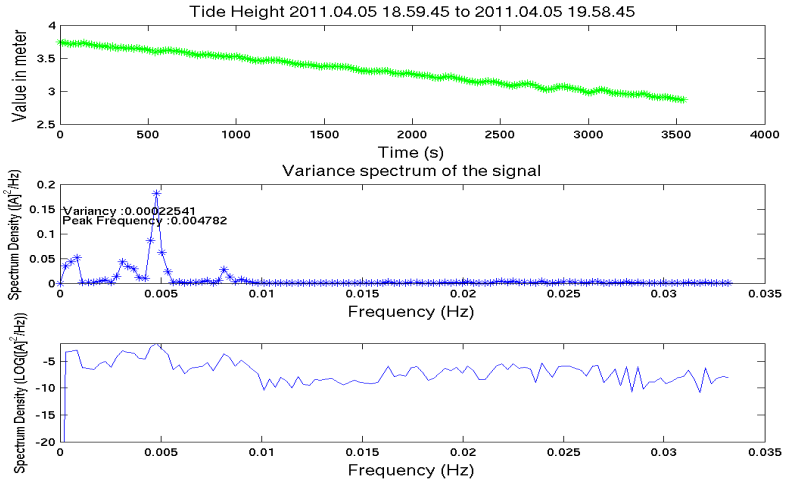

Figure 4.9: *Results of the frequency analysis of the tide signal in Groix April 5 between 6.59 pm and 7.58 pm. The data were recorded every fifteen seconds.*

The peak amplitude is at the frequency $4.7.10^{-3}$ Hz which corresponds to a period of around four minutes. This frequency belongs to the long waves.

The following figures 4.10 shows an example of the time spectrum evolution. The infragravity frequencies are always present in the harbor. But other lower frequencies are observed. They are due to the weather conditions.

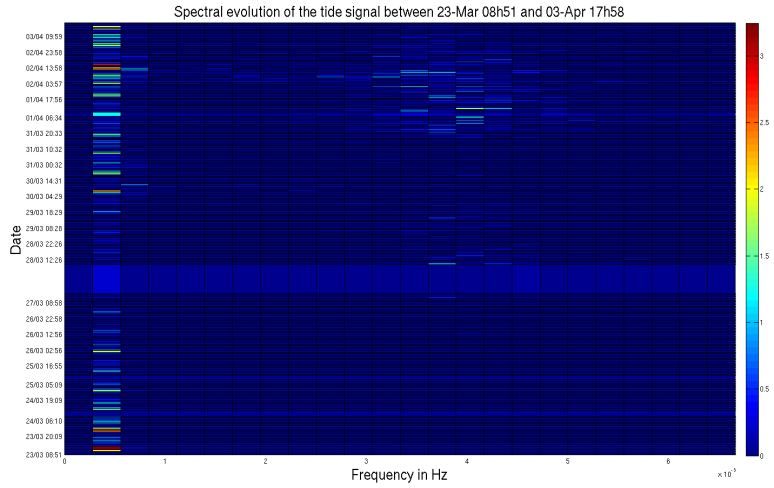

Figure 4.10: *Spectral evolution between March 23 and April 3 2011 in Groix. The data were recorded every minute.*

The long waves energy is lower than the other waves energy. The next step is to study the infragravity waves outside the harbor, with the pressure sensors and the model predictions.

4.4 Pressure Sensors.

In this section, I am going to present the location and installation of the pressure sensors.

The pressure sensors were located around Groix between February 24 and June 8 2011. The following map illustrates their location (fig. 4.11) :

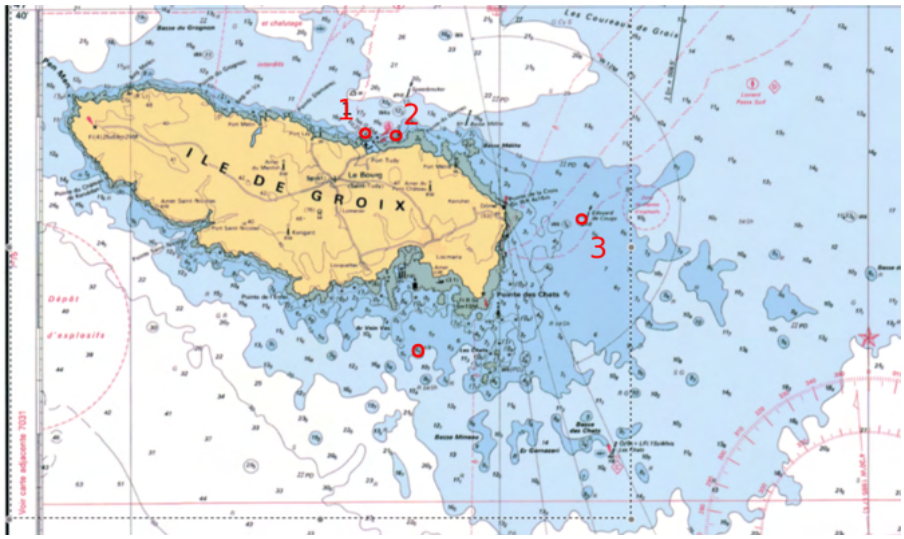

Figure 4.11: *Pressure sensors positions around Groix.*

On the last point situated in the south of Groix, no sensor was placed because of the swell that day. The sensors were protected by a table. Here is a schema of the assembly (fig. 4.12), a photo of the equipment used and the sensor on the bottom (fig 4.13) :

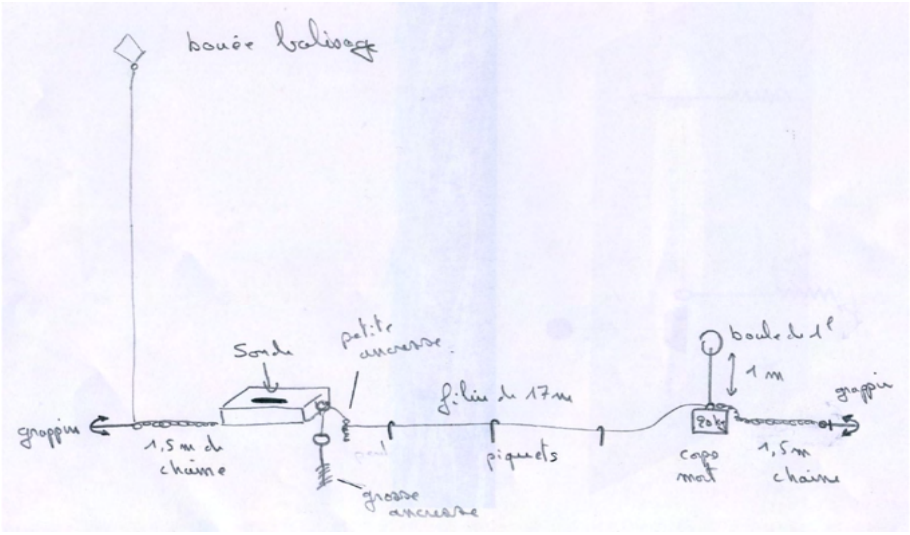

Figure 4.12: *Schema of the pressure sensor assembly located around Groix.*

Figure 4.13: *Equipment used in the assembly (on the left photo) and sensor on the seabed (on the right photo).*

4.5 Long Waves Inside And Outside The Harbor.

With the island of Groix and the rising bottom, the swell is refracted. The waves go each side of Groix and thus have a deviated trajectory. Then they interact in the basin of "Courreaux de Groix" and create infragravity waves.

In this case, I use the spectrum from the tide signal to calculate the significative long waves height inside the harbor (the calculation is explained in appendix E) and the sepctrums from the pressure sensors and WAVEWATCH III model to calculate the significative height of the long waves outside the harbor. As I had observations outside the harbor with the pressure sensors, I did not use the model. The nearest buoy was in Oléron, which is too far away from Groix. So I could not use observations from a buoy.

As the data has not been recorded on the same period, I studied the long waves on the common periods.

I compared the significative long waves height inside and outside the harbor. The significative height inside the harbor is calculated with the spectrum from the tide signal and outside the harbor I used the pressure sensor data. The method is described in appendix E. The following figure 4.14 shows the results between March 23 and April 5 2011 :

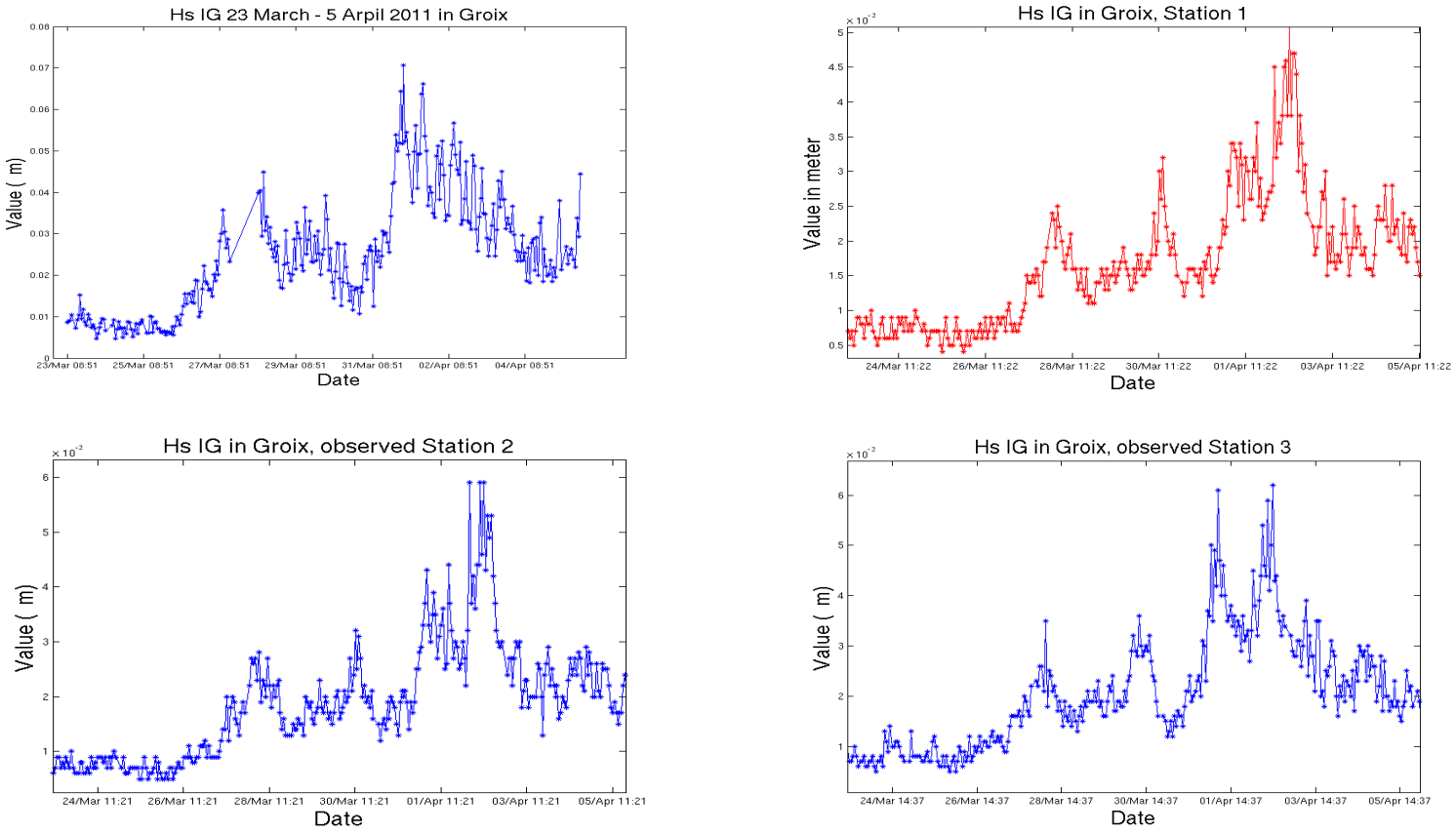

Figure 4.14: *Significative height of the long waves calculated in the harbor with the tide signal (on the top left figure) and calculated with significative height outisde the harbor calculated with the pressure sensors (on the down figures) between March 23 and April 5 2011.*

The correlation coefficient is 0.8. The infragravity waves are amplified by a factor of approximately ten inside the harbor. The other results are presented in appendix F.

When I use the spectrums, I obtained the following figures 4.15, 4.16, 4.17 and 4.18 of the full and infragravity spectrums for the same period, which is between March 23 and April 1 2011 :

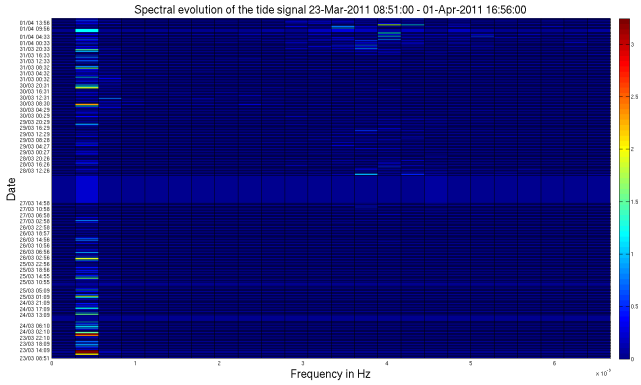

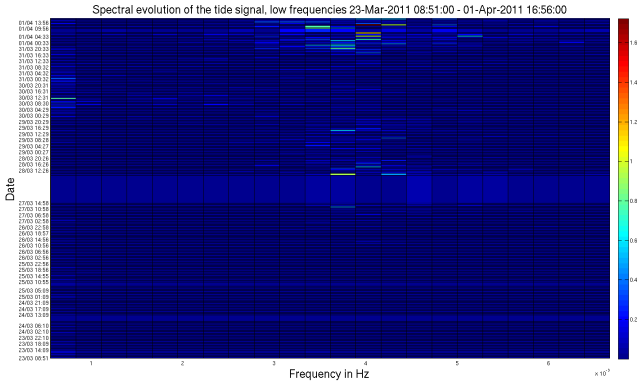

Figure 4.15: *Full spectrum evolution (on the left figure) and infragravity spectrum (on the right figure) calculated inside the harbor using tide data between March 23 and April 1 2011.*

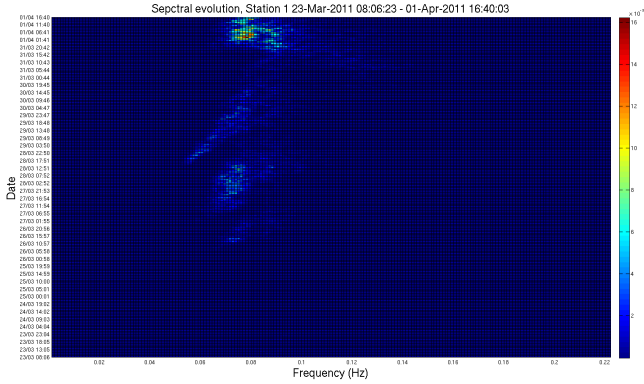

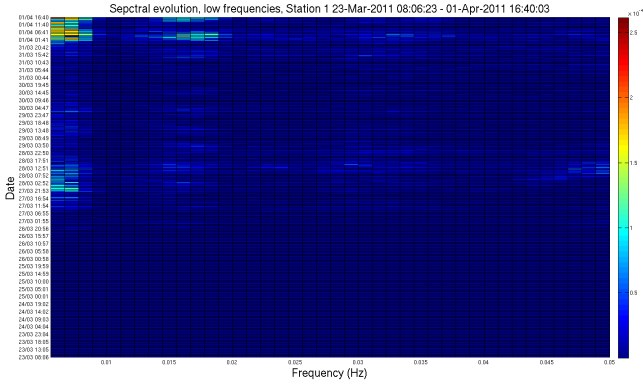

Figure 4.16: *Full spectrum evolution (on the left figure) and infragravity spectrum (on the right figure) calculated outside the harbor using pressure data for Station 1 between March 23 and April 1 2011.*

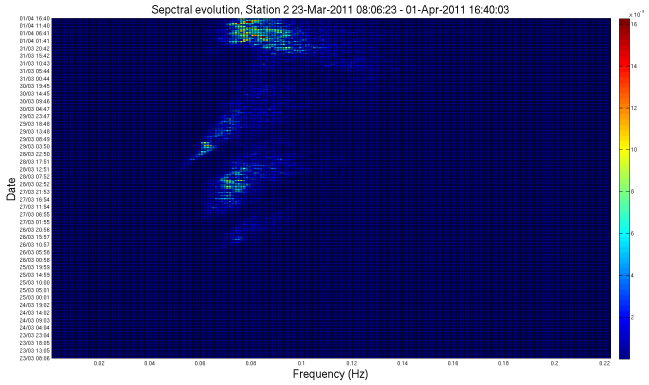

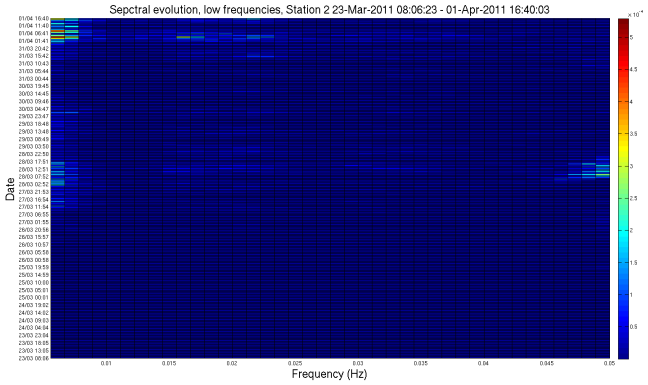

Figure 4.17: *Full spectrum evolution (on the left figure) and infragravity spectrum (on the right figure) calculated outside the harbor using pressure data for Station 2 between March 23 and April 1 2011.*

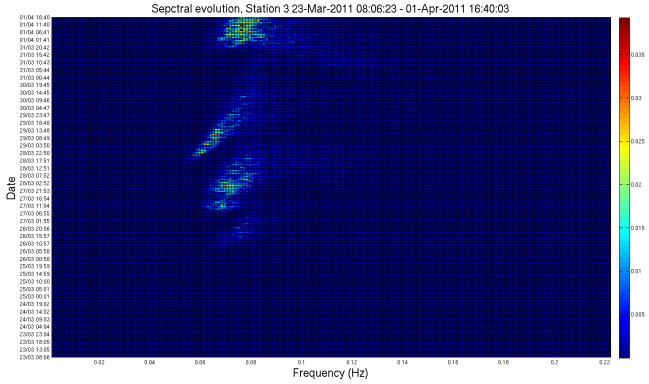

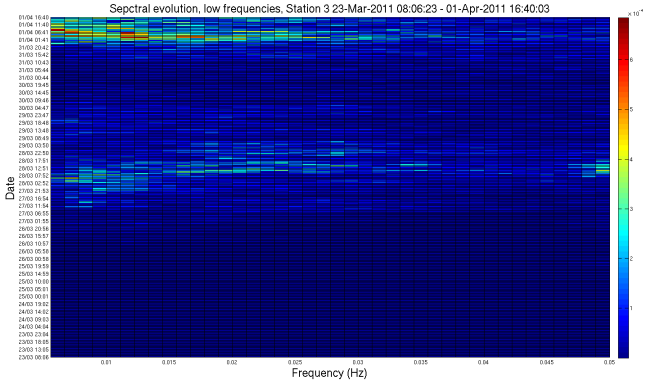

Figure 4.18: *Full spectrum evolution (on the left figure) and infragravity spectrum (on the right figure) calculated outside the harbor using pressure data for Station 3 between March 23 and April 1 2011.*

The long waves outside the harbor are present inside the harbor. More the swell frequency is low, more easily are the long waves created and higher is their energy. But here other frequencies due to weather conditions are also present. Indeed in the basin "Coureaux de Groix" outside the harbor, atmospheric pressure variations exist. These varaitions create a wave which propagate in the entire basin and inside the harbor. The other results are presented in appendix F.

5

Study Case In Royan

Concerning the Royan harbor, I obtained the tide gauge data for the last three years. They come from MEDDTL/DDTM17/SPC-Littoral Atlantique and are avaible on the website of reference networks of tide gauge obsertations (REFMAR)[1].But it would have been too long to treat all data. As the aim is to study a seiche, I did not study the all data but only when a seiche happened. Thus a seiche happened this year in February 2011, between the 15 and the 16. This seiche has caused strong currents in the harbor. About twenty boats have been damaged and sixty meters of a pontoon has been torn. The pontoon at the harbor entrance was pulled out. The swell outside was eight meters high. However the tidal coefficient was not very large.[2] So I only studied this period.

5.1 Harbor Configuration.

The harbor is situated on the Atlantic coast, at the mouth of the Gironde. The following photos (fig. 5.1 and fig. 5.2) show satellite views of the harbor and its orientation :

[1] refmar.shom.fr
[2] Sud Ouest, 17th of February 2011.

Figure 5.1: *Harbor location at the mouth of the Gironde (on the top photo) and its orientation (on the down photo).*

Figure 5.2: *Royan harbor.*

The harbor is quite well protected from the swell and the wind. The west dyke attenuates but also diffracts the swell. It turns around the end of the dyke. The swell is quickly attenuated into the harbor while the long waves propagates. Indeed the swell loses energy while propagating whereas the infragravity waves lose a little energy. Moreover the harbor entrance is near a beach, which amplifies and refracts the long waves. The tide gauge location is indicated with a red cross on the figure 5.2. At this place, the tide gauge is protected. So in theory, only the tide and the long waves will be seen by the tide gauge. The other small

waves created by wind are filtered by the well stilling. Therefore one can assume that one of the infragravity frequencies is the harbor resonance frequency and these long waves come from outside.

5.2 Seiche Detection.

It seems that the seiche which happened in February 2011 was caused by the infragravity waves outside the harbor. The seiche can be seen with the observed tide. The seiche happened during the flow and is not repeated at the next flow. The phenomenon lasts few hours and has an amplitude of one meter. The following figure 5.3 shows the observed and predicted tides :

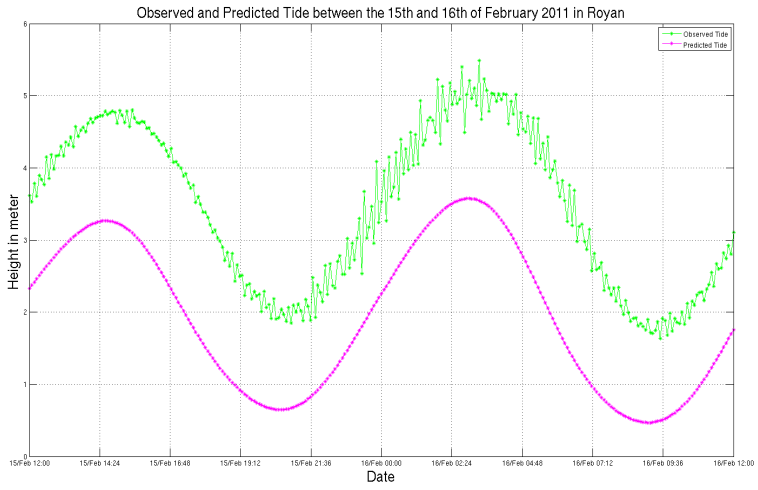

Figure 5.3: *Observed (in green) and predicted (in pink) tides in Royan between February 15 and February 16 2011.*

The predicted and observed tides have a constant difference. Maybe the tide gauge has a calibration problem. However, it is not a problem for the frequency analysis. The difference between the observed and predicted tides is :

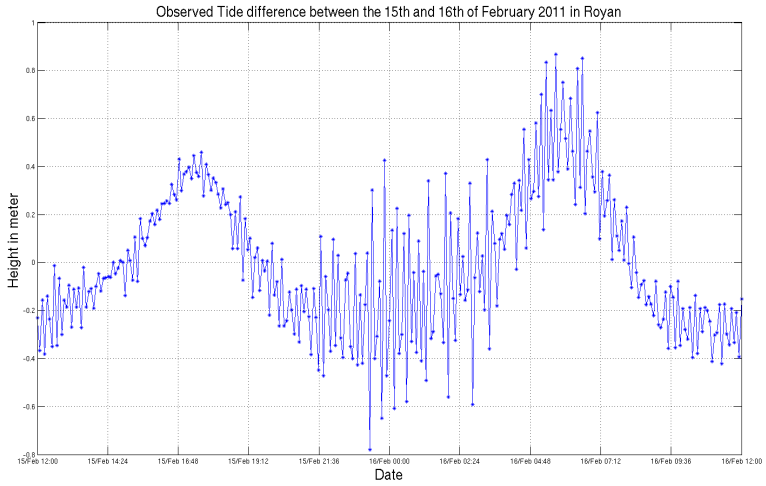

Figure 5.4: *Difference between the observed and predicted tides in Royan between February 15 and February 16 2011.*

On this figure, the seiche amplitude has a maximum of one meter. But a residual tidal signal remains. Using a frequency analysis, I obtained the following spectrum :

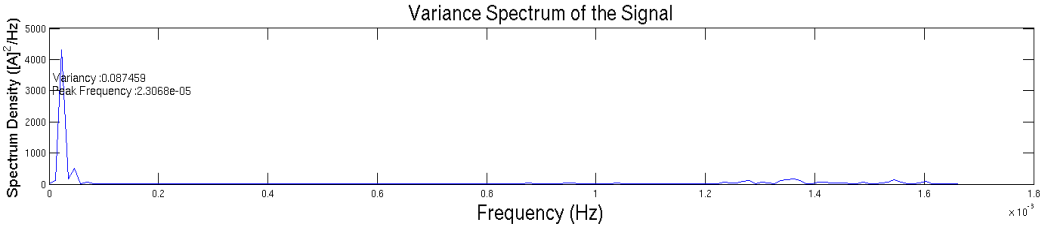

Figure 5.5: *Frequency analysis of the difference between the observed and predicted tides between February 15 and February 16 2011 in Royan.*

The peak frequency is at $2.3.10^{-5}$ Hz which corresponds to the tidal signal. However, others frequencies can be seen around $1.4.10^{-3}$ Hz which correspond to infragravity waves. The following figure (fig. 5.6) shows these frequencies:

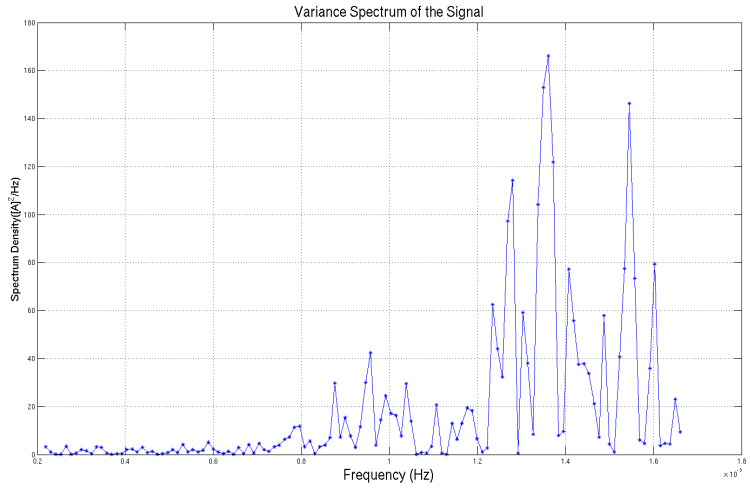

Figure 5.6: *Frequency analysis of the difference between the observed and predicted tides between the February 15 and February 16 2011 in Royan. The frequencies observed here are* $0.2.10^{-3}$ *to* $1.8.10^{-3}$ *Hz.*

Few peaks can be detected. The main peak is about $1.3.10^{-3}$ Hz which is a period of twelve minutes. The two other peaks have $1.5.10^{-3}$ Hz and $1.2.10^{-3}$ Hz which are periods of about ten and thirteen minutes.

The same results were observed by the SHOM[3] on the website "refmar" [4]:

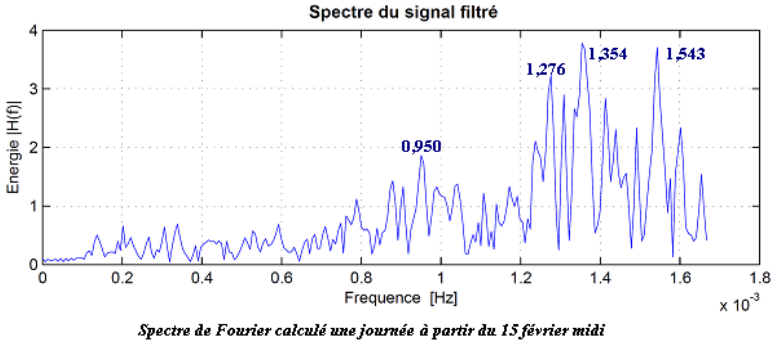

Figure 5.7: *Frequency analysis in Royan, made by the SHOM. The studied period is between the February 15 and February 16 2011.*

These frequencies are the seiche frequencies and belong to the infragravity frequencies. In the harbor, only the tide and the long waves are present. Indeed the frequency analysis on the tide signal using one hour of data, before and after the seiche, shows the long waves.

[3]Service Hydrographique et Océanographique de la Marine

[4]http://refmar.shom.fr/spip.php?article233

5.3 Frequency Analysis Using One Hour Of Data.

With the frequency analysis using one hour of data, the spectrum evolution can be monitored during the seiche. The following figure 5.8 shows a result of the analysis using one hour data during the seiche :

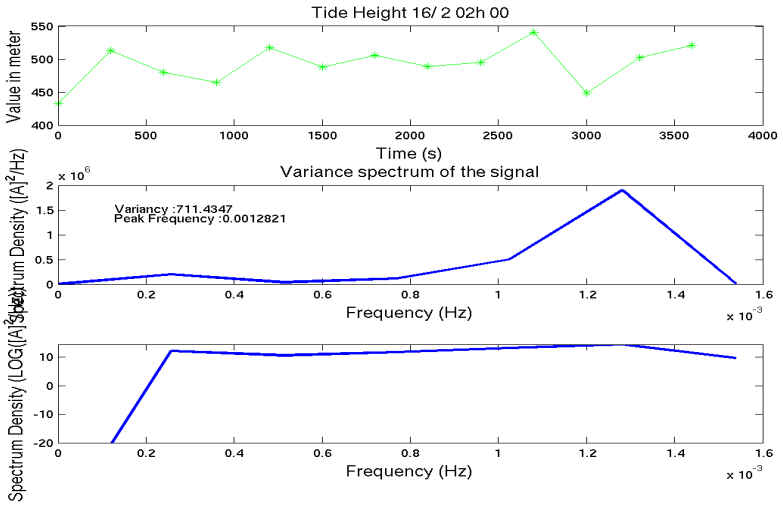

Figure 5.8: *Frequency analysis in Royan using one hour data, February 16 2011, during the seiche in the harbor.*

The frequency peak observed is the seiche frequency. During the storm, the spectrum evolution is (fig. 5.9) :

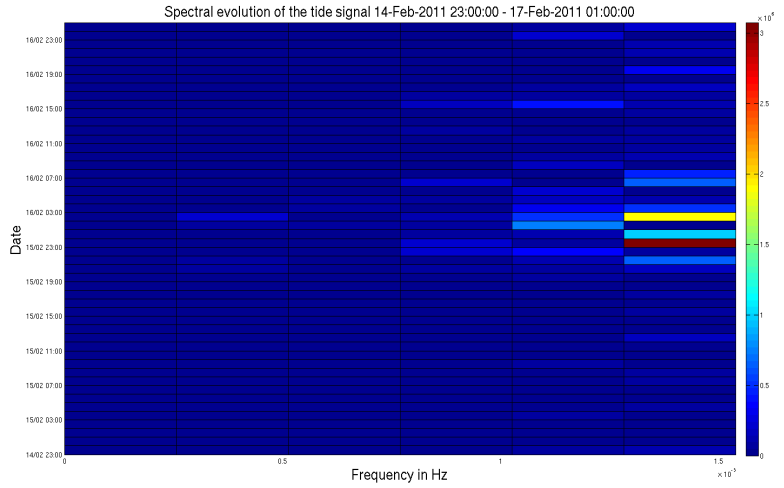

Figure 5.9: *Spectrum evolution between February 15 and February 17 2011 in Royan.*

The seiche corresponds to the energy peak. The infragravity frequencies are always present in the harbor. But their energy is less high than their energy during the storm. However, in this study some infragravity frequencies are missing because the measurements were done every five minutes.

As the seiche frequency is the resonance frequency of the basin, the long waves are responsible for the seiches. However, sometimes the infragravity frequencies in the harbor are almost the same as the resonance frequency but no seiche happens. Therefore the long waves amplitude outside the harbor also influences the phenomenon.

5.4 Long Waves Inside And Outside The Harbor.

Near Royan, the closest buoy is Oléron (see appendix G), which is quite away from the harbor. Indeed the figures in the appendix G shows a correlation coefficient of 0.58 between the model in Royan and the buoy observations, and a correlation coefficient of 0.65 between the observations in the harbor and at the buoy. Moreover a shelf (fig. 5.1) is onshore near the harbor. This shelf filters the waves because they can break on it (see appendix G). However the long waves are not filtered. But the WAVEWATCH III model calculates the significative height on a point which is near Royan harbor and an other point is Oléron. Therefore if the comparison between the observations and the model are stisfying in Oléron, I will use the model in Royan to predict the significative long waves height outside the harbor. Then I will make a comparison between the significative height inside and outside the harbor for the infragravity waves.

5.4.1 Comparison Between The Model And The Buoy Observations In Oléron.

The following figure 5.10 shows the significative long waves height foreseen by the model and observed with the buoy in Oléron. As the model and the buoy did not have the band frequency, I used the method explained in 2 to calculate the long waves spectrum and then their significative height. The common period is between January and February 2011.

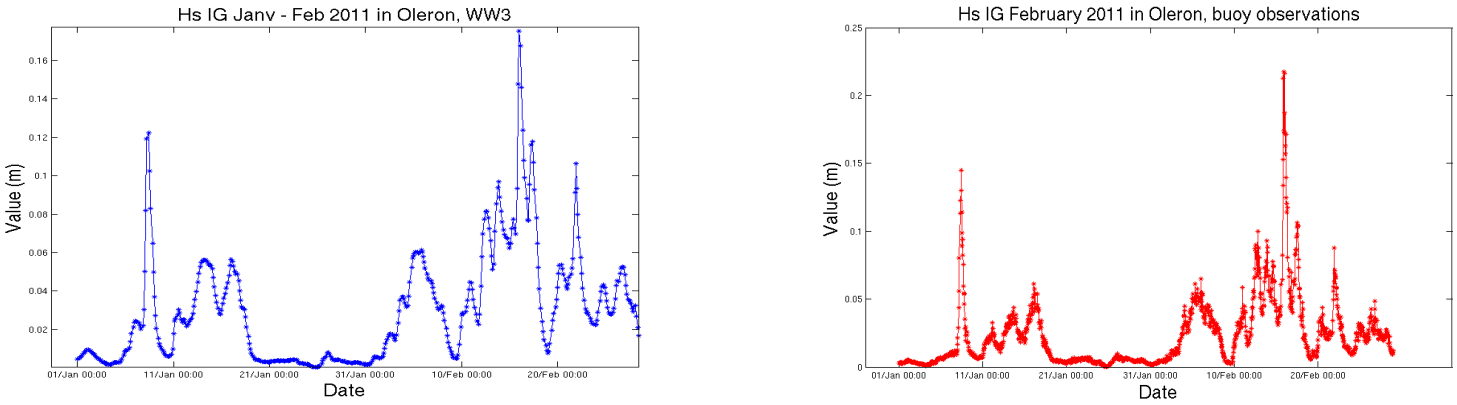

Figure 5.10: *Significative long waves height calculated with WAVEWATCH III model (on the left figure) and observed with a buoy (on the right figure) in Oléron. The comparison is made between January and February 2011.*

The correlation coefficient is 0.9. The high amplitude peak correponds to the seiche which happened in Royan harbor. The model is quite realistic and gives satisfying estimations of the significative infragravity waves height. Therefore I will use the model predictions for Royan to compare the significative long waves height inside and ouuside the harbor.

5.4.2 Comparison Between The Model And The Tide In Royan.

I compared the significative long waves height inside and outside the harbor. The significative height inside the harbor is calculated with the spectrum from the tide signal as explained in appendix E. The following figure 5.11 shows the significative height calculated inside the harbor and the outside the harbor with the WAVEWATCH III model :

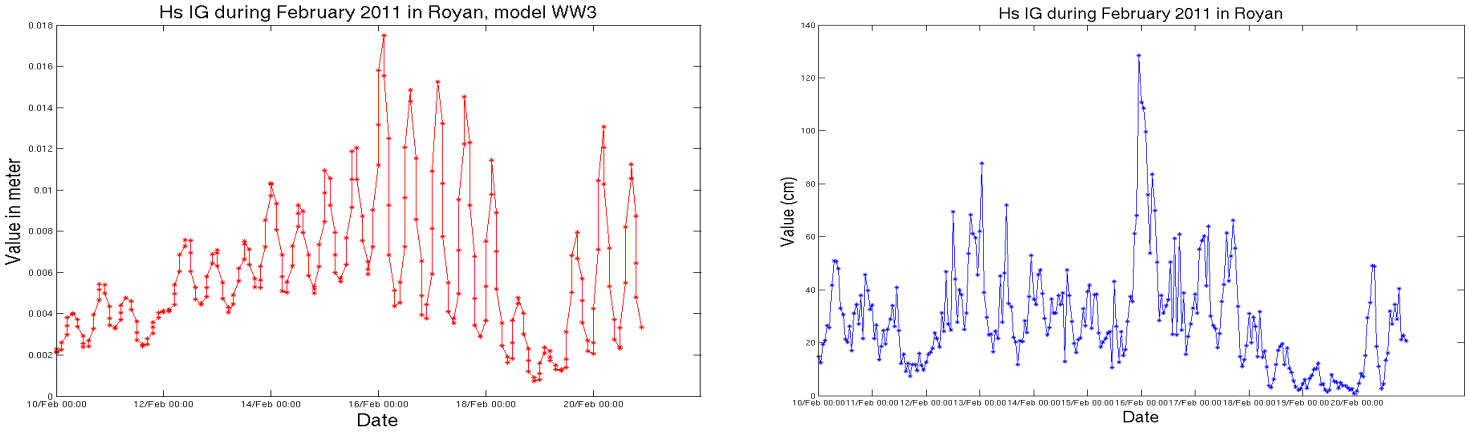

Figure 5.11: *Significative infragravity waves height calculated outside the harbor with the WAVEWATCH III model (on the left figure) and the significative height calculated inside the harbor from the tide gauge data (on the right figure). The period is between February 10 and February 20 2011.*

The significative height was calculated each hour. A residual tidal signal remains or the tide may modulate the infragravity signal. The seiche corresponds to the highest peak on the right figure. In the harbor the long waves are amplified. On the following figure, the significative long waves height observed inside the harbor and calculated with WAVEWATCH 3 are plotted (fig. 5.12) :

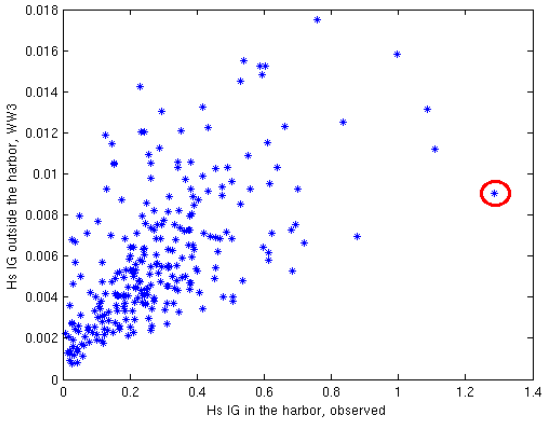

Figure 5.12: *Significative infragravity waves height calculated outside the harbor in comparison with the observed significative height inside the harbor. Values in meter.*

The correlation coefficient is 0.6. The red circle corresponds to the seiche observed February 16 2011. The long waves are amplified in the harbar by a factor of appoximately ten.

When I use the spectrums, I obtained the following figures 5.13 and 5.14:

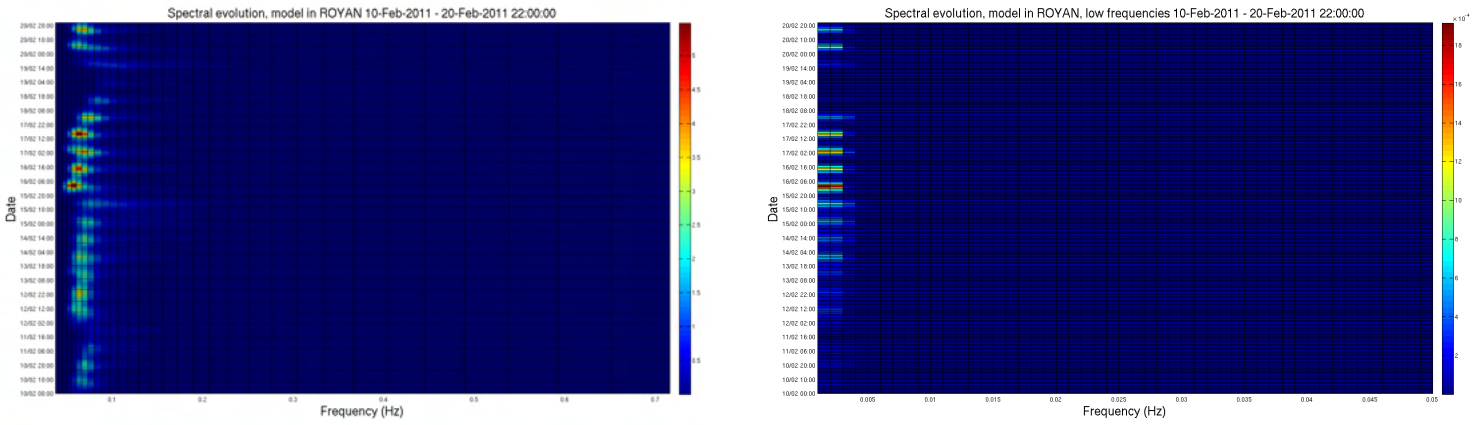

Figure 5.13: *Spectrum evolution (on the left) calculated with WAVEWATCH III model in Royan in February 2011. The long waves spectrum is represented on the right figure.*

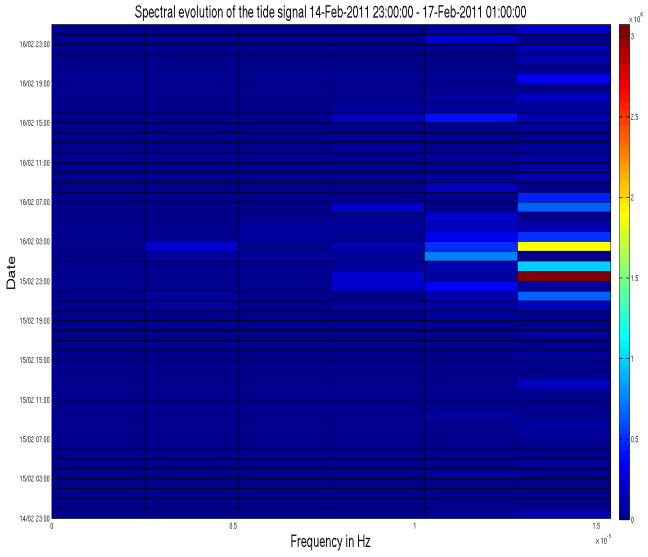

Figure 5.14: *Spectrum evolution of the long waves inside the harbor in February 2011.*

The long waves outside the harbor are present inside the harbor. More the swell frequency is low, more easily are the long waves created and higher is their energy. It seems that the hours following the seiche, the swell frequency outside the harbor was a little different so the long waves energy has changed and was lower. However, the infragravity frequencies were the same. In the harbor, other oscillations happened but with a lower amplitude. They can be again seen as small seiches.

5.5 Seiche Prediction.

Using a similar figure as the previous figure, one could know when a seiche will happen with the significative long waves height outside the harbor. Indeed if all seiches are listed with their height assiociated with the significative long waves height outside the harbor, they will be predictible. However, this piece of information is not sufficient. The following figure 5.15 shows the prediction made by the model in Royan for February 2011 :

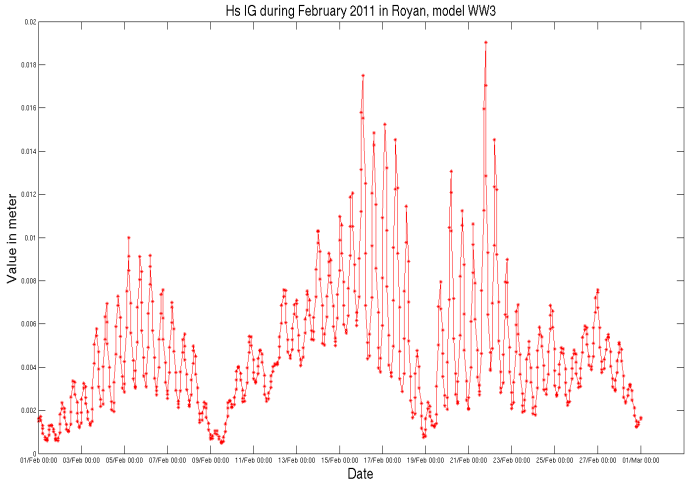

Figure 5.15: *Significative infragravity waves height calculated outside the harbor in Royan in February 2011 using WAVEWATCH III model.*

On the figure, it seems that around February 22 2011, the significative height is the same as the height during the seiche. But no seiche happened as shown on the following figure 5.16:

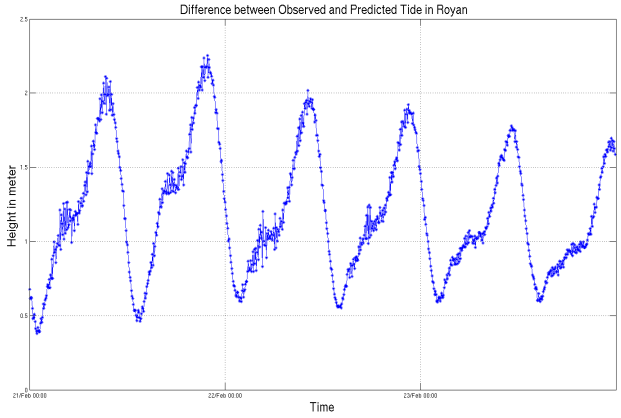

Figure 5.16: *Difference between the observed and predicted tides between February 21 and February 24 2011 in Royan.*

The amplitude is too law and the oscillations are at middle tide. Thus the frequency analysis shows that the infragravity frequencies are present but not really the seiche frequencies (fig. 5.17).

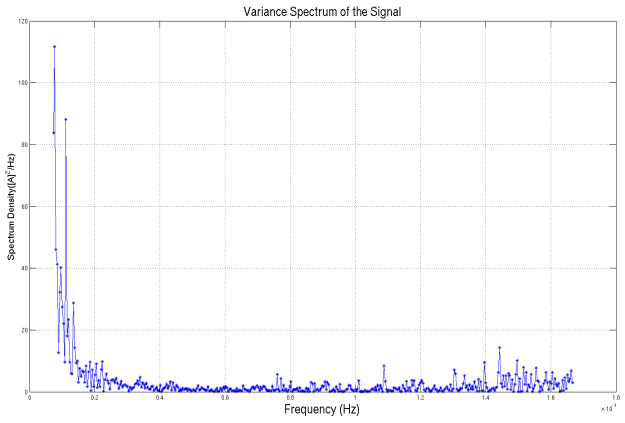

Figure 5.17: *Frequency analysis of the difference between the observed and predicted tides between February 21 and February 24 2011 in Royan.*

As the resonance frequency is not reached, the significative long waves height inside the harbor is amplified but no seiche happened.

To really be able to predict a seiche, all seiches must be listed, with their frequencies and the frequencies and height of the long waves outside the harbor. Using a plot such as the figure 5.12 at any time will conduct to really determinate when a seiche happens, depending on the long waves outside the harbor. The same plot should be done with the frequencies. Indeed it seems that a seiche happens when the infragravity frequencies have the basin resonance frequency and when the significative long waves height outside the harbor is high enough.

Conclusion

Over the last five months, I have studied the infragravity waves and their relation with seiches. My main objectives were to calculate the long wave generation and to model their propagation. Then an other aim was to study the seiches in Groix and Royan harbors to see their relation with the infragravity waves.

In this project, to model the infragravity waves, I understood and used programs written by F.Ardhuin. I adapted them to calculate the long waves caracteristics using a wave field. These carateristics will be use as a forcing in L.Leballeur code. I used his program to propagate the long waves. At the beginning the model attenuated the waves but I solved it by linearizing the schema. It contributed to increase my knowledge in modeling. As the code from L.Leballeur is a 1D cross-shore model, the next step would be to model in 2D using the MARS model from Ifremer.

Then to study the relation between seiches and infragravity waves, I processed and exploited the data from the tide gauges and pressure sensors. I created a method to treat them.

In Port-Tudy, no seiche happened during the interesting period. Indeed it was when the pressure sensors were on the seabed. However, the long waves are amplified inside the harbor. It would be interesting to follow the study but before March 23 2011, the tide gauge data were not numeric and some problems would occur with the scanning. Instead of using pressure sensors data, the results from WAVEWATCH III can be used to compare the long waves inside and outside the harbor.

In Royan, I could studied the seiche which happened in February 2011. The long waves are responsible. To really be able to predict a seiche, the corresponding frequency-significative height between long waves inside and outside the harbor should be continued, and highlight when a seiche happended.

Now one can say that the infragravity waves are responsible for the seiches. As the long waves spectrum is predictible, the seiche height and its occurence could be foresee.

Finally this internship gave me the opportunity to work in a research center and discover this field.

Appendices

Appendix A

Numerical Analysis.

In this appendix, the LU and Runge-Kutta methods to solve systems are going to be described. The LU method is used to solve the system for the circulation model and the Runge-Kutta method is used to solve the system for the wave propagation model.

A.1 The LU method.

In the circulation model, the system to solve is the following:

$$\eta_j^{n+1} + \theta_1 \frac{\Delta t}{\Delta x}\left((hu)_{j+1/2}^{n+1} - (hu)_{j-1/2}^{n+1}\right) = \eta_j^n - (1-\theta_1)\frac{\Delta t}{\Delta x}\left((hu)_{j+1/2}^{n} - (hu)_{j-1/2}^{n}\right) \quad \text{(A.1a)}$$

$$u_{j+1/2}^{n+1} + g\theta_2 \frac{\Delta t}{\Delta x}\left(\eta_{j+1}^{n+1} - \eta_j^{n+1}\right) = u_{j+1/2}^{n} - g(1-\theta_2)\frac{\Delta t}{\Delta x}\left(\eta_{j+1}^{n} - \eta_j^{n}\right) \quad \text{(A.1b)}$$

The code is written in Fortran 90. The language has a package LAPACK (Linear Algorithmic Package) which solves directly the systems. With this package, the resolution is with a LU factorization. This kind of resolution is interesting to use with iteratif algorithmics. The factorization is the following:

$$\begin{pmatrix} b_1 & c_1 & 0 & \cdots & 0 \\ a_2 & b_2 & c_2 & \ddots & \vdots \\ 0 & \ddots & \ddots & \ddots & 0 \\ \vdots & \ddots & \ddots & \ddots & c_{n-1} \\ 0 & \cdots & 0 & a_n & b_n \end{pmatrix} = \begin{pmatrix} p_1 & 0 & \cdots & \cdots & 0 \\ a_2 & p_2 & \ddots & \ddots & \vdots \\ 0 & a_3 & p_3 & \ddots & \vdots \\ \vdots & \ddots & \ddots & \ddots & 0 \\ 0 & \cdots & 0 & a_n & p_n \end{pmatrix} \begin{pmatrix} 1 & -q_1 & 0 & \cdots & 0 \\ 0 & 1 & -q_2 & \ddots & \vdots \\ \vdots & \ddots & \ddots & \ddots & 0 \\ \vdots & \ddots & \ddots & \ddots & -q_{n-1} \\ 0 & \cdots & \cdots & 0 & 1 \end{pmatrix} \quad \text{(A.2)}$$

Then by developping, the equation system is:

$$\begin{cases} p_1 &= b_1 \\ -p_k q_k &= c_k \\ -a_k q_{k-1} + p_k &= b_k \end{cases}$$

The unknowns are the vectors p and q. The system has one solution. After this factorization, one resolves:

$$LX' = Y \text{ then } UX = X'.$$

A.2 The Runge-Kutta Method.

The Runge-Kutta methods are methods of numerical analysis to approximate solutions to differential equations. These methods are based on the iteration principle, which means that the first solution estimation is used to calculate the second solution estimation which is more precised, and else. More the iterations number is high, better is the precision of the solution. In this resolution, the order is 4. The problem is the following:

$$y' = f(t, y) \text{ and } y(t_0) = y_0.$$

The Runge-Kutta method at the 4th order is given by the equations:

$$\begin{aligned} y_{n+1} &= y_n + \frac{h}{6}(k_1 + 2k_2 + 2k_3 + k_4) \\ k_1 &= f(t_n, y_n) \\ k_2 &= f(t_n + \frac{h}{2}, y_n + \frac{h}{2}k_1) \\ k_3 &= f(t_n + \frac{h}{2}, y_n + \frac{h}{2}k_2) \\ k_4 &= f(t_n + h, y_n + hk_3) \end{aligned} \tag{A.3}$$

The value y_{n+1} is approximated by the sum of the current value y_n and the product of the interval size by the estimated slope. The slope is obtained with the pondered slope mean: $(k_1 + k_2 + k_3 + k_4)/6$.

Appendix B

Test Of The Circulation Model.

B.1 Test Of $\theta_{continuity}$ And θ_{qdm}.

In the chapter 3, one has seen that the model attenuates the infragravity waves, which is a problem because no viscosity nor friction was added. In this appendix, different values of the parameters $\theta_{continuity}$ and θ_{qdm} were tested. First $\theta_{continuity}$ and θ_{qdm} are equal to 0.5 and then one parameter is modified. The system tested is the circulation model described in the chapter :

$$\eta_j^{n+1} + \theta_1 \frac{\Delta t}{\Delta x}\left((hu)_{j+1/2}^{n+1} - (hu)_{j-1/2}^{n+1}\right) = \eta_j^n - (1-\theta_1)\frac{\Delta t}{\Delta x}\left((hu)_{j+1/2}^{n} - (hu)_{j-1/2}^{n}\right) \quad \text{(B.1a)}$$

$$u_{j+1/2}^{n+1} + g\theta_2 \frac{\Delta t}{\Delta x}\left(\eta_{j+1}^{n+1} - \eta_j^{n+1}\right) = u_{j+1/2}^{n} - g(1-\theta_2)\frac{\Delta t}{\Delta x}\left(\eta_{j+1}^{n} - \eta_j^{n}\right) \quad \text{(B.1b)}$$

The other parameters have the following values:

- $tfin = 3600$ sec (simulation time).
- $dt = 5$ sec (interval time).
- long = 50 km (total cross-shore distance).
- nb couche l = 1000 (number of stitches on the horizontal).
- period = 240 sec (wave period).
- channel with a flat seabed.
- Boundary condition a the end of the channel : a wall.

First θ_{qdm} and $\theta_{continuity}$ are equal to 0.5. Then one of the values is modified.

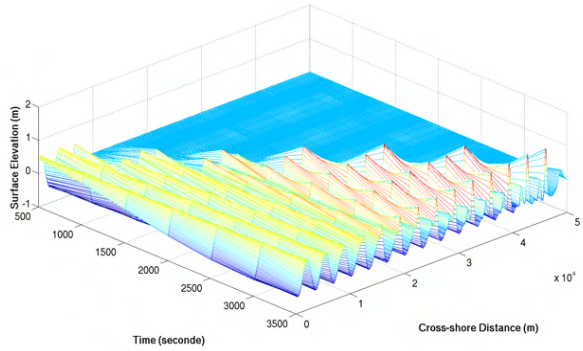

(a) *3D View.*

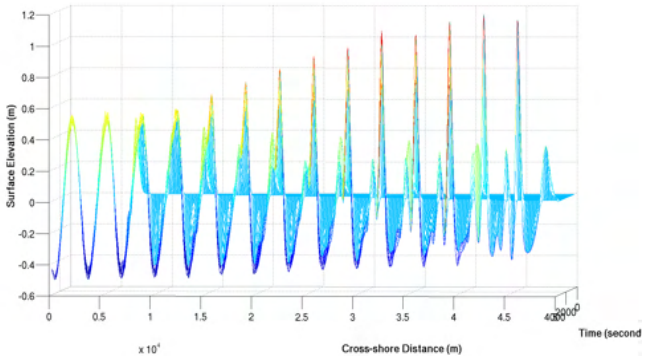

(b) *Surface elevation depending on the cross-shore distance.*

Figure B.1: $\theta_{continuity} = 0.5$ *and* $\theta_{qdm} = 0.5$.

The waves are not attenuated but a little amplified. However, the wave form is changed. Then $\theta_{qdm} = 0.5$ and $\theta_{continuity}$ takes different values.

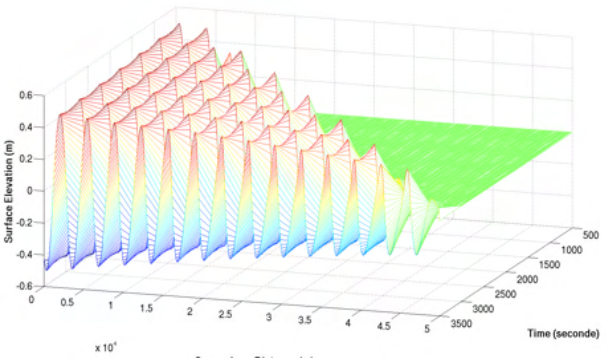

(a) *3D View.*

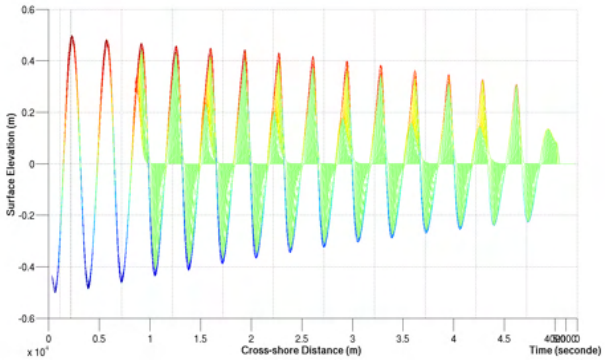

(b) *Surface elevation depending on the cross-shore distance.*

Figure B.2: $\theta_{qdm} = 0.5$ *and* $\theta_{continuity} = 0.6$.

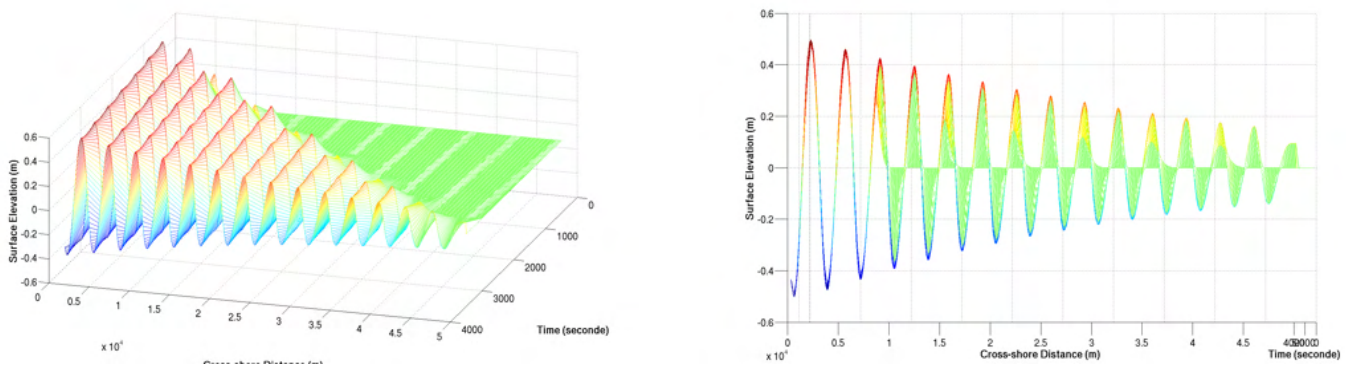

(a) *3D View.* (b) *Surface elevation depending on the cross-shore distance.*

Figure B.3: $\theta_{qdm} = 0.5$ *and* $\theta_{continuity} = 0.7$.

The wave is too much attenuated when $\theta_{continuity}$ is increased.

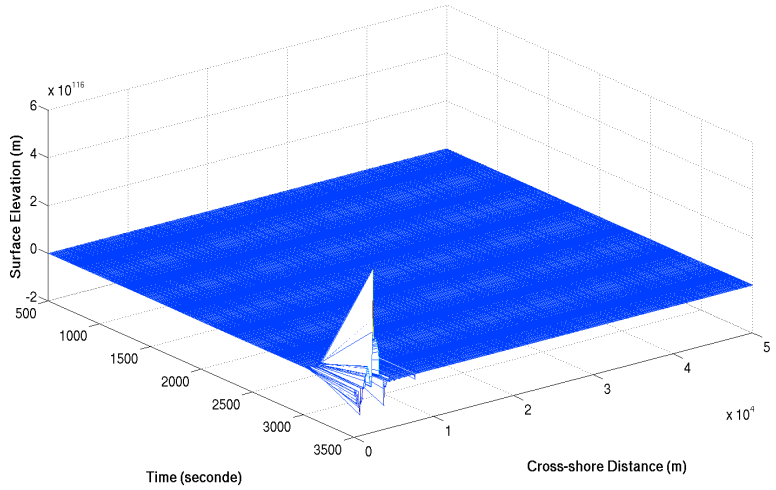

Figure B.4: $\theta_{qdm} = 0.5$ *and* $\theta_{continuity} = 0.4$.

When $\theta_{qdm} = 0.5$ and $\theta_{continuity}$ decreases, the model exploses.

Then $\theta_{continuity} = 0.5$ and θ_{qdm} takes different values. The following figures show the results.

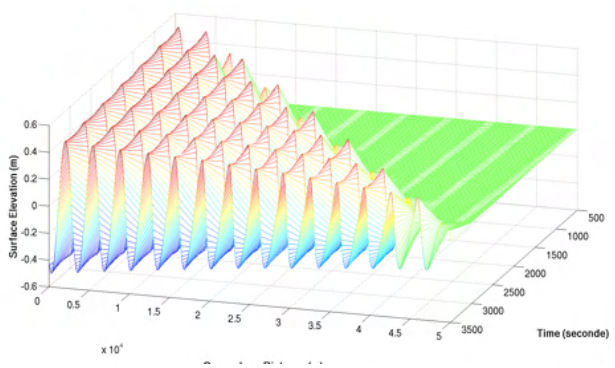

(a) *3D View.*

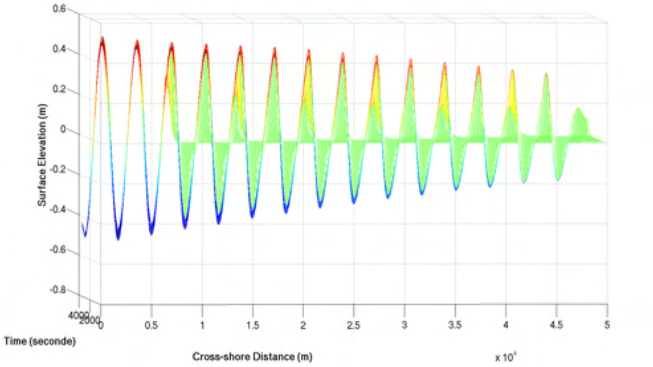

(b) *Surface elevation depending on the cross-shore distance.*

Figure B.5: $\theta_{qdm} = 0.6$ *and* $\theta_{continuity} = 0.5$.

One can observe that the result is the same if $\theta_{qdm} = 0.5$ and $\theta_{continuity} = 0.6$. The two parameters can be interchanged. The following figure shows it again:

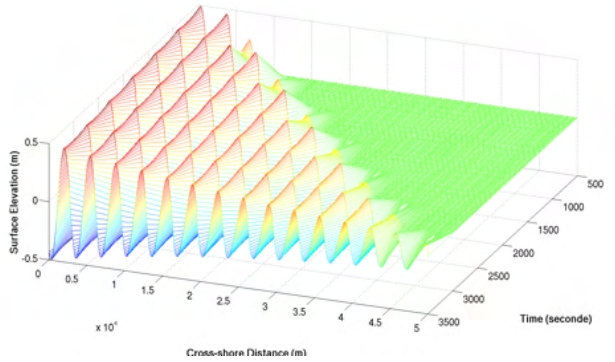

(a) *3D View.*

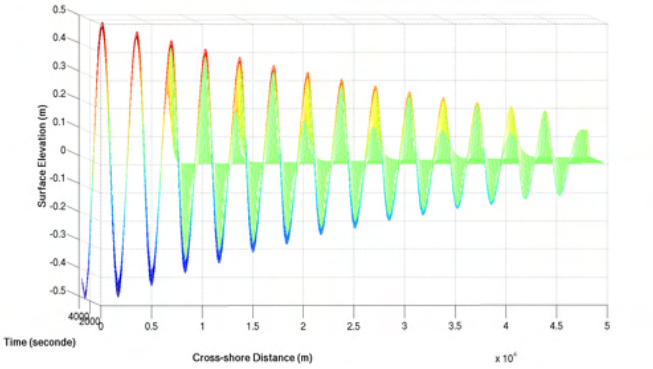

(b) *Surface elevation depending on the cross-shore distance.*

Figure B.6: $\theta_{qdm} = 0.7$ *and* $\theta_{continuity} = 0.5$.

Here it seems that when $\theta_{qdm} = 0.5$ and $\theta_{continuity} = 0.6$, the wave is less attenuated.

Then $\theta_{qdm} = 0.4$ and $\theta_{continuity}$ takes different values.

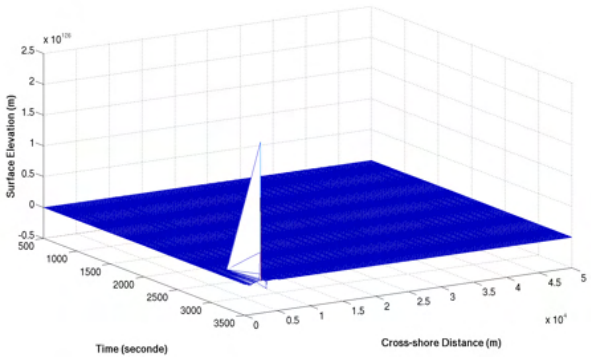

(a) $\theta_{qdm} = 0.4$ *and* $\theta_{continuity} = 0.4$.

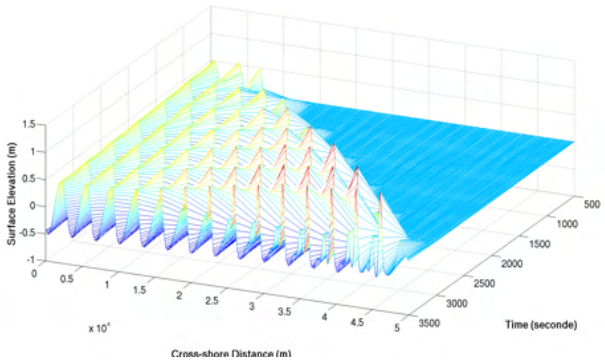

(b) $\theta_{qdm} = 0.4$ *and* $\theta_{continuity} = 0.6$.

Figure B.7: *Test with* $\theta_{qdm} = 0.4$ *and* $\theta_{continuity} = 0.4$ *and* 0.6

Then $\theta_{qdm} = 0.6$ and $\theta_{continuity}$ takes different values.

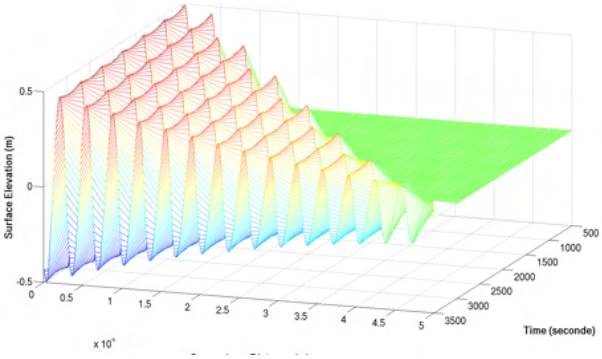

(a) $\theta_{qdm} = 0.6$ *and* $\theta_{continuity} = 0.6$.

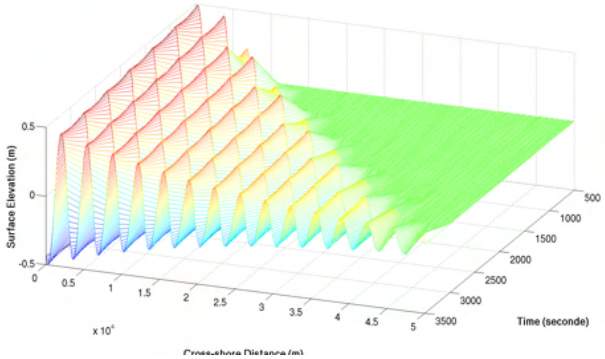

(b) $\theta_{qdm} = 0.6$ *and* $\theta_{continuity} = 0.7$.

Figure B.8: *Test with* $\theta_{qdm} = 0.6$ *and* $\theta_{continuity} = 0.6$ *and* 0.7

So for the moment the best values for θ_{qdm} and $\theta_{continuity}$ are 0.5 and 0.6.

Then the interval between $\theta_{continuity}$ and θ_{qdm} is modified. The following figures show the results when the interval increases or decreases.

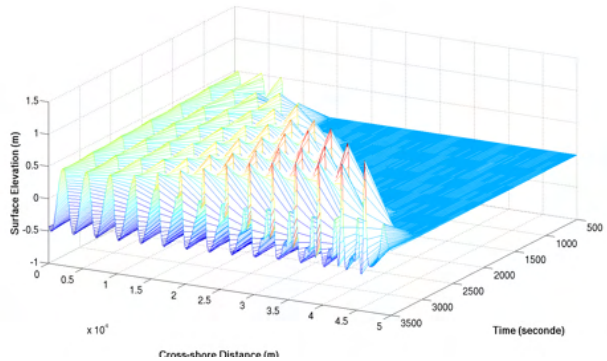

(a) $\theta_{qdm} = 0.3$ *and* $\theta_{continuity} = 0.7$.

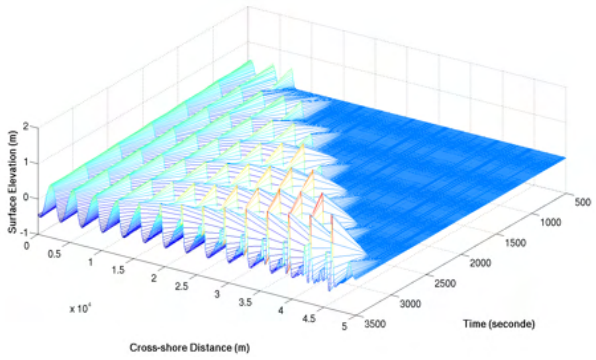

(b) $\theta_{qdm} = 0.2$ *and* $\theta_{continuity} = 0.8$.

Figure B.9: *Interval between* θ_{qdm} *and* $\theta_{continuity}$ *of 0.4 and 0.6.*

The waves are amplificated, which is not satisfying. So the best maximum interval is 0.1 with $\theta_{qdm} = 0.5$ and $\theta_{continuity} = 0.6$ or the contrary. The result is reminded with the following figure:

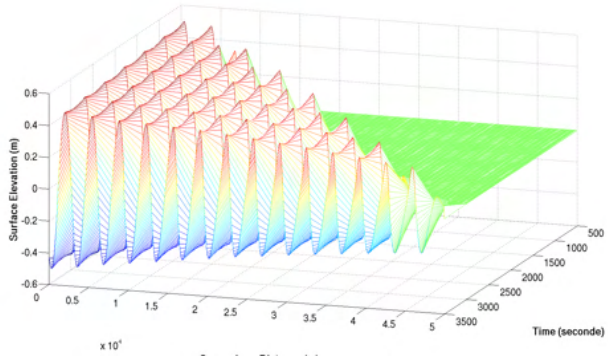

(a) *3D View.*

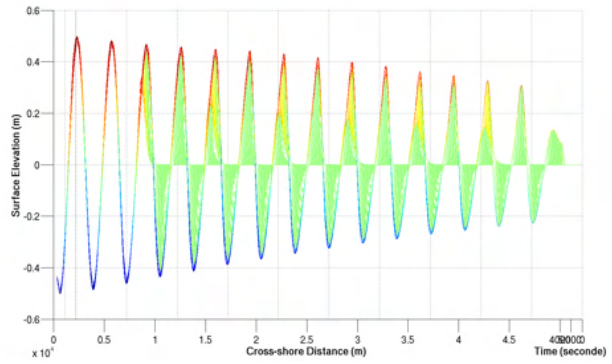

(b) *Surface elevation depending on the cross-shore distance.*

Figure B.10: $\theta_{qdm} = 0.5$ *and* $\theta_{continuity} = 0.6$, *the best maximum interval.*

Then this interval is decreased. $\theta_{continuity} = 0.5$ and θ_{qdm} takes different values between 0.5 and 0.6.

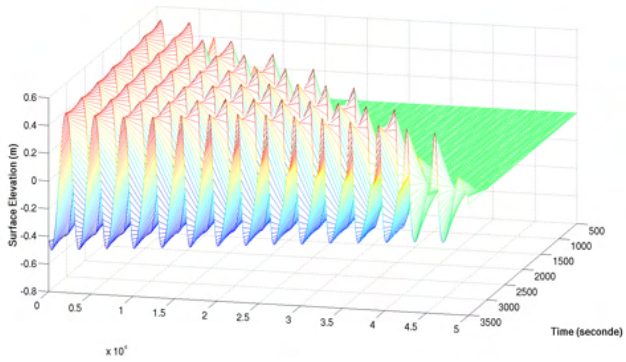

(a) *3D View.*

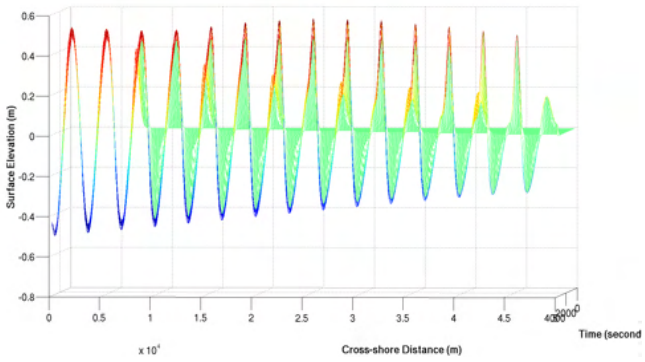

(b) *Surface elevation depending on the cross-shore distance.*

Figure B.11: $\theta_{qdm} = 0.55$ *and* $\theta_{continuity} = 0.5$.

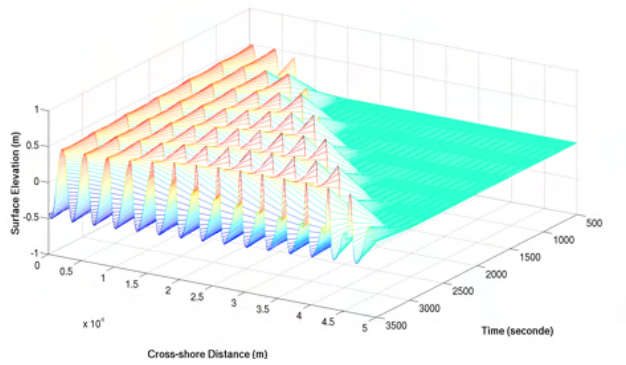

(a) *3D View.*

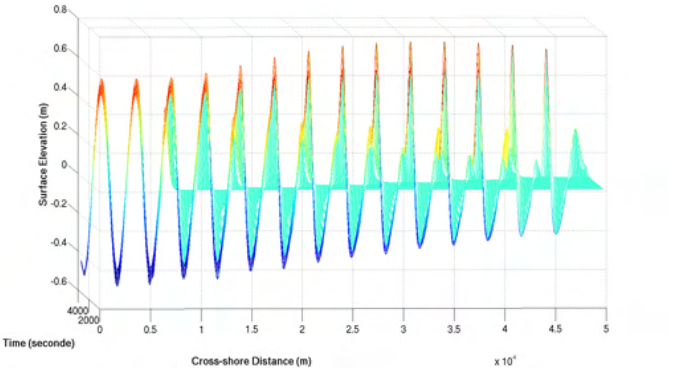

(b) *Surface elevation depending on the cross-shore distance.*

Figure B.12: $\theta_{qdm} = 0.53$ *and* $\theta_{continuity} = 0.5$.

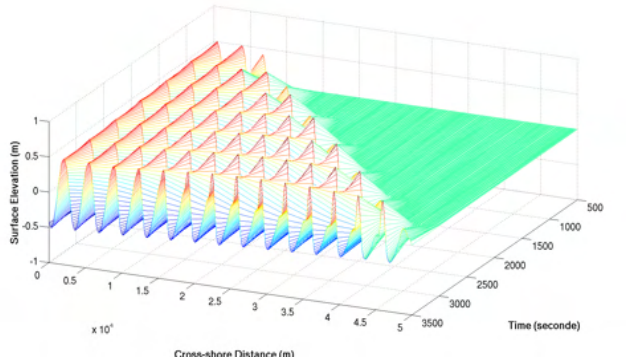

(a) *3D View.*

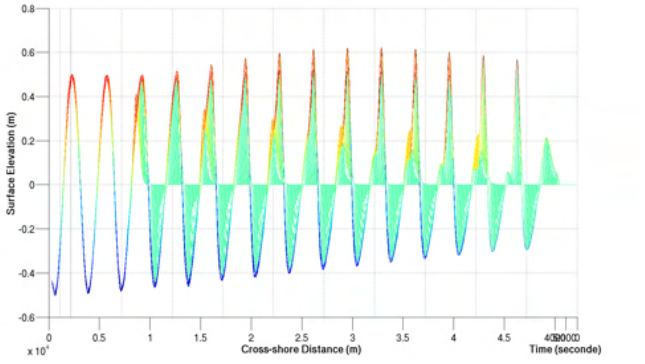

(b) *Surface elevation depending on the cross-shore distance.*

Figure B.13: $\theta_{qdm} = 0.54$ *and* $\theta_{continuity} = 0.5$.

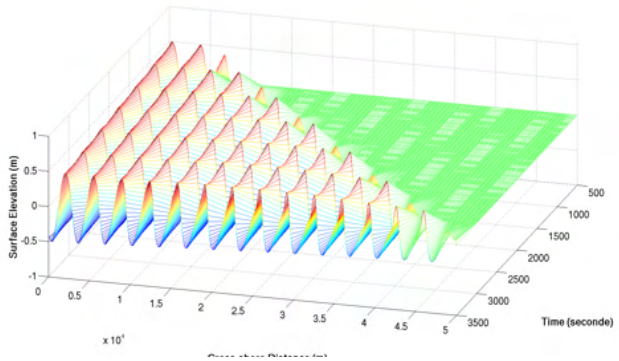

(a) *3D View.*

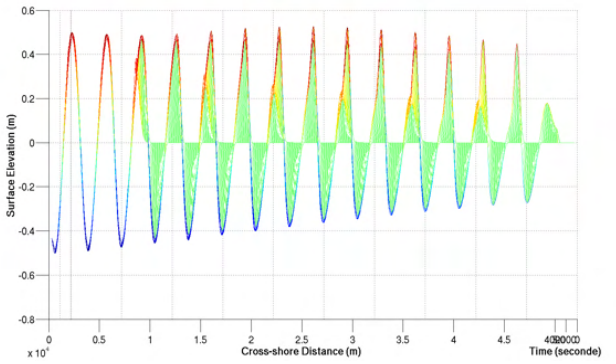

(b) *Surface elevation depending on the cross-shore distance.*

Figure B.14: $\theta_{qdm} = 0.56$ *and* $\theta_{continuity} = 0.5$.

The wave is still a little attenuated. Now one can test values between 0.53 and 0.55 for θ_{qdm} and 0.49 and 0.51 for $\theta_{continuity}$.

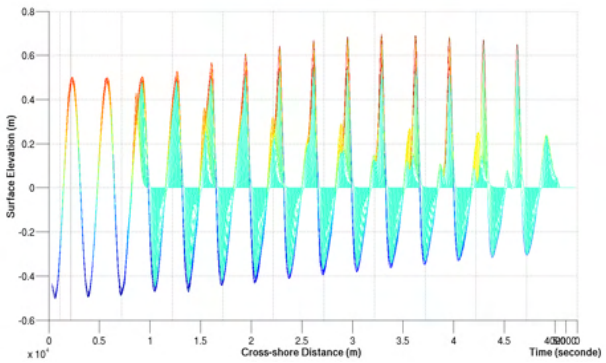

(a) $\theta_{qdm} = 0.54$ *and* $\theta_{continuity} = 0.49$.

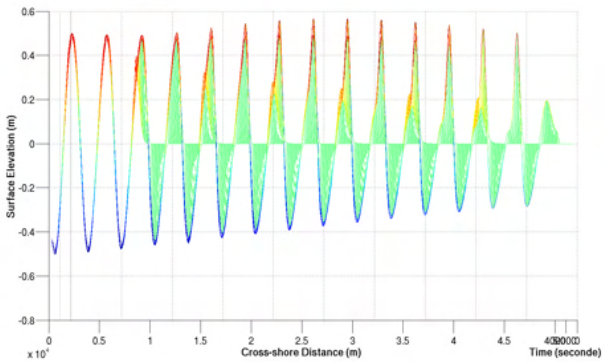

(b) $\theta_{qdm} = 0.54$ *and* $\theta_{continuity} = 0.51$.

Figure B.15: *Test with* $\theta_{qdm} = 0.54$ *and* $\theta_{continuity} = 0.49$ *and* 0.51.

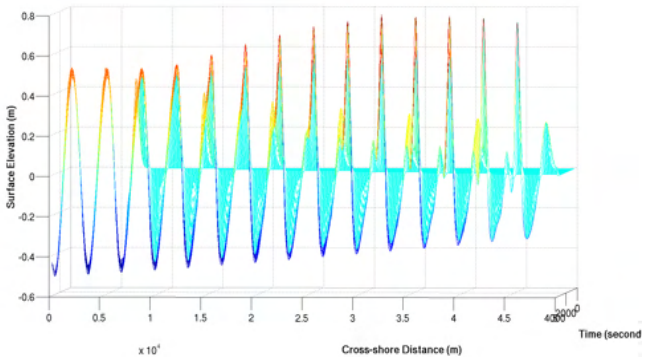

(a) $\theta_{qdm} = 0.53$ *and* $\theta_{continuity} = 0.49$.

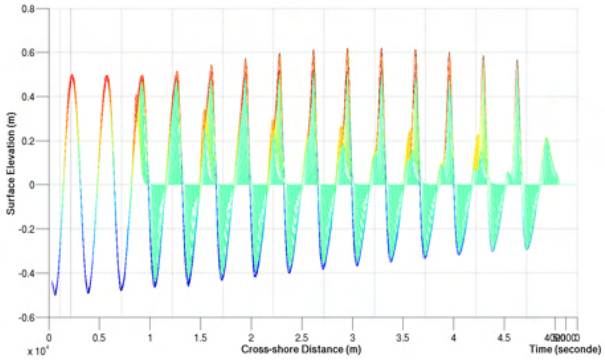

(b) $\theta_{qdm} = 0.53$ *and* $\theta_{continuity} = 0.51$.

Figure B.16: *Test with* $\theta_{qdm} = 0.53$ *and* $\theta_{continuity} = 0.49$ *and* 0.51.

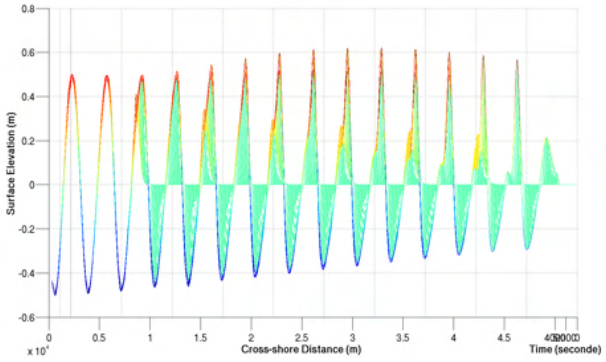

(a) $\theta_{qdm} = 0.55$ *and* $\theta_{continuity} = 0.49$.

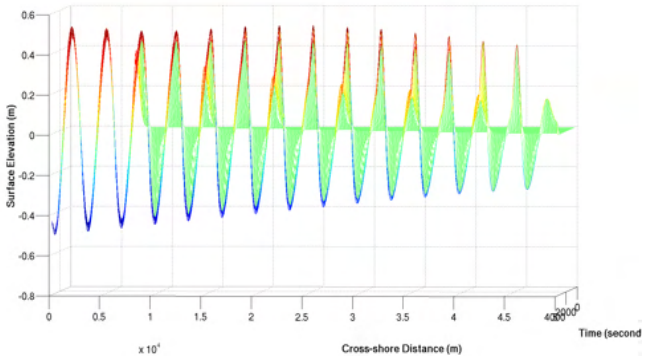

(b) $\theta_{qdm} = 0.55$ *and* $\theta_{continuity} = 0.51$.

Figure B.17: *Test with* $\theta_{qdm} = 0.55$ *and* $\theta_{continuity} = 0.49$ *and* 0.51.

If $\theta_{continuity}$ is equal to 0.5 or 0.51, the result does not change a lot. So the best values for θ_{qdm} and $\theta_{continuity}$ are:

$$\theta_{qdm} = 0.54$$
$$\theta_{continuity} = 0.5$$

However the wave form at the end is not a sinusoid like the forcing. At the end, the sinusoid is more like a wave, with crests and hollows. The wave crests are higher than the wave hollows. This phenomenon is happening because the channel is not deep enough in comparison with the wave height. Here the waves are considered no dispersive. (Non linear interactions ?)

If the wave height is decreased, the following figure is obtained, with the same parameters used in the figure B.13:

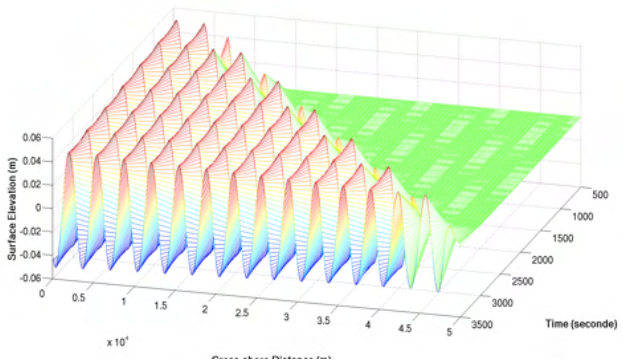

(a) *3D View.*

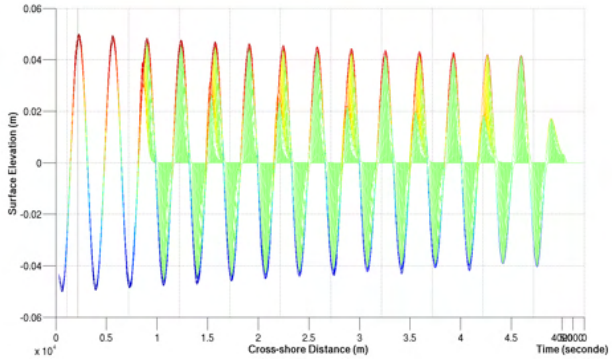

(b) *Surface elevation depending on the cross-shore distance.*

Figure B.18: $\theta_{qdm} = 0.54$ *and* $\theta_{continuity} = 0.5$. *The wave height has been decreased by a 10 factor.*

Previously the ratio between the depth and the wave height was $\frac{1}{40}$. But if the ratio is smaller, for example $\frac{1}{200}$, the wave is less attenuated.

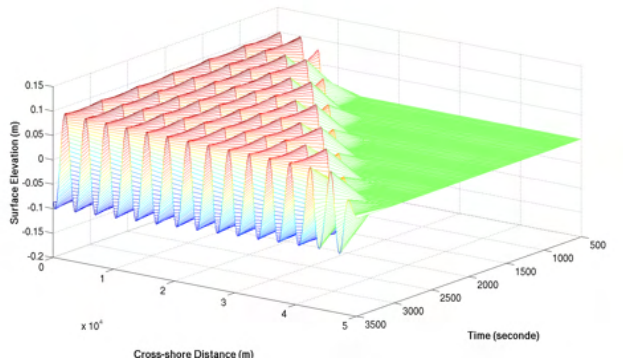

(a) *3D View.*

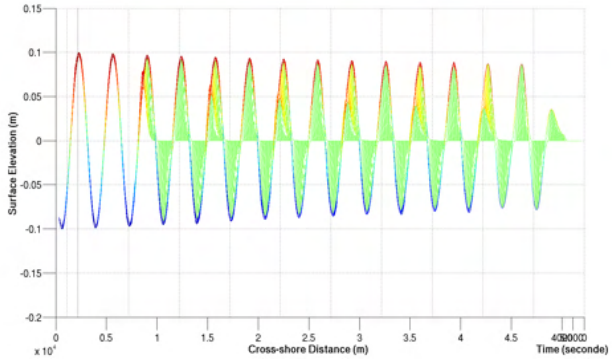

(b) *Surface elevation depending on the cross-shore distance.*

Figure B.19: $\theta_{qdm} = 0.54$ *and* $\theta_{continuity} = 0.5$. *The wave height has been decreased by a 5 factor.*

It seems also that the wave amplitude must be taken into account, after having the right parameters. Indeed if θ_{qdm} and $\theta_{continuity}$ are not equal to 0.5 or have a maximum interval of 0.1, the system exploses or the wave is too much attenuated.

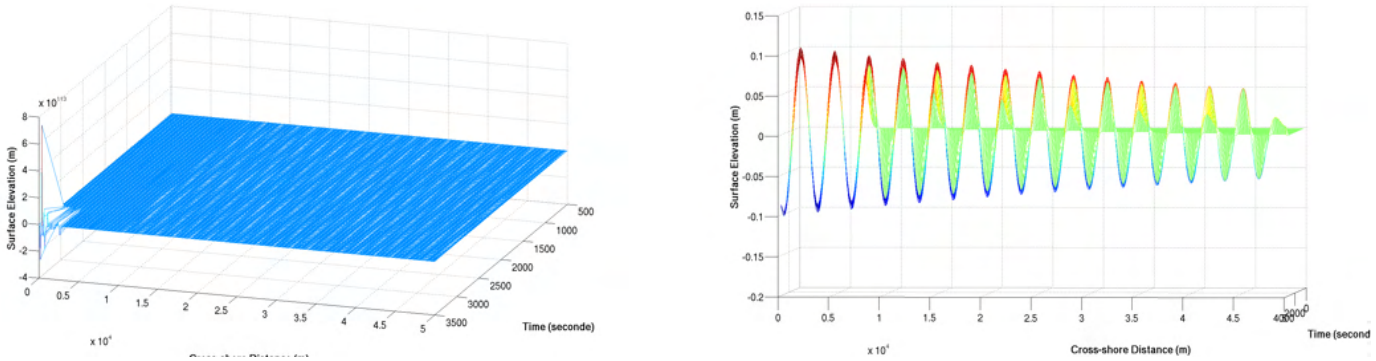

(a) $\theta_{qdm} = 0.5$ *and* $\theta_{continuity} = 0.4$.

(b) $\theta_{qdm} = 0.5$ *and* $\theta_{continuity} = 0.6$.

Figure B.20: *Test with a wave height which has been decreased by a 5 factor.*

However even if the wave is less attenuated with the right parameters, the results are not good for the use that we wanted. Indeed the model will have to propagate a wave on more that 50 km long.

B.2 Test Of The Explicit Schema.

Then the explicit schema has been tested. It means that θ_{qdm} and $\theta_{continuity}$ are equal to zero. However, the schema must repsect the stability condition which is the following condition:

$$\sqrt{gh}\frac{dt}{dx} < 1 \tag{B.2}$$

First, the more adjustable parameter is dt. Indeed $dx = \frac{long}{nbcouchel}$ can not really be modified. The precision depends on it. The other parameters are:

- $tfin = 3600$ sec (simulation time).
- long = 50 km (total cross-shore distance).
- nb couche l = 1000 (number of stitches on the horizontal).
- period = 240 sec (wave period).

The condition on dt is then:

$$dt < 3.57 \tag{B.3}$$

But when this condition is respected, the system exploses.

Appendix C

Waves Propagation Model

C.1 Equations.

The model is an energetic waves model propagation. It is based on the equilibrium of the energy flux divergence. The waves are propagating to the coast. For one dimention one has the relation :

$$\frac{\partial \rho g E C_g cos\theta}{\partial x} = \langle \varepsilon_b \rangle \tag{C.1}$$

In the previous formula, E is the energy density ($E = H_{rms}^2/8$), $C_g cos\theta$ is the composant of the group speed, which is oriented to the coast. $\langle \varepsilon_b \rangle$ is the dissipation due to the wave breaking.

Then to take into account the wave propagation in the surf area, a Rayleigh distribution is used. Indeed the wave heigth distribution in the surf area is modulated with the enery loss. The distribution is then :

$$p(H) = \frac{2H}{H_{rms}^2} e^{-\left(\frac{H}{H_{rms}}\right)^2} \tag{C.2}$$

Then a modulation function is used so that no waves break in deep water and all waves at the coast have broken. The modulation function is the following :

$$W(H) = \left(\frac{H_{rms}}{\gamma h}\right)^4 \tag{C.3}$$

By integrating the energy dissipation, the mean total dissipation is :

$$\langle \varepsilon_b \rangle = \frac{3}{16} \rho g \sqrt{\pi} \frac{B^3}{\gamma^4 h^5} f_p H_{rms}^7 \tag{C.4}$$

After calculations and by substituting E in the equation, one obtains a differencial equation at the first order C.5:

$$\frac{\partial}{\partial x}\frac{1}{8}\rho g H_{rms}^2 C_g cos\theta = \frac{3}{16}\rho g\sqrt{\pi}\frac{B^3}{\gamma^4 h^5} f_p H_{rms}^7 \tag{C.5}$$

C.2 System Resolution.

The previous differencial equation is resolved with the Runge-Kutta method. The method is at the fourth order (see appendix A).

But first γ and some empirical parameters have to be determinated. Thus the value B depends of the type of breaking considered. In general this parameter is close to 1. In his code, L.Leballeur has fixed B to 1 and has seen that this parameter does not really influence the results.

Concerning γ, Ruessink has proposed a parametrization of γ which depends on the wave number k and on the depth h:

$$\gamma = 0.76kh + 0.29 \tag{C.6}$$

Other formulas are possible but this previous formula is used in the code.

C.3 Results.

In the model, I simulated a channel with a flat bottom and an infragravity wave as a forcing. So the bathymetry is constant. To force the model, I imposed the first H_s offshore and the model evaluates the other heights in each point of the grid: the waves are propagating.

The significant height does not change because here the bathymetry is constant and the H_s is modified with the bathymetry. This result was expected.

Appendix D

Coupling Model.

D.1 Principle.

The following diagram (fig.D.1) shows the principle of the coupling:

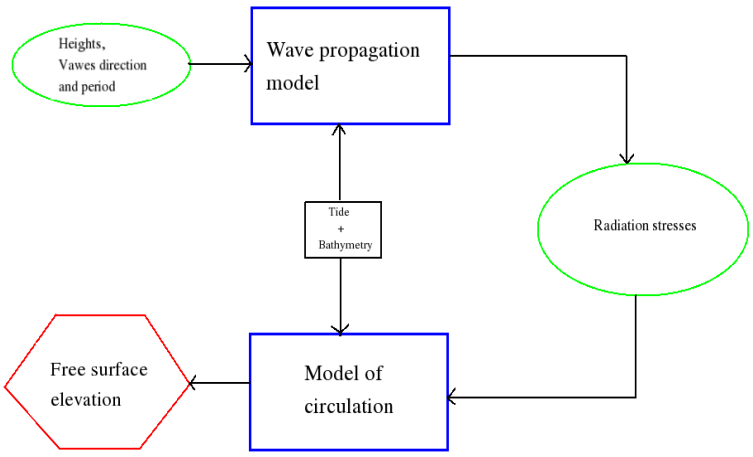

Figure D.1: *Schema illustrating the coupling realized between the circulation and wave propagation models.*

The forcing is realized with S_{xx} which is the radiation stresses.

D.2 Radiation Stresses.

The notion of tensor radiation is generally known in electromagnetics. Indeed when a wave touches an object, the movement quantity conservation implies that a force is exerted on it, which is equal to the movement quantity variation. This is the radiation stress which can be consider as an excess of movement quantity flux.

Indeed electromagnetic radiation impinging on a surface produces a force which is referred to as the "radiation pressure". A similar phenomenon occurs in the case of acoustic waves and of waves on the surface of fluids. In each case the force is principally in the direction of wave propagation.

Longuet-Higgins and Stewart ([LS64]) have worked on this and have modelled it. They have introduced a radiative stress tensor which represents a flux of momentum. It is the flux divergence which cause the particules acceleration.

Surface waves possess momentum which is directed parallel to the direction of propagation and is proportional to the square of the wave amplitude. Now if a wave train is reflected from an obstacle, its momentum must be reversed. Conservation of momentum then requires that there be a force exerted on the obstacle, equal to the rate of change of a wave momentum. This force is a manifestation of the radiation stress, which must be defined as the excess flow of momentum due to the presence of waves.

First if one considers an undisturbed body of water of uniform depth, the pressure p at any point is equal to the hydrostatic pressure :

$$p = -\rho g z \tag{D.1}$$

z is the distance measured upwards from the mean surface, ρ and g denote density and gravity. Thus the total flux of horizontal momentum between the surface and bottom ($z = -h$) is :

$$\int_{-h}^{0} p dz \tag{D.2}$$

Since this quantity is independant of x, the flux of momentum across an adjacent plane $(x + dx)$ just balances the flux across the first plane, and there is no net change of momentum between the two planes.

Now if one consider the momentum flux in the presence of a simple progressive wave, the surface elevation $z = \nu$ is given approximatively by:

$$\eta = a cos(kx - \sigma t) \tag{D.3}$$

a is the amplitude, k the wavelength and σ the period. The particle orbits are roughly ellipses, with the major axes horizontal in general. The corresponding components of velovity

are then:

$$u = a\omega \frac{cosh(k(z+h))}{sinh(kH)} cosh(kx - \omega t) \tag{D.4a}$$

$$v = a\omega \frac{sinh(k(z+h))}{sinh(kH)} sin(kx - \omega t) \tag{D.4b}$$

Then the instantaneous flux of horizontal mouvment quantity through a vertical surface is : $p + \rho u^2$. One can notice that by intregration on the vertical, the total flux is obtained:

$$\int_{-h}^{\nu} (p + \rho u^2) dz \tag{D.5}$$

The main component (in the propagation direction) of the stress tensor is the time mean of the last equation, and one substracte the mean flux whithout waves. So one obtains:

$$\begin{aligned} S_{xx} &= \overline{\int_{-h} (p + \rho u^2) dz} - \int_{-h}^{0} p_0 dz \\ S_{yy} &= \overline{\int -h(p + \rho v^2) dz} - \int_{-h}^{0} p_0 dz \\ S_{xy} &= \overline{\int -h(p + \rho uv) dz} - \int_{-h}^{0} p_0 dz \end{aligned} \tag{D.6}$$

One obtains for a direction propagation on (Ox) with an angle θ:

$$\begin{aligned} S_{xx} &= \rho g E \frac{C_g}{C} cos^2\theta \\ S_{yy} &= \rho g E \frac{C_g}{C} sin^2\theta \\ S_{xy} &= \rho g E \frac{C_g}{C} sin\theta cos\theta \end{aligned} \tag{D.7}$$

In the formula S_{xx}, the first term represents the advection of the movement quantity and the second term represents the pressure. The pressure matters only in normal components of the stress.

In the code, one consideres that the waves have a normal incidence at the coast and propagate in the (Ox) direction. So the previous formulas become:

$$\begin{aligned} S_{xx} &= \rho g E \left(\frac{C_g}{C} + \frac{1}{2} \frac{2kH}{sinh(2kH)} \right) \\ S_{yy} &= \rho g \frac{E}{2} \left(2\frac{C_g}{C} - 1 \right) \\ S_{xy} &= 0 \end{aligned} \tag{D.8}$$

D.3 Wave Effects On the Mean Circulation.

As one saw previously and according to *Longuet-Higgins and Steward*, the waves act on the water surface with the radiation stress.

The principle is to integrate on the vertical the Navier-Stokes equations , and mean them on a wave period. The Coriolis force is supposed to be insignificant. The viscosity and the friction are also supposed to be insignificant at this level. Therefore one has the following equations D.9:

$$\frac{\partial U}{\partial t} + U\frac{\partial U}{\partial x} + g\frac{\partial \bar{\eta}}{\partial x} = -\frac{1}{\rho(h+\bar{\eta})}\frac{\partial S_{xx}}{\partial x} \tag{D.9a}$$

$$\frac{\partial \bar{\eta}}{\partial t} + \frac{\partial}{\partial x}((h+\bar{\eta})U) = 0 \tag{D.9b}$$

So the energy gradients of waves are responsible for the induced propagation with waves.

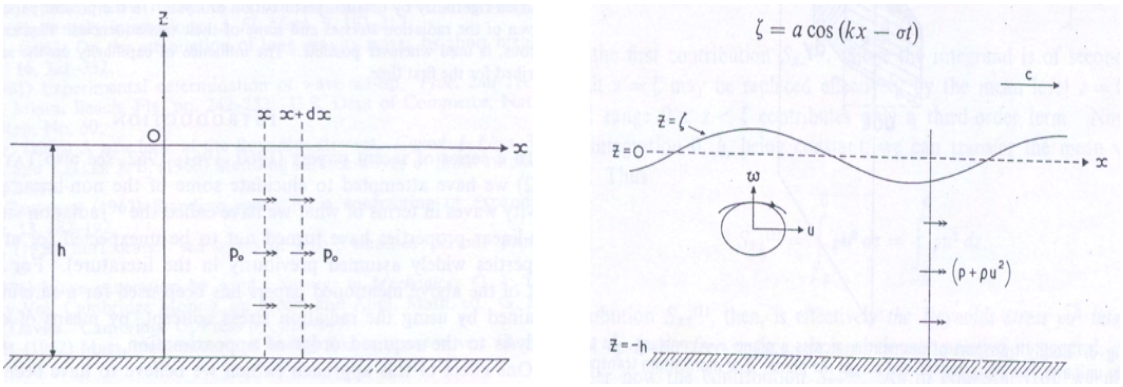

Figure D.2: *The momentum flux in a stationary fluid (on the left) and in a progressive wave (on the right).*

The previous equations are used in the coupling model and the bottom friction is added because of the shallow water. Then the bottom friction must be parametrized. Several different parametrizations exist.

Appendix E

Explanations Of The Data Processing.

To study the infragravity waves and to see their relation with seiches, two harbors have been studied, which are Royan and Port-Tudy in Groix (fig. E.1).

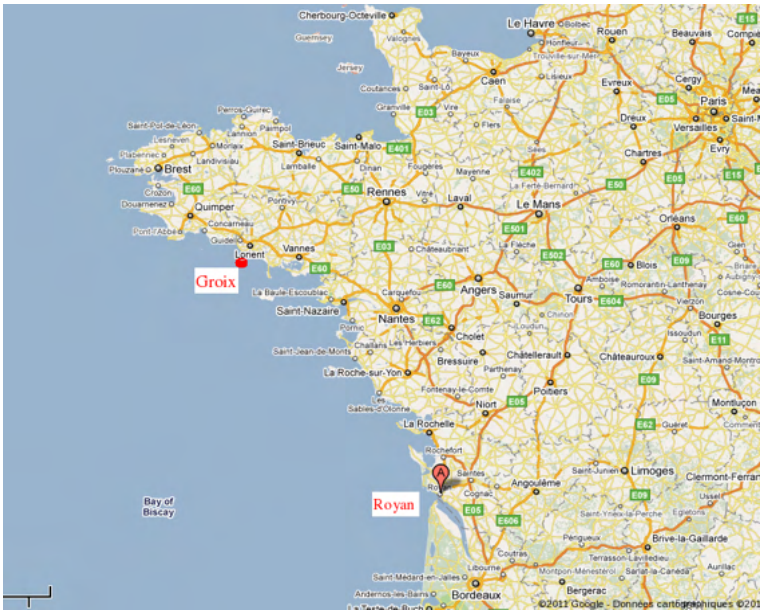

Figure E.1: *Groix and Royan harbors.*

For each harbor, I got data from tide gauges, frequency-direction spectrum from the WAVEWATCH III model and observed frequency-direction spectra from buoys and pressure sensors (only for Groix). For the two harbors, the same method was applied to process the data. Then all results have been analysed.

In this part, I am going to explain the data processing. Then the results will be presented

for each harbor (in the next chapters). First, the data from the tide gauges were processed, then the spectra and at the end the pressure sensors data.

E.1 Tide Gauge Data Processing.

E.1.1 Frequency Analysis Of One Hour Of Data.

The data come from the SHOM and are used to study the infragravity waves in the harbor, to see their time evolution and to detect seiche. The tide gauges in the harbors filter the little waves and the swell. So only the tide and the infragravity waves remain.

To study the long waves in the harbor and their time evolution, I use the observed tide and realize a frequency analysis. To reduce the tide, the analysis is made each hour. If a seiche happened, its frequency will appear. However the observed tide has holes which are caused by the sensor. If a hole has a duration which is small enough (less than few hours), a linear interpolation is done. Otherwise, the file is cut when the linear interpolation gives wrong points or cuts the curve. Moreover some wrong data are removed. The following figure E.2 shows an example of the linear interpolation made for Groix:

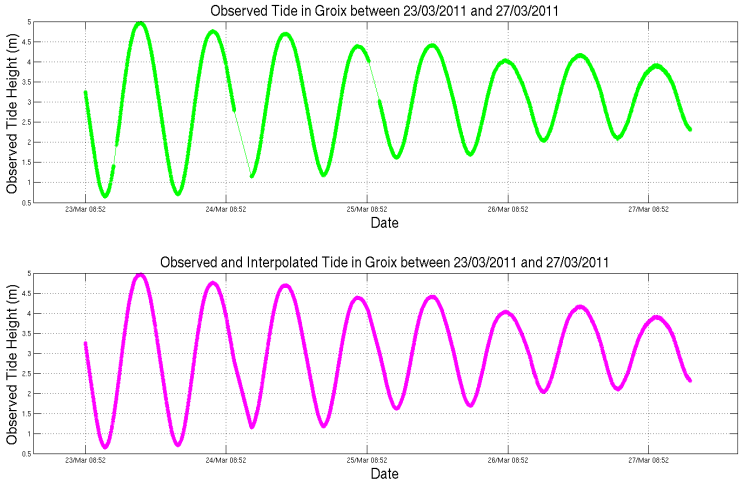

Figure E.2: *Result of the linear interpolation of the observed tide in Groix from March 23 to March 27, 2011. The data were recorded every minute.*

When the data have a hole, the wrong values were not replaced by a special value to avoid having a high frequency which can pollute the frequency analysis. The following figure E.3 shows an example of the result of the analysis on one hour for Groix:

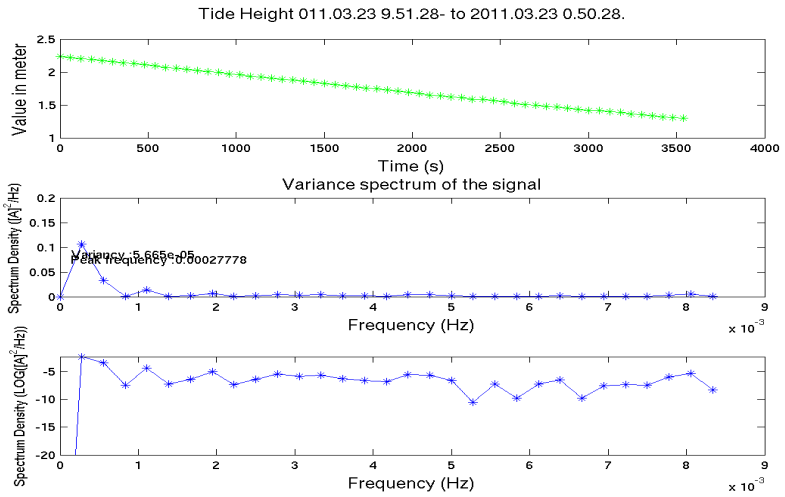

Figure E.3: *Result of the frequency analysis of the tide signal in Groix for March 24 2011, between 2.10 am and 3.09 am.*

Then the evolution of the results is monitored hour by hour. The figure E.4 shows an example of the spectral evolution from March 23 to May 2, 2011, in Groix:

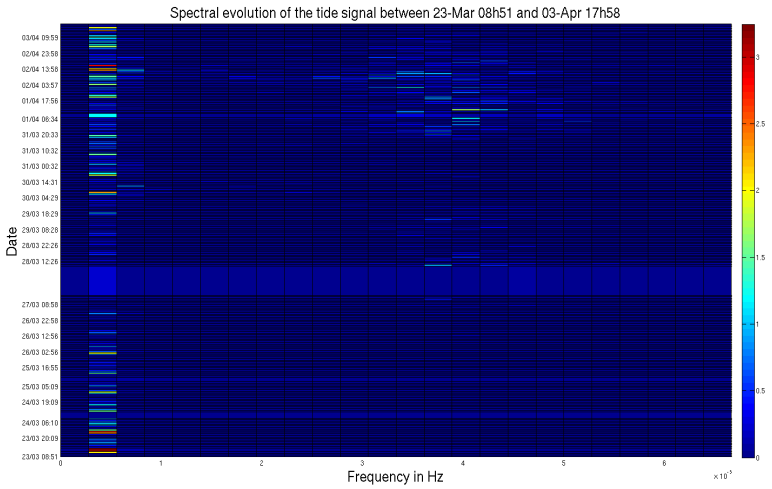

Figure E.4: *Spectral evolution of the tide in Groix from March 23 to May 2, 2011. The data were recorded every minute.*

With the spectrum, the significative height is calculated. The formula used is the following:

$$Hs = 4(\int E(f)df)^{1/2}$$

$E(f)$ is the wave spectrum. So to calculate the long waves significative height Hs_{IG} I

use the previous formula and I integrate with the infragravity frequencies. The integration is approximated with a sum :

$$Hs_{IG} = 4(\sum_{f_{1IG}}^{f_{2IG}} E(f)\Delta f)^{1/2}$$

Δf is the interval between two frequencies and $E(f)$ is constant on each spectral element. As the spectrum is calculated each hour, the significative height can also be known.

E.1.2 Seiche Detection.

Then to really detect a seiche, the observed and predicted tides are compared. The difference between the two tides is analysed. If this difference is very high (more than fifty centimeters) and is oscillating with a period between four and ten minutes, it means that a seiche has happened. Indeed the surcotes and decotes can be fifty centimeters and more during a storm, but they do not fluctuate. However here, the surcotes and decotes are not known and sometimes the peak is due to them. The following figure E.5 shows an example of the observed tide and the predicted tide from May 6 to May 9, 2011 :

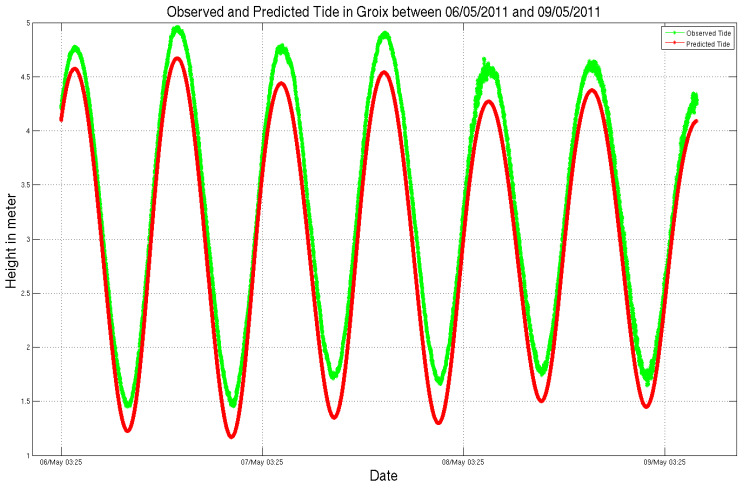

Figure E.5: *Observed (in green) and predicted (in red) tide in Groix from May 6 to May 9, 2011.*

The predictions are shifted in comparison with the observed tide. But the two curves are always shifted in the same direction. Then the difference is calculated and a frequency analysis is realized. Here is an example with the figure E.6 :

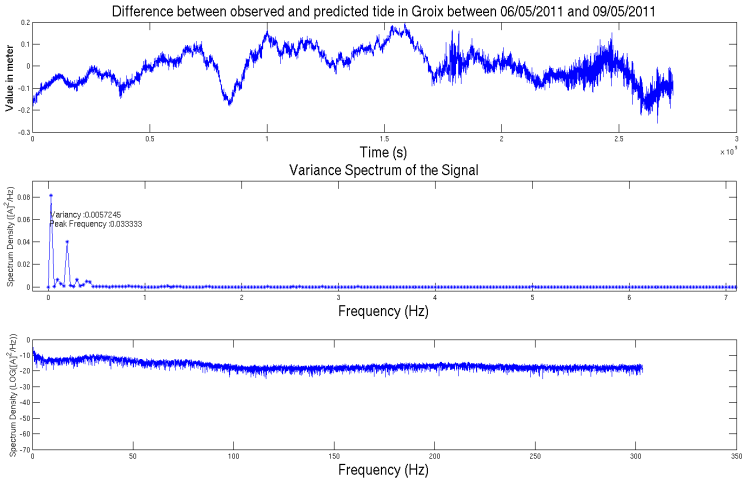

Figure E.6: *Result of the frequency analysis of the difference between the observed and predicted tide in Groix. The analysis is realized from May 6 to May 9, 2011.*

E.2 Spectral Processing.

Then the observed spectrums and those obtained with the WAVEWATCH III model are analysed. To perform it, I use a Matlab program wrote by F.Ardhuin. The program reads the spectrum, calculates the second order spectrum and the infragravity wave caracteristics such as the significative height. Indeed the observed and modeled spectrums do not have the infragravity band frequency.

E.3 Pressure Sensors Data Processing.

The pressure sensors were only located around Groix (see chap. 4 to see the location of the sensors and other information). The processing is quite similar to the tide data processing. The aim is to study the infragravity waves and their time evolution. Then when a seiche happens in the harbor, they can be used to see the sea conditions outside the harbor.

First I had to put the data in a more suitable format. An example of the format of the raw file is shown on the figure E.7:

```
Y11,M02,D23,H10,M44,S15,F02,L00,I01,N003,Z00,X03,T10,R0000,

Y11,M02,D23,H10,M45,S00,
+0.0201,+0.0195,+0.0189,+0.0184,+0.0180,+0.0090,+0.0222,+0.0218,+0.0215,+0.0215,+0.0211,+0.0211,+0360,
+0.0200,+0.0204,+0.0204,+0.0145,+0.0182,+0.0188,+0.0178,+0.0175,+0.0146,+0.0174,+0.0181,+0.0167,+0360,
+0.0176,+0.0179,+0.0168,+0.0165,+0.0163,+0.0162,+0.0160,+0.0160,+0.0159,+0.0158,+0.0157,+0.0156,+0360,
+0.0155,+0.0141,+0.0111,+0.0141,+0.0217,+0.0221,+0.0141,+0.0260,+0.0228,+0.0212,+0.0193,+0.0194,+0360,
+0.0188,+0.0182,+0.0178,+0.0174,+0.0171,+0.0168,+0.0166,+0.0164,+0.0162,+0.0160,+0.0159,+0.0158,+0360,
+0.0156,+0.0156,+0.0155,+0.0154,+0.0153,+0.0152,+0.0152,+0.0152,+0.0151,+0.0150,+0.0150,+0.0150,+0360,
+0.0149,+0.0149,+0.0149,+0.0149,+0.0148,+0.0148,+0.0148,+0.0147,+0.0147,+0.0147,+0.0147,+0.0147,+0360,
```

Figure E.7: *Example of raw file from a pressure sensor situated around Groix.*

The first line of the header corresponds to the moment when the file was created and the second one corresponds to the moment when the data started to be recorded. But then the time is not recorded. So after reading the file, I had to recreate a time vector. The pressure measurement is saved every half second and a file lasts three days. Therefore between two files, a time interval exists. This is a problem for the frequency analysis because the data record is not continuous. So the frequency analysis was done for each file and then each hour. The tide needed only to be reduced for the frequency analysis for each file.

E.3.1 Frequency Analysis Of Each File.

Here is an example of the observed pressure in the suitable form (fig. E.8). The pressure is as a function of time. The data are not corrected from the atmospheric pressure.

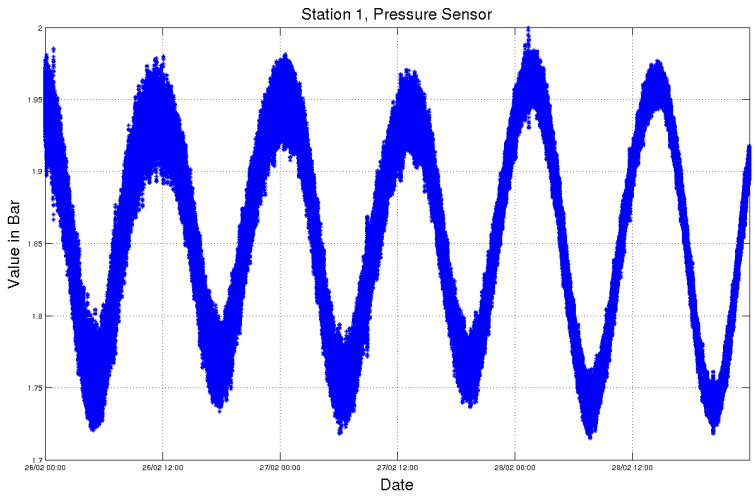

Figure E.8: *Example of raw file from the pressure sensor situated around Groix, in the adapted form.*

The data processing includes the removal of some wrong points such as the measurements at the beginning and at the end. Indeed the sensors were put into the water after the recording had already started so the first and last values are totally incorrect. Otherwise the sensors are really reliable because in each file, there is no hole at all. The following figure E.9 shows an example of the beginning of the recording for the station 1 in Groix:

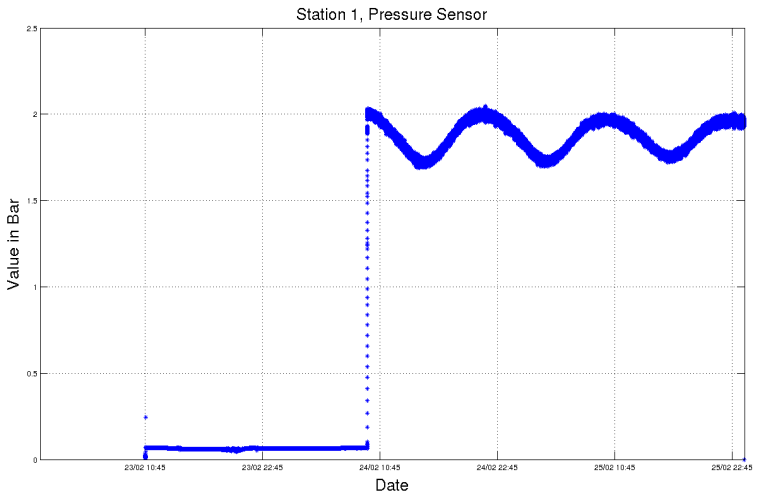

Figure E.9: *Example of raw file from the pressure sensor situated around Groix, in the adapted form. The file is the first recording.*

To realize a frequency analysis on each file, the tide signal has to be removed. However the sensors were placed on the bottom, so the surface elevation is not directly known and the tide can not be directly substracted. Moreover, I worked with the bottom pressure because if I had tried to calculate the surface elevation, I would surely have got wrong points. To have the surface elevation, a correction coefficient must be applied. But the infragravity waves include the forced waves and the free waves. For each kind of wave, the correction coefficient is not the same. These two kinds of waves can be hardly discriminated. So some information and some waves would be lost. In this situation, as the infragravity frequencies are not filtered by the depth, this correction is not required.

The tide signal can not be substracted using the tide predictions. So to realize it, I smoothed the signal and substrated it to the raw pressure. To smooth the signal, I use a filter with the Hanning window, applied on thirty minutes. Half hour corresponds to 3600 points. I used this filter because it cancels the points at the window border and highlights the peaks. The best smoothing is obtained with this filter. The following figures are a reminder of the Hanning window and the results of the filtering (fig. E.10):

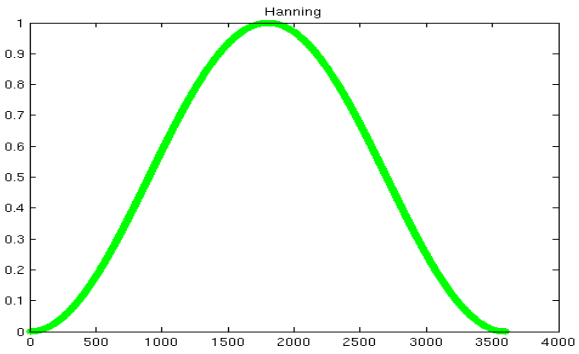

(a) *Hanning window used to smooth the pressure signal.*

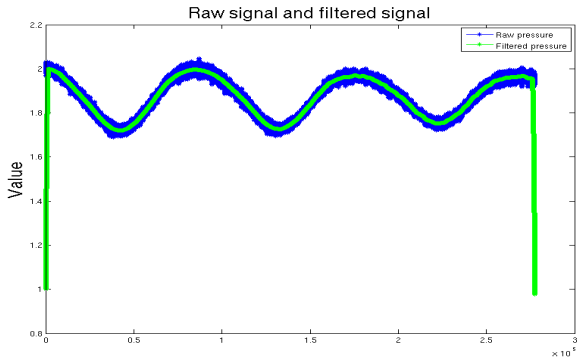

(b) *Results of the Hanning filtering. Raw pressure (in blue) and filtered pressure (in green).*

Figure E.10: *Hanning window and the results of the filtering.*

However, the Hanning filter adds points in each side of the file. I removed them. Moreover, I had to take away the beginning and the end of the file because the filter produce erroneous points and these points would affect the frequency analysis. The filtered signal corresponds to the tide only as the frequency analysis shows (fig. E.11):

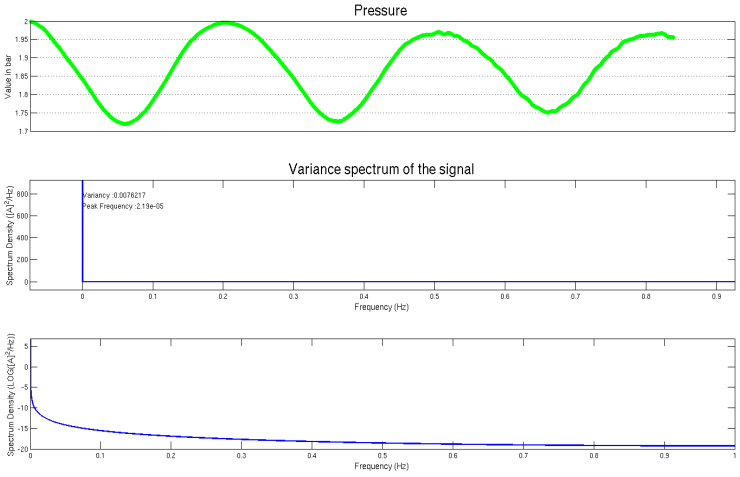

Figure E.11: *Results of the Hanning filtering. Frequency analysis.*

The peak frequency corresponds to the tide (The peak has a frequency of $2.1.10^{-5}$ Hz). So this pressure signal due to the tide is substracted to the raw pressure. After the tide reduction, the difference is analysed. Here is an example of the frequency analysis done after (fig. E.12):

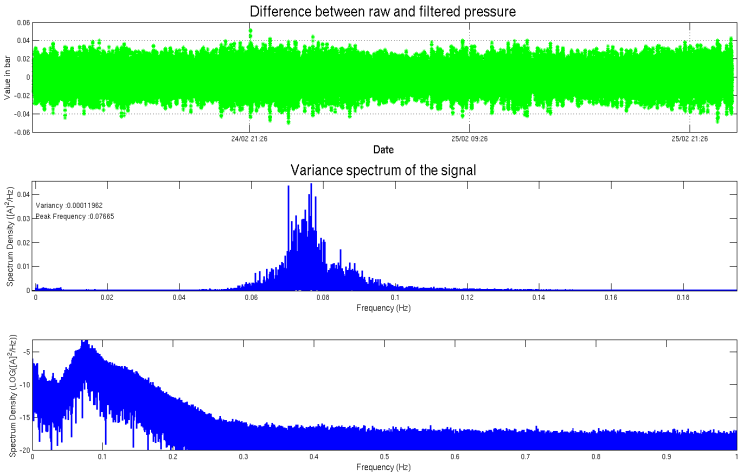

Figure E.12: *Results of the frequency analysis after the filtering and the tide signal removal, in Groix for the Station 1.*

Then the time evolution of the spectrum is plotted. The following figure shows an example using the infragravity spectrum (fig. E.13):

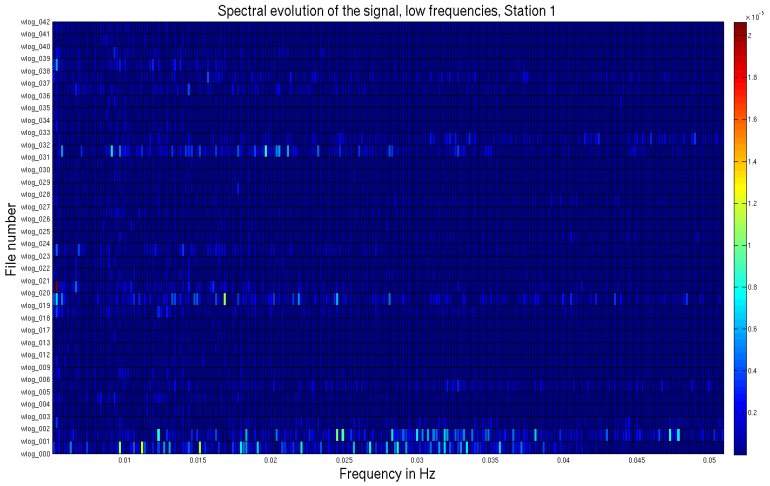

Figure E.13: *Time evolution of the spectrum, in Groix for the Station 1.*

E.3.2 Frequency Analysis Of One Hour Of Data.

To cut the files hour by hour, I use a Matlab program realized by F.Ardhuin. This program cuts the pressure files, performs the frequency analysis and calculates the significative height.

The program calculates seven spectrums (a spectrum is done with about fifteen minutes of data) and then the mean spectrum is calculated and saved. I adapted it so that the data be corrected from the atmospheric pressure.

Appendix F

Results In Groix

In this appendix, all results will be presented in details except the figures already shown in the chapters. First I will show all figures that prove that no seiche happened between February and May 2011. Then the significative long waves height inside and outside the harbor will be compared. Finally the full and infragravity spectrums will be presented. The significative long waves height is calculated with spectrums from the pressure sensors and the tide gauge.

But sometimes the period is not in continue and has holes. I merged the dates. Moreover sometimes the significative height was kown each hour whereas in other file it was known each two half hours.

F.1 Seiche Dectection.

F.1.1 Seiche Detection Using Data Recorded Every Minute.

Observed and predicted tides between March 28 and April 5 2011 :

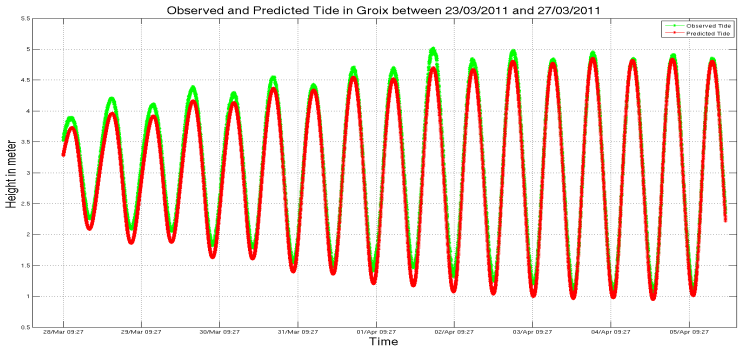

Figure F.1: *Observed and predicted tides in Groix between March 28 and April 5 2011.*

Difference between the observed and predicted tides between March 28 and April 5 2011 :

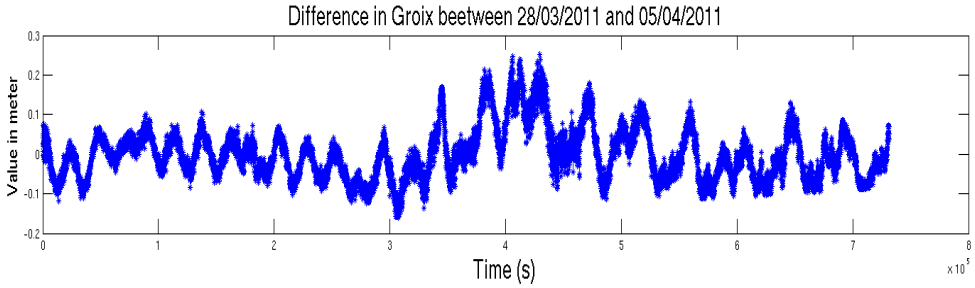

Figure F.2: *Difference between observed and predicted tides in Groix between March 28 and April 5 2011.*

F.1.2 Seiche Detection Using Data Recorded Every Fifteen Seconds.

Difference between the observed and predicted tides between April 26 and May 12 2011 :

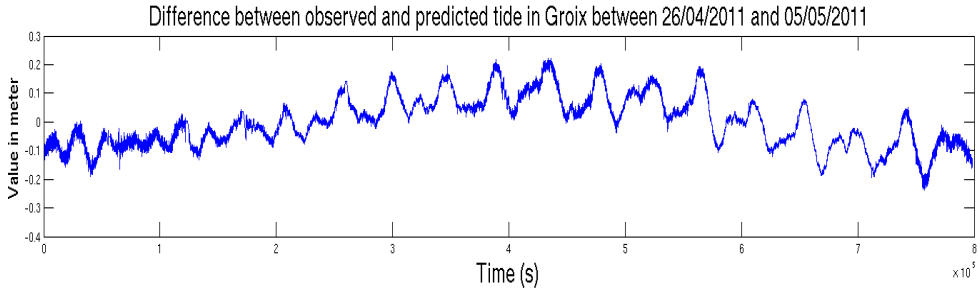

Figure F.3: *Difference between observed and predicted tides in Groix between April 26 and May 5 2011. The data were recorded fifteen seconds.*

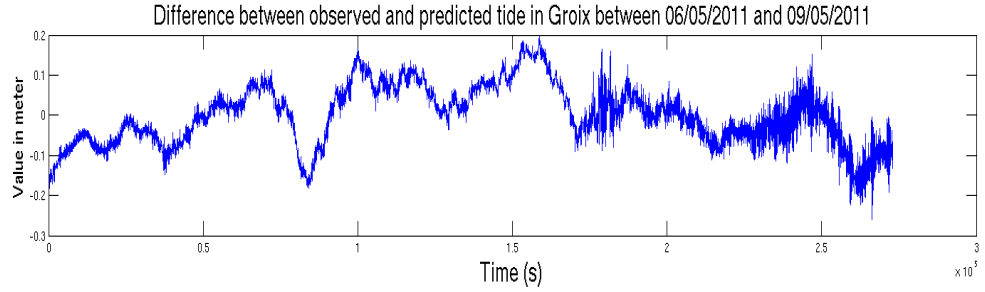

Figure F.4: *Difference betwenn observed and predicted tides in Groix between May 6 and May 9 2011. The data were recorded fifteen seconds.*

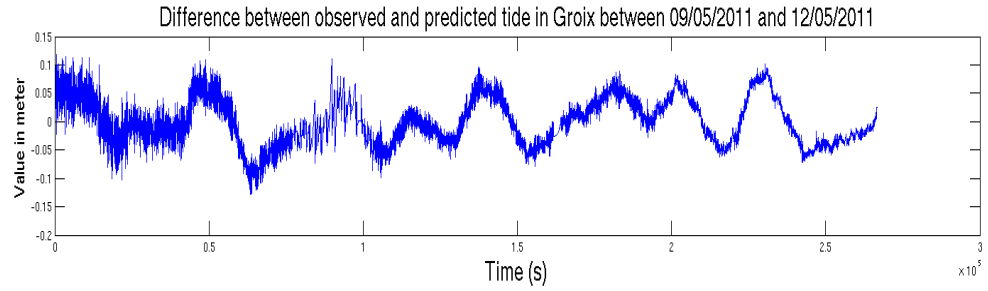

Figure F.5: *Difference between observed and predicted tides in Groix between May 9 and May 12 2011. The data were recorded fifteen seconds.*

F.2 Tide Signal And Pressure Sensors.

The following figures show other relevant results that I obtained. The results concerning the significative long waves height are between April 5 and May 12 2011 and the results concerning the spectrums are between Arpil 4 and April 11 2011:

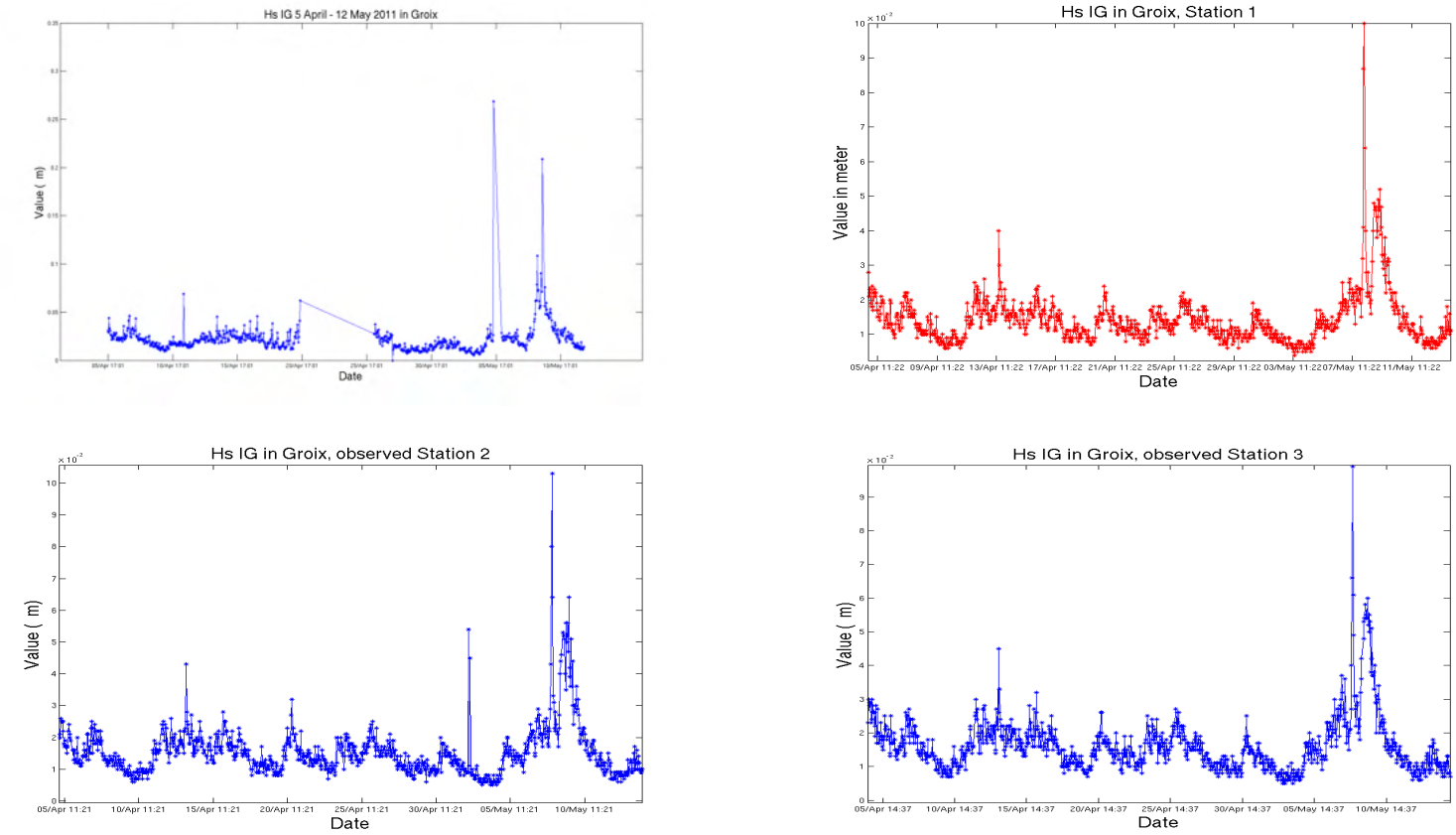

Figure F.6: *Significative long waves height calculated inside the harbor with the tide signal (on the top figure) and outisde the harbor calculated with the pressure sensors (on the down figures) between April 5 and May 12 2011.*

The correlation coefficients are equal to 0.8.

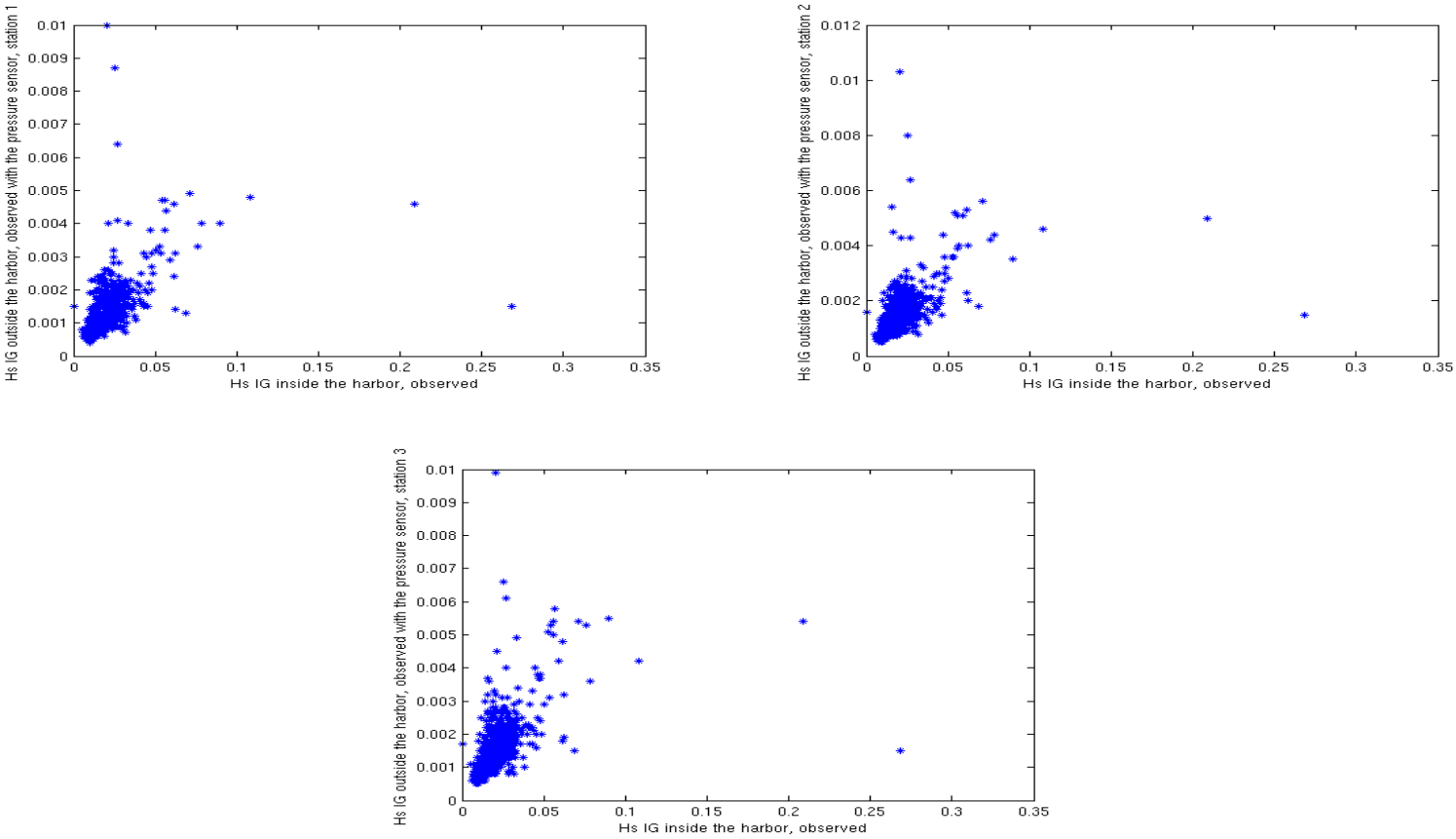

Figure F.7: *Significative height calculated inside the harbor with the tide signal and outside the harbor with the pressure sensors between April 5 and May 12 2011. Values in meter.*

The spectrum evolution between April 5 and April 11 2011 is :

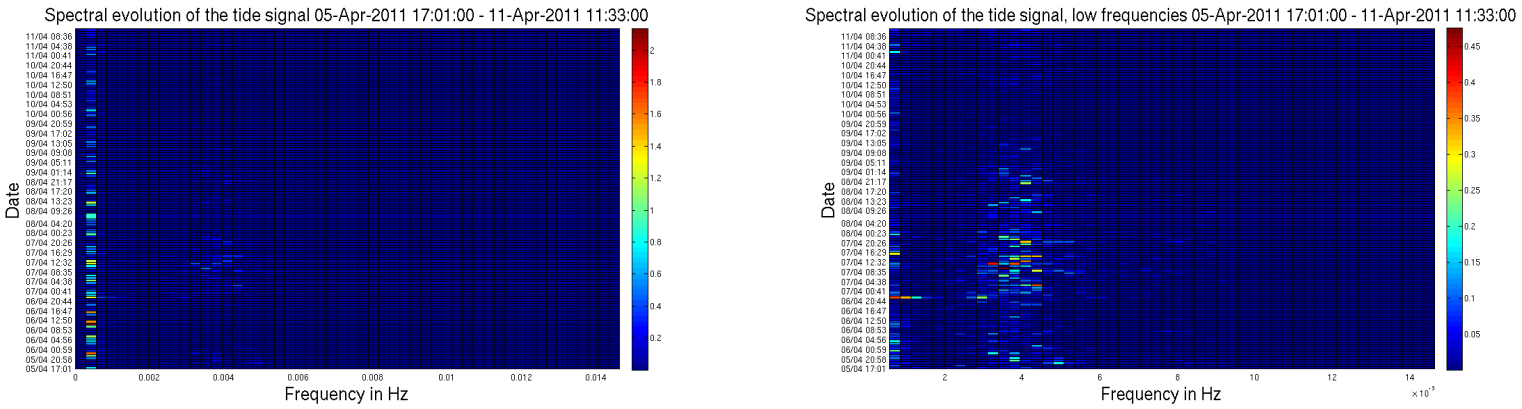

Figure F.8: *Full (on the left) and infragravity (on the right) spectrums calculated using the tide data between April 5 and April 11 2011.*

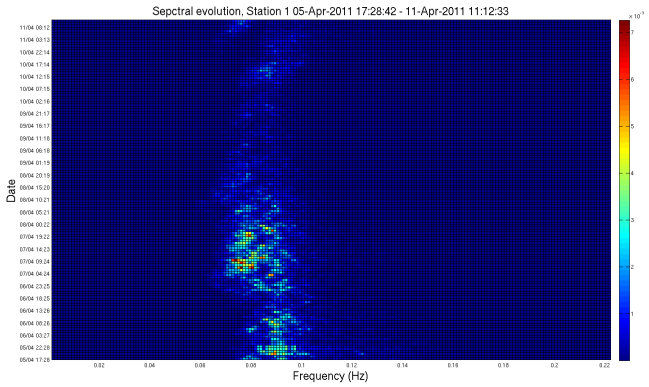

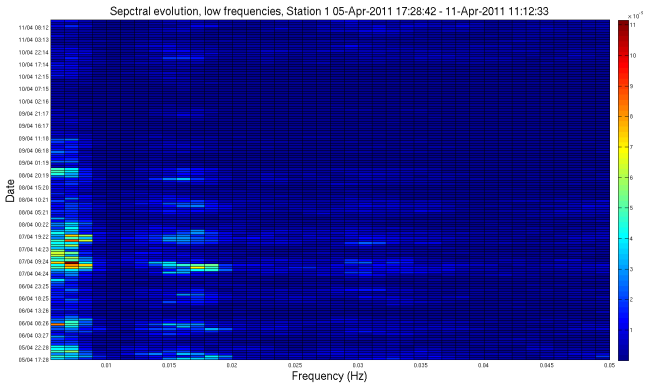

Figure F.9: *Full (on the left) and infragravity (on the right) spectrums calculated using the pressure data in Station 1 between April 5 and April 11 2011.*

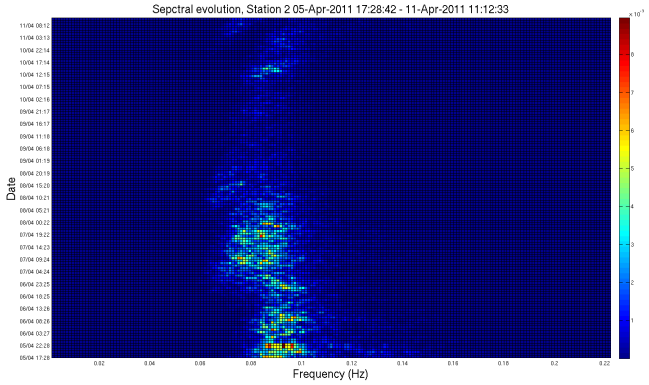

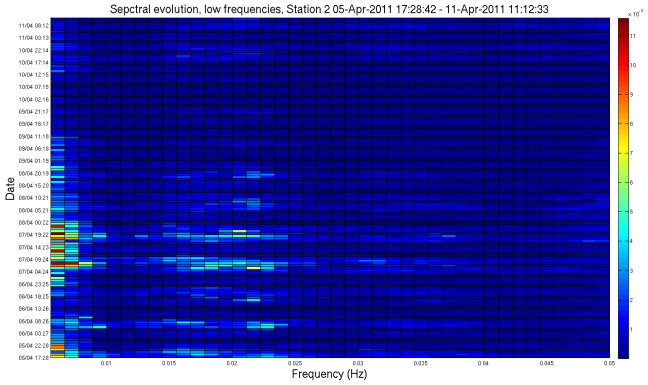

Figure F.10: *Full (on the left) and infragravity (on the right) spectrums calculated using the pressure data in Station 2 between April 5 and April 11 2011.*

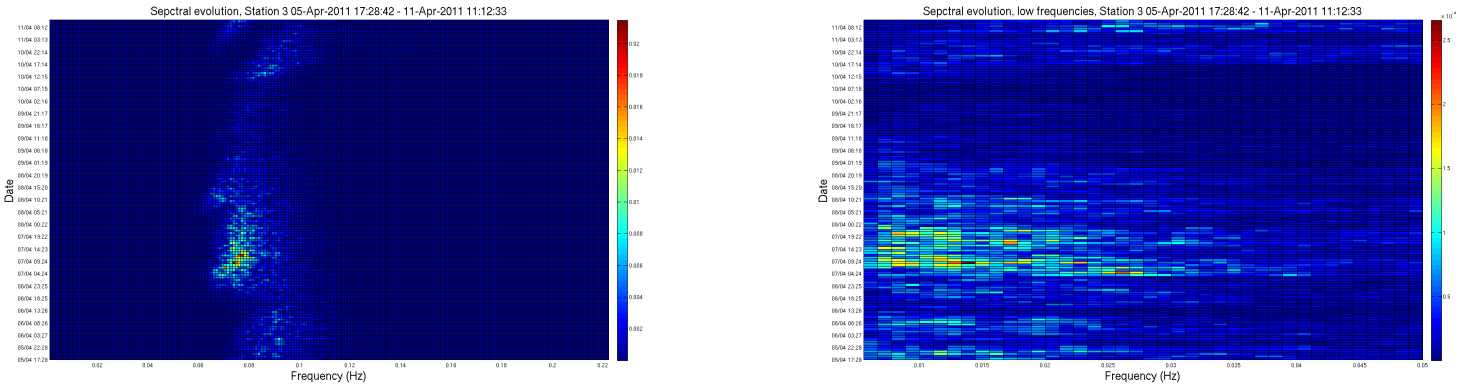

Figure F.11: *Full (on the left) and infragravity (on the right) spectrums calculated using the pressure data in Station 3 between April 5 and April 11 2011.*

Appendix G

Results In Royan

In this appendix, all results will be presented except the figures already shown in the chapters. The significative long waves height inside and outside the harbor will be compared. The height is calculated with spectrums from the pressure sensors, the tide gauge and WAVEWATCH 3 model. The model calculated the height in Oléron and Royan.

But sometimes the period is not in continue and has holes. I merged the dates. Moreover sometimes the significative height was kown each hour whereas in other file it was known each two half hours.

G.1 Locations Of The Calculation Points.

The following figures show the location of different calculation points for WAVEWATCH III, the harbor and the buoy location in Oléron:

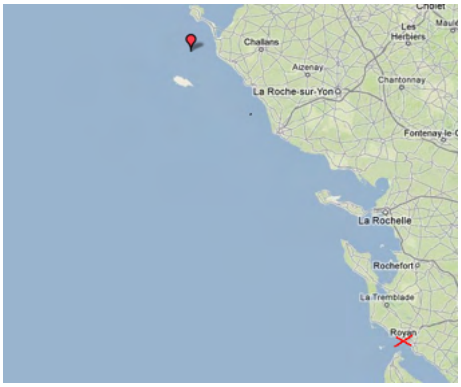

Figure G.1: *The buoy location in Oléron (red point) in comparison with the harbor location in Royan (red cross).*

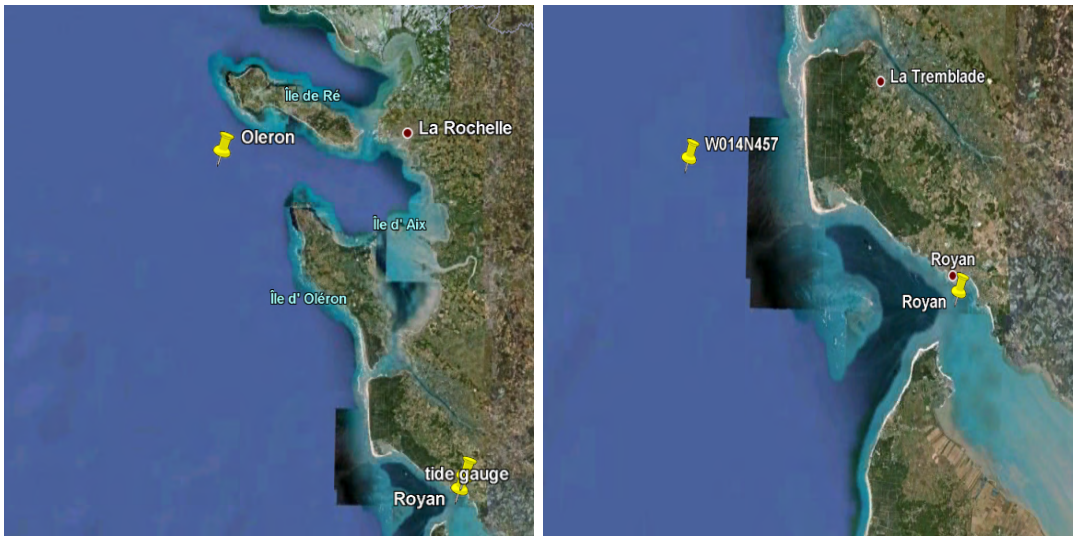

Figure G.2: *Location of the calculation points in Oléron and in Royan (on the left figure) and location of the calculation points in Royan and offshore (on the right figure).*

G.2 Shelf Effects On Waves.

As I previously wrote and is shown on the following figure, a shelf is near the harbor:

Figure G.3: *The shelf near Royan harbor.*

The waves break on the natural shelf. So the waves are filtered but the long waves should remain. Indeed during a break, the infragravity waves are liberated. That was a possible mechanism to generate long waves (see chap. 2). Using the data from WAVEWATCH III in

Royan and in "W014N457" I compared the significative long waves height before and after the shelf and also the significative height of the waves field. The following figures show the results:

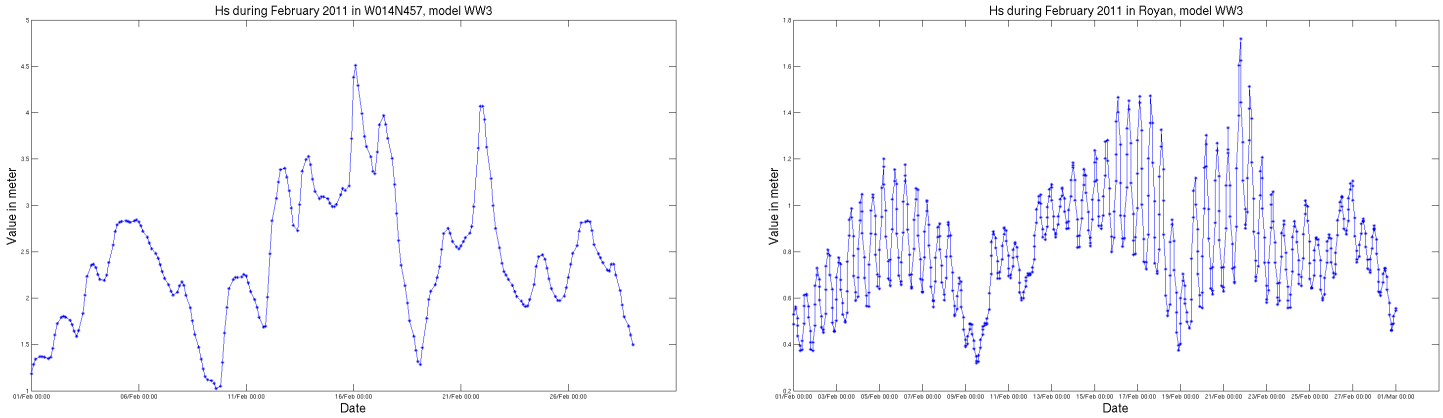

Figure G.4: *Significative height of the wave field calculated before the shelf in "W014N457" (on the left figure) and after the shelf in Royan (on the right figure) between February 1 and March 1 2011.*

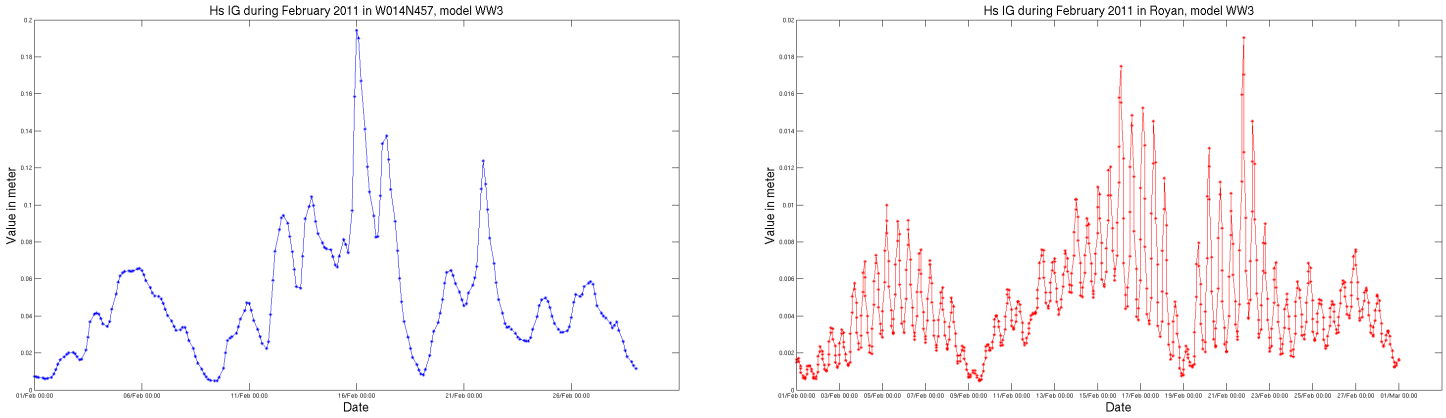

Figure G.5: *Significative long waves height calculated before the shelf in "W014N457" (on the left figure) and after the shelf in Royan (on the right figure) between February 1 and March 1 2011.*

The waves are attenuated except for the long waves.

G.3 Comparison Between The Model In Royan And The Buoy Observations In Oléron.

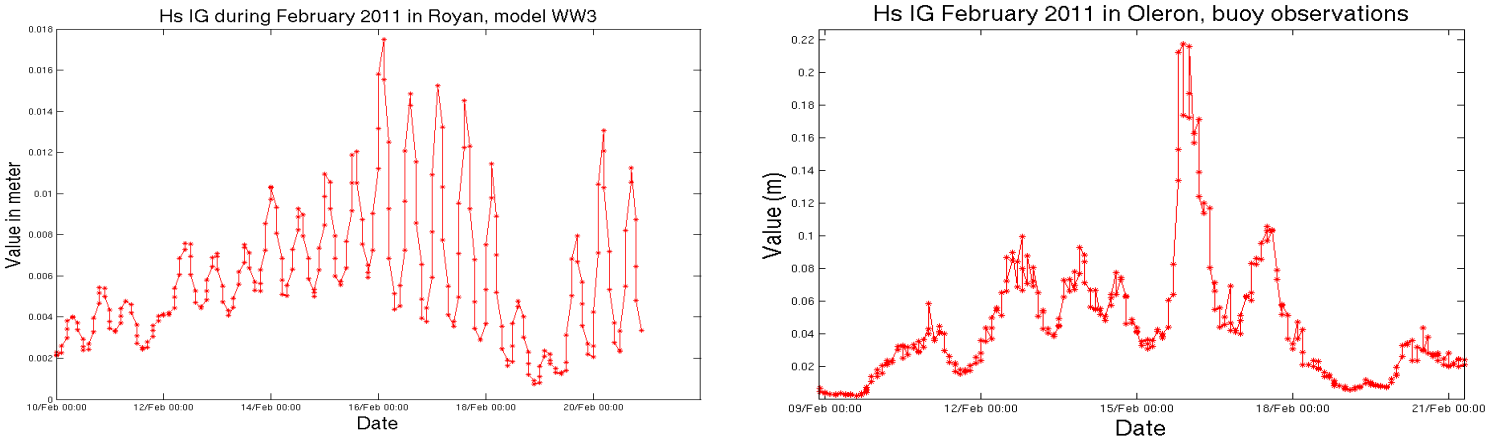

Figure G.6: *Significative infragravity waves height calculated outside the harbor with the WAVEWATCH 3 model in Royan (on the top figure) and the significative height observed outside the harbor using the buoy in Oléron (on the down figure). The period is between February 10 and February 20 2011.*

The correlation coefficient is 0.58. The spectrum evolution is :

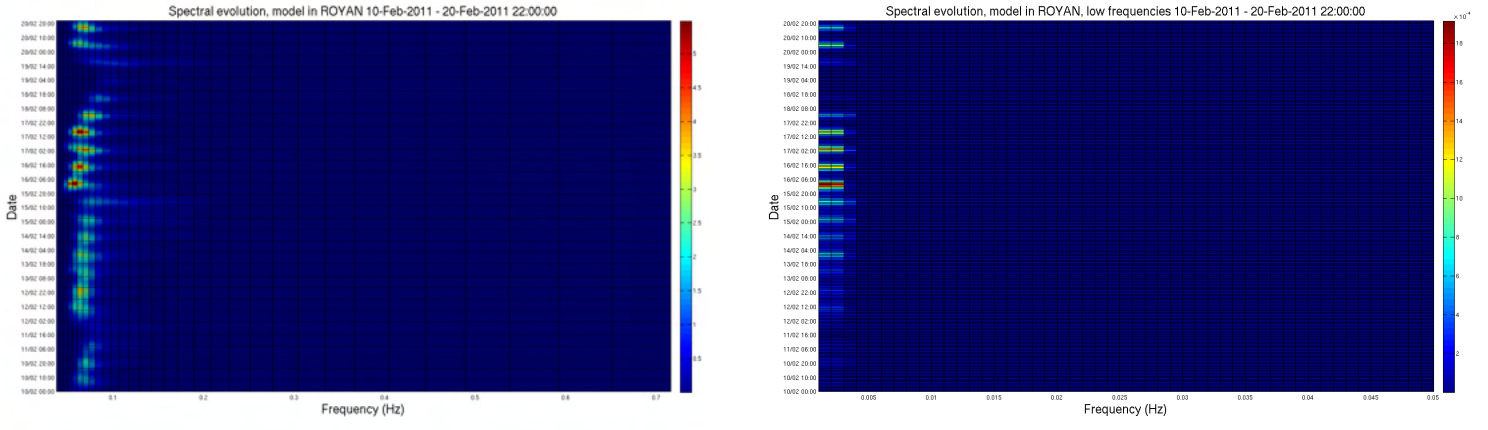

Figure G.7: *Full (on the left) and infragravity (on the right) spectrums in Royan calculated with the model between February 10 and February 20 2011.*

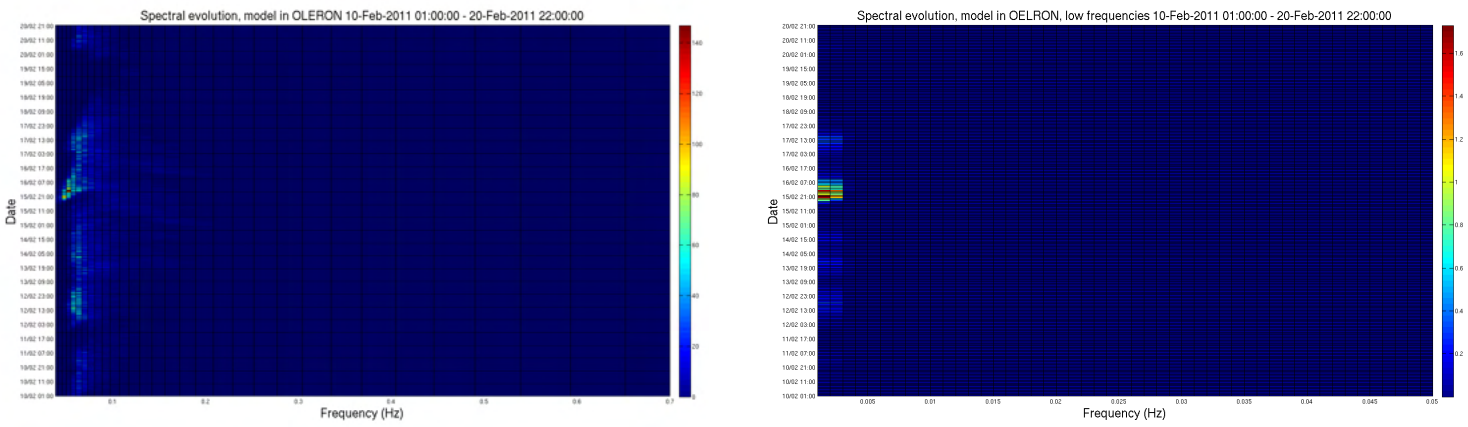

Figure G.8: *Full (on the left) and infragravity (on the right) spectrums in Oléron observed by the buoy between February 10 and February 20 2011.*

G.4 Comparison Between The Tide In The Harbor And The Buoy Observations In Oléron.

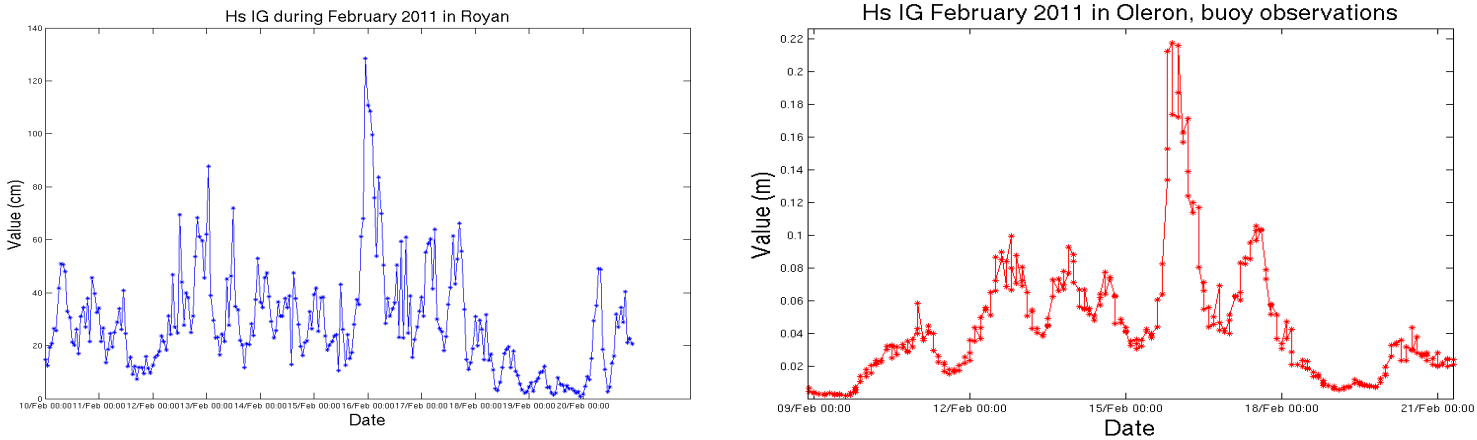

Figure G.9: *Significative infragravity waves height calculated inside the harbor with the tide in Royan (on the top figure) and the significative height observed outside the harbor using the buoy in Oléron (on the down figure). The period is between February 10 and February 20 2011.*

The correlation coefficient is 0.65.

Bibliography

[ADP10] F. Ardhuin, E. Devaux, and L. Pineau-Guillou. Observation et prévision des seiches sur la cote Atlantique française. *Journées Génie Côtier Génie Civil*, June 2010.

[Bal05] A. Balanche. Etude des ondes infragravitaires en zone de surf. Master's thesis, Universite Bordeaux 1, 2005.

[Dev09] E. Devaux. Analyse de seiches à partir de l'exploitation de données marégraphiques. Master's thesis, ENTPE, 2009.

[Fle04] J.B. Fleitour. Etude relative au phenomène de seiche dans le port de Groix. Master's thesis, ENSIETA Brest, 2004.

[For00] Forristall. Wave crest distribution: observations and second-order theroy. *Journal of physical oceanography*, vol. 30:1931–1943, August 2000.

[Gal71] B. Gallagher. Generation of surf beat by non-linear wave interactions. *J.Fluid Mech*, vol. 49:1–20, 1971.

[Her94] T.H.C. Herbers. Infragravity-frequence (0.005-0.05 Hz) motions on the shelf, part I: forced waves. *Journal of Physical Oceanography*, pages 917–927, 1994.

[Leb08] L. Leballeur. *Modélisation couplée houle-courant en zone littorale.* PhD thesis, ENSIETA, 2008.

[LGE+99] S. Lentz, R.T. Guza, S. Elgar, F. Feddersen, and T.H.C. Herbers. Momentum balance on the North California inner shelf. *Journal of geophysical research*, vol. 104:18.205–18.226, August 1999.

[LS64] M.S. Longuet-Higgins and R.W. Stewart. Radiation stress in water waves: a physical discussion, with applications. *Deep-sea research*, vol. 11:529–562, June 1964.

[OGS92] Okihiro, Guza, and Seymour. Bound infragravity waves. *Journal of geophysical research*, vol. 97:11.453–11.469, July 1992.

[OGS93] M. Okihiro, R.T. Guza, and R.J. Seymour. Excitation of seiche observed in a small harbor. *Journal of geophysical research*, vol. 98:18.201–18.211, October 1993.

[OH89] J. Oltman-Shay and K. Hathaway. Infragravity energy and its implications in nearshore sediment transport and sandbar dynamics. Technical Report CERC-89-8, US Army Corps of Engineers, 1989.

[Per07] C. Perherin. Contribution à l'analyse des phenomènes de surcôtes et de submersions marines. Master's thesis, ENTPE, 2007.

[Pug87] D.T. Pugh. *Tides, surges and mean-sea level, chap 5.* 1987.

[Ran04] D.A. Randall. *An Introduction to Atmospheric Modeling.* je sais pas, 2004.

[RGE+09] A.J.H.M. Reniers, M.J. Groenewegen, K.C. Ewans, S. Masterton, G.S. Stelling, and J. Meek. Estimation of infragravity waves at intermediate water depth. *Coastal Engineering*, pages 52–61, November 2009.

[RRT04] Reiners, Roelvink, and Thorton. Morphodynamic modeling of an embayed beach under wave group forçing. *Journal of geophysical research*, vol. 109, 2004.

[RVBT02] A.J.H.M. Reniers, A.R. Van Dongeren, J.A. Battjes, and E.B. Thornton. Linear modeling of infragravity waves during Delilah. *Journal of geophysical research*, vol. 107:3137–3155, October 2002.

[TG86] Thorton and Guza. Surf zone longshore currents and random waves: field data and research. *Journal of physical hydrography*, vol. 16:1165–1178, July 1986.